UNIVERSIDADE FEDERAL DO PARANÁ

RICARDO SCHUMACHER

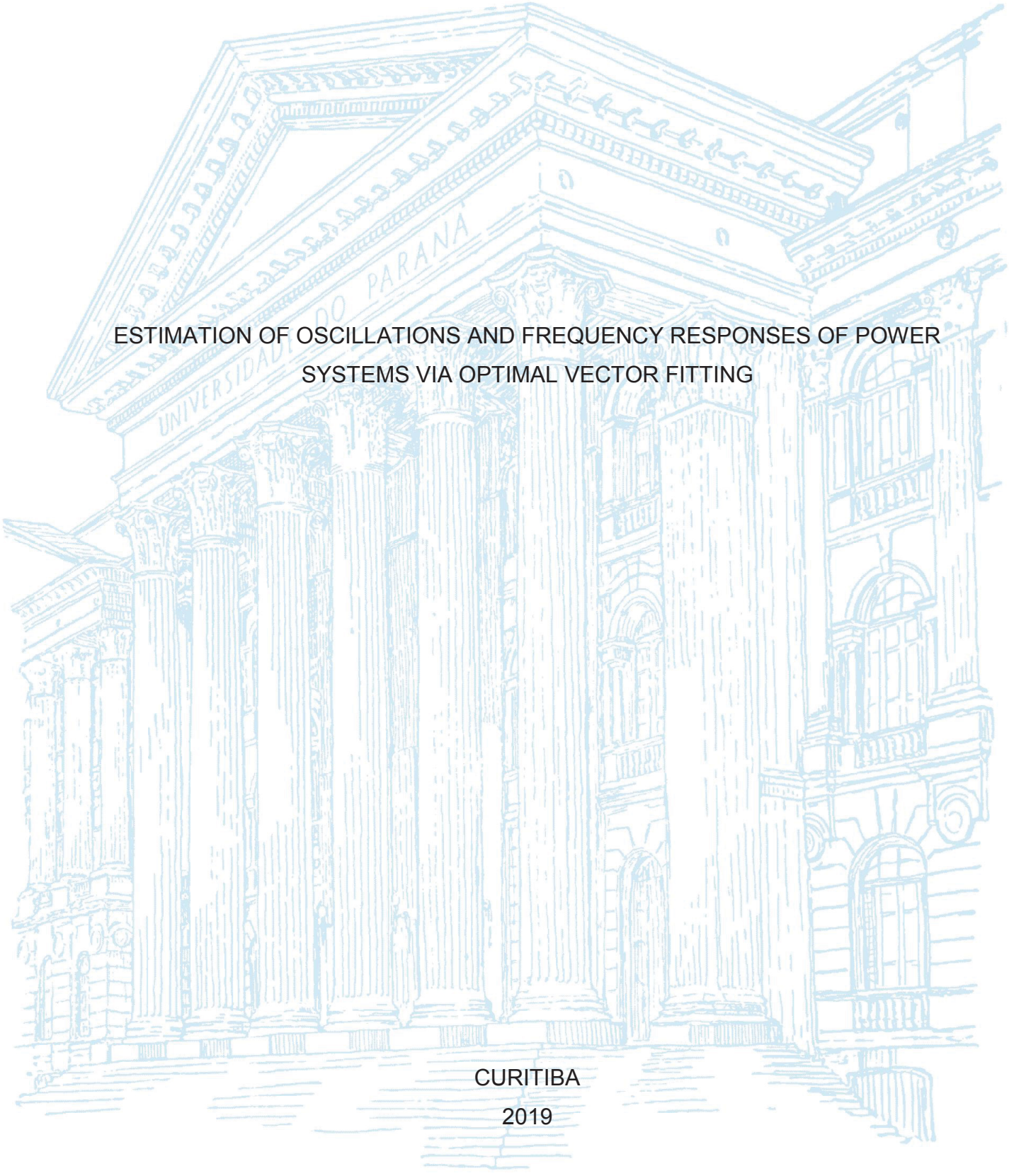

ESTIMATION OF OSCILLATIONS AND FREQUENCY RESPONSES OF POWER SYSTEMS VIA OPTIMAL VECTOR FITTING

CURITIBA

2019

RICARDO SCHUMACHER

ESTIMATION OF OSCILLATIONS AND FREQUENCY RESPONSES OF POWER SYSTEMS VIA OPTIMAL VECTOR FITTING

Tese apresentada ao Programa de Pós-Graduação em Engenharia Elétrica, Área de Concentração Sistemas de Energia, Departamento de Engenharia Elétrica, Setor de Tecnologia, Universidade Federal do Paraná, como requisito parcial à obtenção do título de Doutor em Engenharia Elétrica.

Orientador: Prof. Dr. Gustavo Henrique da Costa Oliveira

Coorientador: Prof. Dr. Rôman Kuiava

CURITIBA

2019

Catalogação na Fonte: Sistema de Bibliotecas, UFPR
Biblioteca de Ciência e Tecnologia

S392e Schumacher, Ricardo
Estimation of oscillations and frequency responses of power systems via optimal vector fitting [recurso eletrônico] / Ricardo Schumacher – Curitiba, 2019.

Tese - Universidade Federal do Paraná, Setor de Tecnologia, Programa de Pós-Graduação em Engenharia Elétrica.
Orientador: Gustavo Henrique da Costa Oliveira
Coorientador: Rôman Kuiava

1. Variáveis (Matemática). 2. V*ector Fitting* (Algorítmos). 3. Identificação de sistemas. I. Universidade Federal do Paraná. II. Oliveira, Gustavo Henrique da Costa III. Kuiava, Rôman. IV. Título.

CDD: 511.8

Bibliotecária: Roseny Rivelini Morciani CRB-9/1585

MINISTÉRIO DA EDUCAÇÃO
SETOR DE TECNOLOGIA
UNIVERSIDADE FEDERAL DO PARANÁ
PRÓ-REITORIA DE PESQUISA E PÓS-GRADUAÇÃO
PROGRAMA DE PÓS-GRADUAÇÃO ENGENHARIA
ELÉTRICA - 40001016043P4

TERMO DE APROVAÇÃO

Os membros da Banca Examinadora designada pelo Colegiado do Programa de Pós-Graduação em ENGENHARIA ELÉTRICA da Universidade Federal do Paraná foram convocados para realizar a arguição da tese de Doutorado de **RICARDO SCHUMACHER** intitulada: **Estimation of oscillations and frequency responses of power systems via optimal Vector Fitting**, após terem inquirido o aluno e realizado a avaliação do trabalho, são de parecer pela sua aprovação no rito de defesa.

A outorga do título de doutor está sujeita à homologação pelo colegiado, ao atendimento de todas as indicações e correções solicitadas pela banca e ao pleno atendimento das demandas regimentais do Programa de Pós-Graduação.

CURITIBA, 19 de Junho de 2019.

GUSTAVO HENRIQUE DA COSTA OLIVEIRA
Presidente da Banca Examinadora (UFPR)

LUCIA VALÉRIA RAMOS DE ARRUDA
Avaliador Externo (UTFPR)

GIDEON VILLAR LEANDRO
Avaliador Interno (UFPR)

FRANCISCO DAMASCENO FREITAS
Avaliador Externo (UNB)

To Paulo and Jennifer

ACKNOWLEDGMENTS

First and foremost, I would like to thank God for his enigmatic presence in my life.

I also would like to thank Prof. Gustavo Henrique da Costa Oliveira for providing me invaluable support, encouragement and guidance throughout the years I have researched under his supervision. He has given me all the freedom to pursue my research, while effectively ensuring that I would not deviate from its goals.

For giving me valuable insights, I also thank Prof. Rôman Kuiava. I extend this thanks to all professors at Federal University of Paraná who have directly or indirectly helped me in my personal and academic formations.

For willingly sharing with us data sets used in this thesis, I would like to thank the authors of (HWANG; LIU, 2017) and (JEREMIAS *et al.*, 2012), as well as Eng. Robson A. Oliveira and Eng. José G. R. Filho, both from Itaipu Hydroelectric.

This study was supported by Fundação Araucária de Apoio ao Desenvolvimento Científico e Tecnológico do Estado do Paraná and by the Energia Sustentável do Brasil (ESBR) research and technological development program, through the P&D ANEEL 06631-0006/2017 project, regulated by the Agência Nacional de Energia Elétrica (ANEEL).

Finally, for supporting me all these years, I am also pleased to acknowledge the importance of my family in my life.

RESUMO

A identificação de sistemas está presente em diversas áreas da engenharia onde um modelo matemático preciso é exigido. Diferentes tipos de algoritmos de estimação têm sido usados para identificar sistemas lineares invariantes no tempo. Contudo, o caso particular que considera a utilização dos chamados métodos iterativos *Vector Fitting* (VF) tem atraído atenção significativa da comunidade científica, especialmente durante as últimas duas décadas. Neste contexto, esta tese aborda o problema de formulação de algoritmos VF para ambos os domínios, do tempo e da frequência. No domínio do tempo, algoritmos VF são aqui desenvolvidos dentro de um contexto *ringdown*, de modo que dinâmicas oscilatórias (assim como dinâmicas puramente exponenciais) de sistemas de potência possam ser efetivamente estimadas através de conjuntos de dados transitórios extraídos desses sistemas. Neste sentido, também é apresentada uma abordagem multi-sinal para estimar simultaneamente múltiplos sinais transitórios possivelmente distribuídos em diferentes localizações do sistema de potência que está sendo modelado. Por outro lado, no âmbito do domínio da frequência, esta tese apresenta um método VF que pode ser aplicado na estimação de modelos formados por bases de funções racionais (BFRs) definidas tanto no tempo contínuo como no tempo discreto. Em ambos os contextos do tempo e da frequência, formulações VF alternativas baseadas em variáveis instrumentais (VI) são também vastamente investigadas neste trabalho. Soluções convergidas fornecidas por essas formulações VF baseadas em VI são provadamente ótimos locais de suas funções objetivo não-lineares correspondentes, sendo essa importante propriedade de otimalidade local independente da natureza do ruído que corrompe os dados de estimação. Exemplos numéricos apresentados neste trabalho focam em dados de resposta em frequência extraídos de transformadores de potência e de potencial indutivo reais assim como em conjuntos de dados transitórios extraídos do sistema de potência interconectado Brasileiro e do sistema de interconexão leste norte americano.

Palavras-chave: identificação de sistemas. *vector fitting*. análise *ringdown*. estimação de respostas em frequência. variáveis instrumentais

ABSTRACT

System identification appears in several areas of engineering where a accurate mathematical model is required. Many different types of estimating algorithms have been used for identifying linear time-invariant systems. Nonetheless, the particular case of using the so-called iterative Vector Fitting (VF) algorithms has been drawing significant attention from scientific community, especially during the last two decades. In this context, this thesis addresses the problem of formulating VF algorithms for both time- and frequency-domain system identification. When it comes to time-domain, VF algorithms are here developed within a ringdown context, so that oscillatory (as well as purely exponential) dynamics of power systems can be effectively estimated through transient (ringdown) data sets extracted from these systems. In this sense, it is also presented a multi-signal approach for simultaneously estimating multiple transient signals possibly distributed over different locations of the power system under modeling. On the other hand, when it comes to frequency-domain, this thesis presents a unifying VF method which can be similarly applied for estimating models formed either by continuous- or discrete-time rational basis functions (RBFs). In both time- and frequency-domain contexts, alternative VF formulations based on instrumental variables (IV) are also intensively investigated throughout this thesis. Converged solutions provided by these IV-based VF formulations are proved to be local optimums of their corresponding nonlinear objective functions, being this important optimality property independent on the nature of the noise that corrupts estimation data. Numerical examples presented in this work focus on frequency response data extracted from actual power and potential transformers as well as on transient data sets extracted from the Brazilian Interconnected Power (BIP) system and from the North American Eastern Interconnection (NAEI) system.

Keywords: system identification. vector fitting. ringdown analysis. frequency response estimation. instrumental variables.

LIST OF FIGURES

LIST OF ABBREVIATIONS AND ACRONYMS

BIP	**B**razilian **I**nterconnected **P**ower
DFT	**D**iscrete **F**ourier **T**ransform
FD	**F**requency-**D**omain
FDR	**F**requency **D**isturbance **R**ecorder
IPT	**I**nductive **P**otential **T**ransformer
IV	**I**nstrumental **V**ariables
MIMO	**M**ultiple-**I**nput **M**ultiple-**O**utput
NAEI	**N**orth **A**merican **E**astern **I**nterconnection
NOF	**N**onlinear **O**bjective **F**unction
PMU	**P**hasor **M**easurement **U**nit
RBF	**R**ational **B**asis **F**unction
RMS	**R**oot **M**ean **S**quare
SISO	**S**ingle-**I**nput **S**ingle-**O**utput
TD	**T**ime-**D**omain
VF	**V**ector **F**itting
WAMS	**W**ide-**A**rea **M**onitoring **S**ystems

LIST OF SYMBOLS

$y(t)$	measured ringdown signal
$\bar{y}(t)$	modeling signal structure
h_{dc}	dc component
M_{OSC}	number of oscillatory modes
M	total number of modes
A_l	amplitude of the l-th mode
σ_l	attenuation of the l-th mode
ω_l	frequency (in rad/s) of the l-th oscillatory mode
φ_l	phase of the l-th oscillatory mode
λ_l	l-th model eigenvalue
K	number of data samples available for estimation
T	sampling time
$\delta(t)$	unit impulse function
N	model order
ρ	differentiation operator
γ	parameter vector
p_i	i-th model pole
θ	alternative parameter vector
$J(\theta)$	objective function to be minimized

$e(\cdot)$	scalar error
$\hat{y}(t)$	alternative signal structure
$\hat{\theta}$	estimate for $\theta^\star$ obtained for a given set of pre-specified poles
$\hat{\theta}_{\mathrm{IV}}$	IV-based estimate for $\theta^\star$ obtained for a given set of pre-specified poles
$\theta^\star$	global minimum of $J(\theta)$
$\mathbf{i}_{(v)}(\cdot)$	instrument vector
$\mathbf{i}'_{(v)}(\cdot)$	instrument vector
$\mathcal{L}^{-1}$	inverse Laplace operator
$\mathcal{L}$	Laplace operator
$U_0(\alpha)$	system input
$Y_0(\alpha)$	system output
$V(\alpha)$	additive disturbance at the system output
α	variable used for determining if the system is described either in continuous-time ($\alpha = s$) or discrete-time ($\alpha = z$)
$\Phi_i(\alpha, \mathbf{p})$	i-th model rational basis function
$\mathbf{p}$	vector containing the poles of $\bar{G}(\alpha)$
$W(\alpha_k)$	weighting function to be selected by the user

CONTENTS

1 INTRODUCTION

The act of formulating models has been part of human life for thousands of years. When children learn to walk, for instance, their brains develop mental models which are capable of relating notions of equilibrium, distance and motor coordination. In a sense, although nature of models may vary significantly, in many daily circumstances one has to deal with the problem of obtaining (estimating) mathematical models that describe the so-called memory effect (dynamic behavior) of physical processes (systems).

Indeed, various areas of engineering demand for mathematical models that appropriately represent physical processes. These models can be applied, for instance, in the design and implementation of new processes, in the design of control systems and in studies involving system stability (EREMIA; SHAHIDEHPOUR, 2013; MUNOZ-HERNANDEZ; MANSOOR; JONES, 2013; LJUNG, 1999; ÅSTRÖM, 1996).

There are, in principle, two ways of constructing mathematical models: physical modeling and system identification (LJUNG; GLAD, 1994). In physical modeling, which is also called white box modeling, considerable knowledge about physical laws that describe the process behavior is used for obtaining mathematical models. The model for a DC motor, for example, can be obtained by using principles of mechanics and electricity. On the other hand, system identification, which is also known as black box or gray box modeling, plays a key role in cases where there is little (gray box) or no (black box) knowledge about physical phenomena involved in the process behavior, although data from such a process is considered to be available for measurement. Therefore, one can say system identification is based on experimentation, being mathematical models built through data extracted from the process under modeling.

One can divide system identification methods into (*i*) time-domain methods (LJUNG, 1999), when estimation data are composed of a sequence of samples discretized in time; and (*ii*) frequency-domain methods (PINTELON; SCHOUKENS, 2012), when, alternatively, estimation data are composed of a sequence of samples discretized in frequency.

Extraction of such data sets may occur directly either in frequency-domain (through direct frequency response measurement) or time-domain (through analysis of input-output data). Nonetheless, one can also transform data from one domain to the other by using, for instance, non-parametric identification or (inverse) discrete Fourier Transform (DFT) (LJUNG, 1999).

Once a (time- or frequency-domain) data set is available, system identification approaches must deal with the definition of a *model structure*, where its parameters are then carefully chosen (estimated) so that the model response gets sufficiently close to the actual response extracted from the system.

When it comes to identifying systems which can be considered to be *linear*, i.e., which satisfy the so-called superposition principle, there are in the literature several well consolidated types of model structures, such as OE, ARX, BJ and ARMAX model structures. System identification methods for estimating the parameters of such structures have already been extensively investigated (AGUIRRE, 2007; LJUNG, 1999; VAN DEN BOSCH; VAN DER KLAUW, 1994). However, in the specific context of OE model structures, especially during the last two decades, the so-called iterative Vector Fitting (VF) algorithms have drawn increasing attention from scientific community (GRIVET-TALOCIA; GUSTAVSEN, 2016; VOORHOEVE *et al.*, 2014; DESCHRIJVER; HAEGEMAN; DHAENE, 2007; HEUBERGER; VAN DEN HOF; WAHLBERG, 2005; GRIVET-TALOCIA, 2003; GUSTAVSEN, 2002).

1.1 VF algorithms

VF algorithms have become popular especially within power systems and microelectronics communities since they may provide satisfactory estimates for transfer function poles of OE model structures (GRIVET-TALOCIA; GUSTAVSEN, 2016; UBOLLI; GUSTAVSEN, 2011; GUSTAVSEN, 2006; GUSTAVSEN; SEMLYEN, 1999). In the particular case of power systems, successful applications of VF comprehend the following areas: modeling of frequency-dependent network equivalents for transient analysis (SCHUMACHER; OLIVEIRA, 2017; UBOLLI; GUSTAVSEN, 2011; RAMIREZ, 2009), wideband modeling of

transmission lines and transformers (GUSTAVSEN, 2006; Gustavsen, 2004; GUSTAVSEN; SEMLYEN, 1999), estimation of electromechanical modes (SCHUMACHER; OLIVEIRA; KUIAVA, 2019; SCHUMACHER; OLIVEIRA; KUIAVA, 2018; PAPADOPOULOS *et al.*, 2016) and passive macromodeling (GRIVET-TALOCIA; GUSTAVSEN, 2016; IHLENFELD; OLIVEIRA; SANS, 2016; OLIVEIRA; RODIER; IHLENFELD, 2016). In the particular case of frequency response modeling of power transformers, estimating wideband dynamic models may improve electromagnetic transient simulations which subsidize, for instance, insulation coordination and system performance studies (GUSTAVSEN, 2010; Cigre WG A2/C4.39, 2014) (see also (THOMAS; SAVADAMUTHU, 2017) for a connection between very fast transients and paper insulation in power transformers).

In VF algorithms, transfer functions are represented by means of a linear combination of rational basis functions (RBFs). In a sense, these algorithms can be also understood as robust reformulations (reinterpretations) of the original Sanathanan-Koerner (SANATHANAN; KOERNER, 1963) and Steiglitz-McBride (STEIGLITZ; MCBRIDE, 1965) iterations (HENDRICKX; DHAENE, 2006), which, in turn, represent transfer functions by means of a ratio between polynomials. Fig. 1 briefly explains the main idea of a generic VF algorithm. As it can be observed, VF algorithms are based on iteratively estimating poles of RBF-based models.

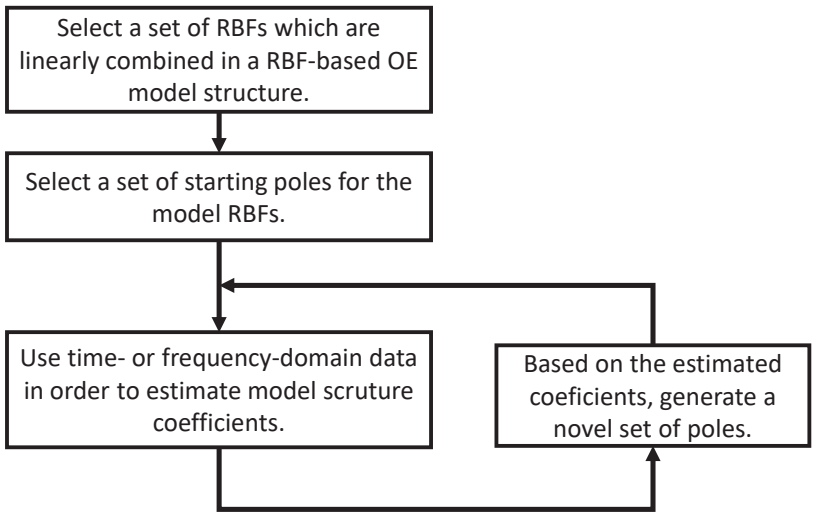

Figure 1 – A generic VF algorithm.

By making use of continuous-time partial fractions as RBFs, VF has been primarily proposed by Gustavsen and Semlyen (GUSTAVSEN; SEMLYEN, 1999; GUSTAVSEN, 2002) in frequency-domain, i.e., for estimating models based on frequency-domain (frequency response) data. Few years later, several modifications and improvements have been incorporated to this standard frequency-domain VF (FD-VF) approach. For instance, by promoting some numerical enhancements for faster convergence (the QR approach) (DESCHRIJVER *et al.*, 2008; KNOCKAERT, 2009) and also the so-called VF relaxation (GUSTAVSEN, 2006), FD-VF has reached the so-called *vectfit3* form, found in (PACKAGE, 2008), which is still one of the most popular implementations of FD-VF.

In (DESCHRIJVER; HAEGEMAN; DHAENE, 2007), the authors have introduced another standard FD-VF algorithm, known as Orthonormal VF, which consists of replacing the original partial fractions with the so-called continuous-time Takenaka-Malmquist orthonormal basis functions (SCHUMACHER; OLIVEIRA, 2018). As mentioned in (DESCHRIJVER; HAEGEMAN; DHAENE, 2007; NOURI; ACHAR; NAKHLA, 2010), improvement in terms of numerical conditioning is considered as one of the benefits of using orthonormal functions as RBFs. In (SCHUMACHER; OLIVEIRA; MITCHELL, 2015), the use of frequency localizing basis functions as RBFs is also studied in the context of FD-VF. Discrete-time counterparts of these FD-VF algorithms can be found, for instance, in (NOURI; ACHAR; NAKHLA, 2010; WONG; LEI, 2008; MEKONNEN; SCHUTT-AINÉ, 2007).

Now, when it comes to system identification based on time-domain data, the continuous-time VF technique introduced by (GRIVET-TALOCIA, 2003) remains as one of the most adopted techniques. However, since time-domain data sets are always in the form of discrete-time samples (meaning that signals are known only at discrete-time instants), practical implementation of such a time-domain VF (TD-VF) method relies on a numerical approximation of convolution integrals (GRIVET-TALOCIA; GUSTAVSEN, 2016; UBOLLI; GUSTAVSEN, 2011; GRIVET-TALOCIA, 2003). In order to cope with this issue, in (SCHUMACHER; OLIVEIRA, 2017) TD-VF has been directly formulated in a discrete time-domain framework whose practical implementation does not rely on

approximating convolution integrals. Such an alternative approach also allows TD-VF to be easily used not only with partial fractions, but also with more general RBF sets, such as discrete-time Takenaka–Malmquist orthonormal basis functions (SCHUMACHER; OLIVEIRA, 2018; HEUBERGER; VAN DEN HOF; WAHLBERG, 2005; VAN DEN HOF; HEUBERGER; BOKOR, 1995).

As discussed in (SCHUMACHER, 2017), both TD-VF and FD-VF algorithms benefit from representing RBF-based OE model structures in a state-space framework. In this sense, Schumacher e Oliveira (2018) propose a unifying method which can be similarly applied for constructing both continuous- and discrete-time RBF sets. In particular, the construction method proposed in (SCHUMACHER; OLIVEIRA, 2018) is designed for finding characterizing matrices of linear RBF state equations, being analytic expressions for the realization of such state-space matrices also developed in this reference. Finally, we also remark that, although VF algorithms are focused on identifying linear time-invariant systems, linear RBF state equations can also be applied in nonlinear system modeling - see, for instance, (SCHUMACHER; LIMA; OLIVEIRA, 2016), where Volterra models based on discrete-time Takenaka–Malmquist orthonormal basis functions are used for behavioral modeling of radio frequency power amplifiers.

1.2 Properties of solutions provided by regular VF implementations

Although regular VF algorithms are worldwide recognized for providing fast and good solutions for system identification problems (and that is actually the main reason for the success of these algorithms) (GRIVET-TALOCIA; GUSTAVSEN, 2016), two key issues still remain unsolved. First, there is no proof of convergence for the VF iterations. When it comes to Fig. 1, this means that estimates for poles and coefficients do not necessarily converge to fixed values. Second, if convergence is indeed achieved, regular VF implementations do not guarantee their converged solutions are local (or the global) optimums of their corresponding nonlinear objective functions (NOFs) (GRIVET-TALOCIA; GUSTAVSEN, 2016). In fact, if data used during estimation are corrupted by colored noise, some recent results on regular VF implementations show they never

converge to any local minimum (SHI, 2016).

In order to effectively overcome the second aforementioned issue, quite recently two instrumental variable (IV)-based VF methods have been proposed: one in time- (SCHUMACHER; OLIVEIRA, 2017) and the other in frequency-domain (SCHUMACHER; OLIVEIRA, 2019). The key advantage of these two IV formulations is that, differently from regular VF implementations, they guarantee that the gradient local optimality condition of their corresponding NOFs are necessarily satisfied after convergence. In other words, converged solutions provided by these IV-based methods are necessarily local (or global) optimums. Moreover, this important result is proved to be independent on the nature of the noise that corrupts the data used during estimation. As a result, more accurate models may be obtained even if this noise is colored. From a practical point of view, the IV formulations in (SCHUMACHER; OLIVEIRA, 2017) and (SCHUMACHER; OLIVEIRA, 2019) can be used to further refine solutions provided by regular VF implementations. Additionally, they can be considered as generalizations of different IV techniques such as those in (VOORHOEVE *et al.*, 2014) and (GILSON; WELSH; GARNIER, 2013).

So far, in this thesis, VF algorithms have been mostly discussed from a generic system identification point of view, meaning applications of these algorithms have been just mentioned, but not detailed. Nonetheless, as highlighted in Section 1.4, two different scopes of application of VF algorithms are focused in this thesis: ringdown response estimation and frequency response estimation.

On the one hand, the idea of frequency response estimation can be directly related to frequency-domain system identification and, more specifically, in this thesis, to FD-VF techniques. On the other hand, since it comprehends a more specific topic within power systems community, the idea of estimating ringdown responses cannot be directly explained in the sense of generic VF algorithms. Therefore, in the following section of this text it is introduced the concept of power system transient (ringdown) analysis as well as how generic VF algorithms have been adapted (modified) to cover this particular scope of application.

1.3 Application of VF to power system transient (ringdown) analysis

Estimation of oscillatory as well as purely exponential dynamics (modes) plays an important role to infer about stability of interconnected power systems (KUNDUR, 1994; CANIZARES *et al.*, 2017). In this context, when a transient (ringdown) event occurs (due to, for instance, a disturbance or a fault), such dynamics are induced in a considerable number of power system signals (power flows, system frequency, etc) (THAMBIRAJAH; BAROCIO; THORNHILL, 2010).

Worldwide, research groups have been expending substantial effort to install entire wide-area monitoring systems (WAMS) in order to collect real-time power system data not only from ringdown events but also from ambient (quasi-stationary) operation. Examples of WAMS based on the so-called Frequency Disturbance Recorders (FDRs) or Phasor Measurement Units (PMUs) are found, for instance, in the Brazilian Interconnected Power (BIP) system (MEDFASEE, 2017) and in the North American Eastern Interconnection (NAEI) system (YE; LIU, 2012; HWANG; LIU, 2014; HWANG; LIU, 2017). In this context, Fig. 2 illustrates the importance of monitoring modes of power systems through ringdown and ambient data. This contrasting scenario shows how tripping of transmission lines or generators may reduce the damping of oscillatory modes, which can in turn lead to a system breakup. In the specific scenario of Fig. 2, as also emphasize Trudnowski *et al.* (2008), 'a mode meter alert during this interval might have allowed system operators to reconfigure the system and perhaps avoid the breakup'.

Both ringdown and ambient data acquired through WAMS encounter their own applications when it comes to estimating power system modes (THAMBIRAJAH; BAROCIO; THORNHILL, 2010). This means estimating methods which process ambient data are usually different from those which deal with ringdown data.

As far as linear methods based on ringdown data are considered, methods can be divided into two groups: time-domain and frequency-domain methods. Time-domain methods such as Prony (HAUER; DEMEURE; SCHARF, 1990) and Matrix Pencil (CROW; SINGH, 2005) consider the roots of characteristic polynomials (or matrices) as modal

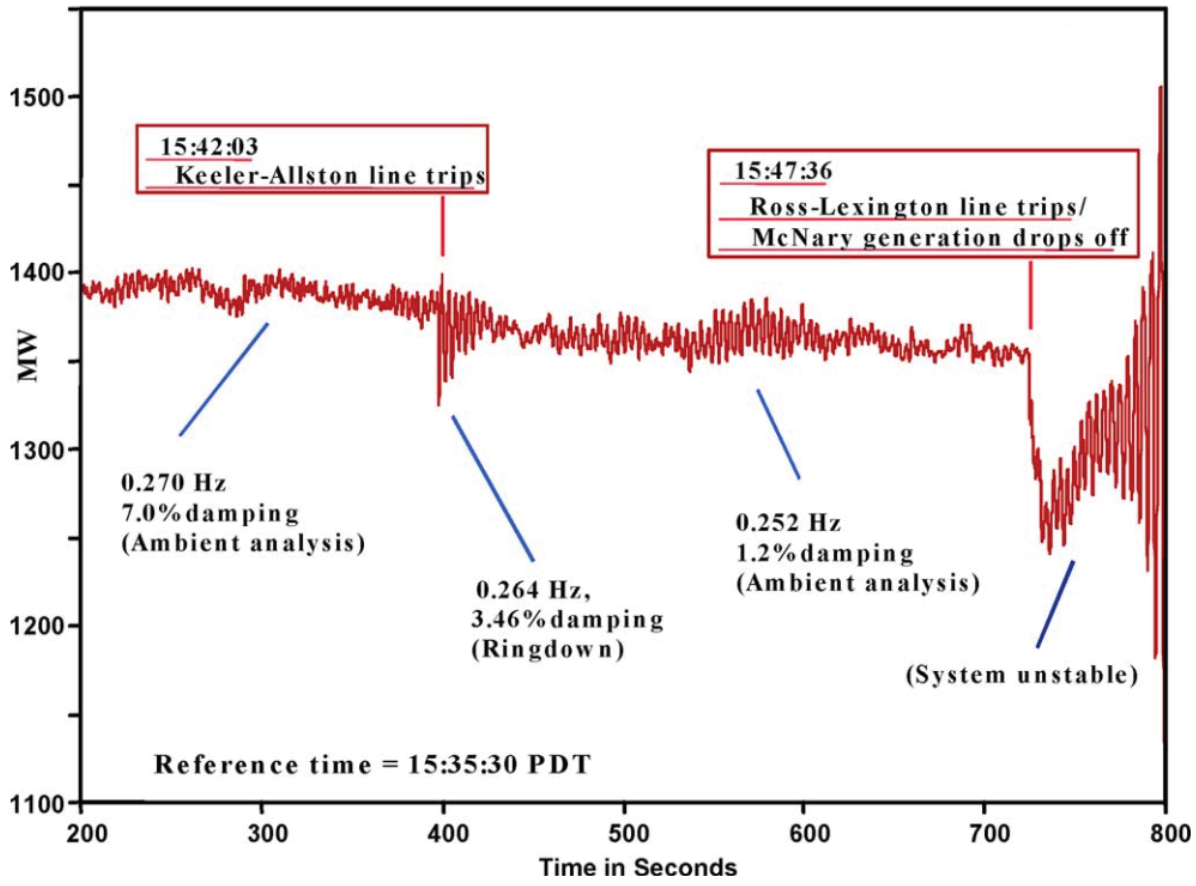

Figure 2 – Power flow on Malin–Round Mountain line of the western North America power system on August 10, 1996.

Source: Trudnowski *et al.* (2008)

estimates. Although widely adopted, these methods may require extensive calculations due to singular value decompositions (GLICKMAN; O'SHEA; LEDWICH, 2007; HAUER; DEMEURE; SCHARF, 1990; HWANG; LIU, 2017). On the other hand, frequency-domain methods may require fewer calculations since they usually generate estimates of oscillatory modes by simply identifying peak frequencies in the DFT of ringdown data sequences. However, since they rely on performing DFTs, frequency-domain techniques may suffer from poor or biased modal estimates due to the well known spectral leakage (windowing) effect. Such a windowing effect is a critical issue especially when ringdown data contain increasing/decreasing dc components. To cope with this issue, recently in (HWANG; LIU, 2017), it has been proposed to remove such dc components by using the difference sequence between two sets of ringdown data.

From a broader perspective, as already discussed in this thesis, regular VF implementations have been first proposed more than a decade ago (GRIVET-TALOCIA, 2003; GUSTAVSEN; SEMLYEN, 1999). However, VF has been only recently adapted for estimating power system modes through ringdown data, in a specific DFT-based setting (PAPADOPOULOS *et al.*, 2016) that reveals the potential of VF for estimation of modal parameters in power systems. Nonetheless, as a 'ringdown frequency-domain Vector Fitting' (RFD-VF) approach, the implementation in (PAPADOPOULOS *et al.*, 2016) naturally suffers from drawbacks which are inherent to DFT computation (poor or biased modal estimates).

Alternatively, the recently proposed 'ringdown time-domain Vector Fitting' (RTD-VF) method (SCHUMACHER; OLIVEIRA; KUIAVA, 2018) proves to be capable of providing superior fitting performance over the worldwide recognized Prony (HAUER; DEMEURE; SCHARF, 1990) and Matrix Pencil (CROW; SINGH, 2005) techniques. In RTD-VF, VF is applied to a suitable time-domain state-space discretization framework which enables ringdown events to be effectively estimated when described as artificial unit impulse responses. When compared with its counterpart RFD-VF approach in (PAPADOPOULOS *et al.*, 2016), the main advantage of RTD-VF lies in the fact that it completely avoids the necessity to perform DFTs. As a consequence, the method can also be naturally applied to ringdown signals with increasing/decreasing dc components, without having to create auxiliary difference sequences (which is an advantage when compared to (HWANG; LIU, 2017)). Nonetheless, although quite robust and effective, there are two problems related to RTD-VF.

The first problem is described in the following. Since it is based on modeling ringdown signals independently, i.e., one at a time, the 'single-signal RTD-VF' method proposed in (SCHUMACHER; OLIVEIRA; KUIAVA, 2018) generates modal estimates that are naturally more related with the particular section of the power system in which the signal under modeling has been measured. In this context, one can expect more realistic estimates for the entire system if multiple signals distributed over different locations are simultaneously used during modal estimation (TRUDNOWSKI; JOHNSON; HAUER,

1999; DOSIEK; PIERRE, 2012; DOSIEK; PIERRE, 2013; KHAZAEI *et al.*, 2016).

Generating a unique set of modal estimates based on multiple data channels (obtained, for instance, from Phasor Measurement Units or Frequency Disturbance Recorders) is of major importance. In (TRUDNOWSKI; JOHNSON; HAUER, 1999), it has been shown Prony analysis based on multiple ringdown signals improves accuracy of modal estimates and, in addition, simplifies the analysis from a user's perspective, since the operator is not left with the problem of determining which set of estimates is more accurate. Recently, in (KONTIS *et al.*, 2018a), an average energy approach based on references (NING; SARMADI; VENKATASUBRAMANIAN, 2015; NING; PAN; VENKATASUBRAMANIAN, 2013) has been used for extending single-signal techniques such as Matrix Pencil (CROW; SINGH, 2005) and Eigenvalue Realization Algorithm (JUANG; PAPPA, 1985) to multi-signal analysis. In (PATERNINA *et al.*, 2019), such an average energy approach is also applied for estimating electromechanical modes based on variational mode decomposition. In (MESSINA; VITTAL, 2007), empirical mode decomposition is used, and in (LI *et al.*, 2018) a multichannel wavelet transform approach is proposed. In (DOSIEK; PIERRE, 2012; DOSIEK; PIERRE, 2013), multi-signal methods are also shown to provide promising results when applied to ambient data. Moreover, techniques based on processing multiple power system signals simultaneously also encounter applications in areas such as, for instance, measurement-based dynamic load modeling (KONTIS *et al.*, 2018b; STOJANOVIĆ; KORUNOVIĆ; MILANOVIĆ, 2008; RENMU; JIN; HILL, 2006; CHOI *et al.*, 2006), coherency identification in multi-machine power systems (BAROCIO *et al.*, 2015; SUSUKI; MEZIC, 2011), steady state model synthesis of power systems (MAHMOOD *et al.*, 2017) and identification of 'dominant inter-area oscillation paths' (CHOMPOOBUTRGOOL; VANFRETTI, 2013).

The second problem related to standard RTD-VF comes from the fact that it can be considered as a regular VF implementation, meaning its converged solutions are not necessarily local (or the global) optimums of their corresponding NOFs (SCHUMACHER; OLIVEIRA, 2017; GRIVET-TALOCIA; GUSTAVSEN, 2016; SHI, 2016). At this point, as discussed in Section 1.2, we remember IV-based VF approaches such as the generic

discrete time-domain method in (SCHUMACHER; OLIVEIRA, 2017) indeed guarantees that local optimums are obtained after algorithm convergence.

1.4 Objectives and contributions of this thesis

This thesis addresses the problem of formulating VF algorithms for both time- and frequency-domain system identification. When it comes to time-domain, VF algorithms are developed within a ringdown context, so that oscillatory (as well as purely exponential) dynamics of power systems can be effectively estimated through transient data sets extracted from these systems. When it comes to frequency-domain, this thesis presents a unifying FD-VF method which can be similarly applied for estimating models formed either by continuous- or discrete-time RBFs. Numerical examples for validating such a FD-VF approach focus mainly on frequency response data extracted from power and inductive potential transformers. IV-based VF formulations which are proved to guarantee local optimums after algorithm convergence are also intensively investigated throughout this thesis.

In what follows, we synthesize the two objectives of this work.

O.1 The first objective consists of presenting, from an objective function perspective, the single-signal RTD-VF method proposed in (SCHUMACHER; OLIVEIRA; KUIAVA, 2018), which can be considered as a natural extension of the regular TD-VF technique (GRIVET-TALOCIA, 2003) to the context of ringdown analysis. In particular, it is shown such a method is capable of providing superior fitting performance over recognized techniques, such as Prony (HAUER; DEMEURE; SCHARF, 1990) and Matrix Pencil (CROW; SINGH, 2005), as well as over its counterpart RFD-VF method previously proposed in (PAPADOPOULOS *et al.*, 2016). Subsequently, single-signal RTD-VF is generalized into the multi-signal RTD-VF approach recently proposed in (SCHUMACHER; OLIVEIRA; KUIAVA, 2019), which is capable of generating modal estimates by simultaneously processing multiple ringdown signals possibly distributed over different locations of a power system. Finally, it is presented

the IV version of multi-signal RTD-VF, which is proved to guarantee local optimums after algorithm convergence. Such a 'multi-signal IV-RTD-VF' method has also been proposed in (SCHUMACHER; OLIVEIRA; KUIAVA, 2019) and is used for further refining solutions provided by regular multi-signal RTD-VF. It should also be mentioned that multi-signal IV-RTD-VF can be regarded as a ringdown version of the generic discrete time-domain IV-based approach in (SCHUMACHER; OLIVEIRA, 2017).

O.2 The second objective of this work consists of presenting, based on a unifying FD-VF approach, the IV-based FD-VF method proposed in (SCHUMACHER; OLIVEIRA, 2019), which is also proved to guarantee local optimums after algorithm convergence. In fact, the IV-based FD-VF method proposed in this chapter consists of a multi-input multi-output (MIMO) generalization of the single-input single-output (SISO) approach in (SCHUMACHER; OLIVEIRA, 2019). The terminology 'unifying' is used to emphasize that such an IV-FD-VF method can be similarly applied for estimating models formed either by continuous- or discrete-time RBFs, being compatible, for instance, with any RBF set listed in (SCHUMACHER; OLIVEIRA, 2018). As will be shown, IV-FD-VF may provide superior fitting performance when compared to standard FD-VF algorithms such as, for instance, *vectfit3* (PACKAGE, 2008), which is still one of the most popular implementations of standard FD-VF.

1.5 Thesis organization

The remainder chapters of this thesis are organized as follows.

Chapter 2: Estimation of power system oscillations through ringdown data

In this chapter it is addressed the problem of formulating VF algorithms which are capable of estimating, based on transient (ringdown) data, oscillatory (as well as purely exponential) dynamics (modes) of power system signals. In this sense, all points listed as objective **O.1** are addressed in this chapter of the thesis.

Numerical examples presented in Chapter 2 focus on actual ringdown data sets extracted from NAEI and BIP systems.

Chapter 3: Frequency-domain system identification

In this chapter it is addressed the problem of formulating VF algorithms for system identification based on frequency-domain data. In this sense, all points listed as objective **O.2** are addressed in this chapter of the thesis.

Numerical examples presented in Chapter 3 focus on frequency response data extracted from actual power and inductive potential transformers.

Chapter 4: Conclusions

This chapter addresses the conclusions of this work.

2 ESTIMATION OF POWER SYSTEM OSCILLATIONS THROUGH RINGDOWN DATA

In this chapter, we address the problem of formulating VF algorithms which are capable of estimating, based on transient (ringdown) data, oscillatory (as well as purely exponential) components of power system signals.

Firstly, based on fundamentals for single-signal modeling, it is presented – from an objective function perspective – the 'single-signal ringdown time-domain Vector Fitting' (RTD-VF) method proposed in (SCHUMACHER; OLIVEIRA; KUIAVA, 2018), which can be considered as a natural extension of the regular TD-VF technique (GRIVET-TALOCIA, 2003) to the context of ringdown analysis. In particular, it is shown such a method is capable of providing superior fitting performance over recognized techniques, such as Prony (HAUER; DEMEURE; SCHARF, 1990) and Matrix Pencil (CROW; SINGH, 2005), as well as over its counterpart 'ringdown *frequency*-domain Vector Fitting' (RFD-VF) method previously proposed in (PAPADOPOULOS *et al.*, 2016). Subsequently, single-signal RTD-VF is generalized into the multi-signal RTD-VF approach proposed in (SCHUMACHER; OLIVEIRA; KUIAVA, 2019), which is capable of generating modal estimates by simultaneously processing multiple ringdown signals possibly distributed over different locations of a power system. Finally, it is presented the IV version of multi-signal RTD-VF, which is proved to guarantee local optimums after algorithm convergence. Such a 'multi-signal IV-RTD-VF' method has also been proposed in (SCHUMACHER; OLIVEIRA; KUIAVA, 2019) and is used for further refining solutions provided by regular multi-signal RTD-VF.

2.1 Single-signal modeling: Fundamentals

Oscillatory as well as purely exponential dynamics (modes) are induced in power system signals (power flows, system frequency, etc) when transient (ringdown) events occur. Such a phenomenon is exemplified through Fig. 3, which depicts a ringdown event occurred during a reconnection of Itaipu Hydroelectric to the Brazilian Interconnected

Power (BIP) system. Itaipu Hydroelectric was disconnected from the rest of the BIP system on September 02, 2011, at 19h43m40.3s UTC, due to an electrical bushing explosion (ONS, 2011). It was reconnected to the BIP system 27m49.7s later (ONS, 2011).

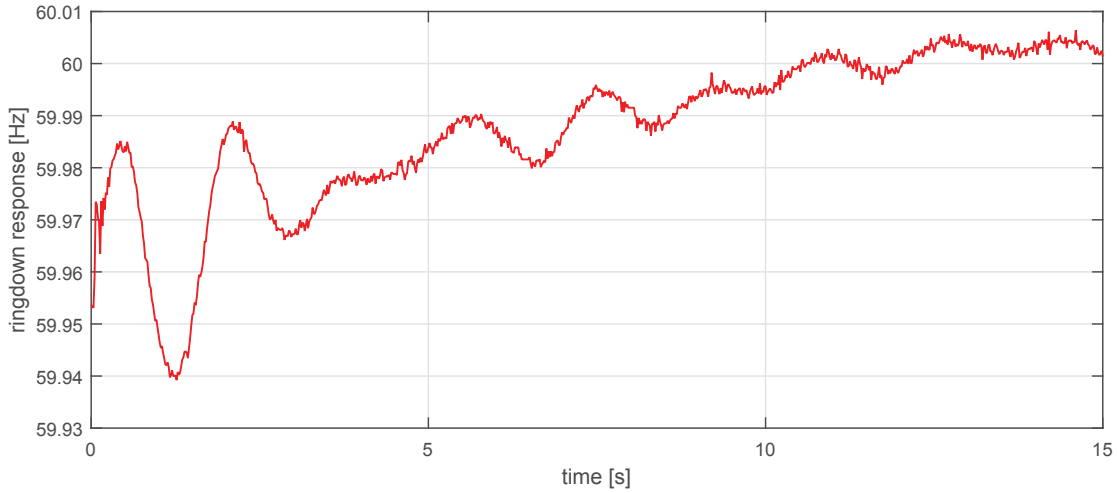

Figure 3 – Example of a typical ringdown response. Measurements (which are composed of 901 samples, from time 19h43m40.3s UTC to 19h43m55.3s UTC) represent system frequency and have been recorded (with a sampling period of (1/60)s) by a frequency disturbance recorder (FDR) installed within Federal University of Santa Catarina (MEDFASEE, 2017).

As suggests Fig. 3, one can assume a generic ringdown response $y(t)$ to have a starting time $t = 0$. As discussed in (SCHUMACHER; OLIVEIRA; KUIAVA, 2018), approximating $y(t)$ for $t \geq 0$ is possible by means of a modeling signal structure $\bar{y}(t)$ which can be assumed to contain not only oscillatory and purely exponential modes, but also a *dc* component h_{dc}:

$$\bar{y}(t) = h_{\mathrm{dc}} + \sum_{l=1}^{M_{\mathrm{OSC}}} A_l \mathrm{e}^{\sigma_l t} \cos(\omega_l t + \varphi_l) + \sum_{l=M_{\mathrm{OSC}}+1}^{M} A_l \mathrm{e}^{\sigma_l t}. \tag{2.1}$$

As it can be observed in equation (2.1), $\bar{y}(t)$ has M_{OSC} oscillatory modes and $M - M_{\mathrm{OSC}}$ purely exponential modes (where M denotes the total number of modes). Each l-th oscillatory mode ($l = 1, \cdots, M_{\mathrm{OSC}}$) is composed of its amplitude A_l, attenuation σ_l, frequency $\omega_l = 2\pi f_l$ and phase φ_l. On the other hand, each l-th purely exponential mode ($l = M_{\mathrm{OSC}} + 1, \cdots, M$) naturally has only an amplitude A_l and an attenuation σ_l.

In this chapter, we deal with the system identification problem of estimating modal parameters of (2.1)-type structures based on a set of K time-domain data samples for

$y(t)$. Since ringdown signal $y(t)$ has been considered to have a starting time $t = 0$, one can assume it has been measured over the following set of discrete-time instants:

$$t = kT, \quad k = 0, \cdots, K-1, \tag{2.2}$$

where T denotes the sampling period used during data acquisition. Ringdown data sets available for modal estimation are then formed by the set of measurements

$$y(kT), \quad k = 0, \cdots, K-1. \tag{2.3}$$

As suggests example from Fig. 3, at least in real case scenarios, ringdown data sets are contaminated by measurement noise, which may affect significantly performance of system identification approaches.

Generating modal estimates for (2.1)-type structures plays an important role to infer about stability of interconnected power systems (KUNDUR, 1994; CANIZARES *et al.*, 2017). From (2.1), one can observe $\bar{y}(t)$ approaches h_{dc} as $t \to \infty$, given that $\sigma_l < 0 \; \forall \; l$. Meanwhile, $\bar{y}(t)$ becomes unbounded for sufficient large values of t if, for any l, we have $\sigma_l > 0$. In principle, the most basic idea of stability monitoring is then to evaluate how close (or how far) σ_l values are from becoming positive.

In a deeper analysis, however, stability monitoring is performed in terms of eigenvalue analysis, being the eigenvalues of $\bar{y}(t)$ in (2.1) defined by[1]

$$\lambda_l = \begin{cases} \sigma_l + j\omega_l & , \quad l = 1, \cdots, M_{\mathrm{OSC}} \\ \sigma_l & , \quad l = M_{\mathrm{OSC}} + 1, \cdots, M \end{cases} \tag{2.4}$$

where $j = \sqrt{-1}$. From (2.4), it becomes clear stability monitoring can also be performed by analyzing eigenvalues in the complex plane, where its stability region is defined by all values of λ_l which satisfy $\Re\mathrm{e}(\lambda_l) = \sigma_l < 0$. From a practical point of view, it is

[1] Eigenvalues are usually related to matrices. Nonetheless, we consider that the λ_l values defined in (2.4) correspond to the eigenvalues of equation (2.1) since it is also possible to express this equation by means of a state-space representation in which the state matrix has eigenvalues $\sigma_l \pm j\omega_l$, $l = 1, \cdots, M_{\mathrm{OSC}}$, and σ_l, $l = M_{\mathrm{OSC}} + 1, \cdots, M$.

well known complex-valued eigenvalues with lower frequencies may be related to poorly-damped oscillations in electromechanical variables (rotor angle from synchronous machines, voltages, etc) of the power system from which ringdown signal $y(t)$ has been measured (WADDUWAGE; ANNAKKAGE; NARENDRA, 2015). In this context, as explained in (WADDUWAGE; ANNAKKAGE; NARENDRA, 2015), unacceptable damping for such low-frequency complex-valued eigenvalues (which are also called electromechanical modes and usually present frequencies within a frequency range from 0.2Hz up to 3Hz) may indicate that the power system is operating close to instability (collapse).

Direct estimation of modal parameters in equation (2.1) is difficult since they are nonlinearly related to each other. However, by means of the unit impulse function $\delta(t)$, one can alternatively express such an equation by the following partial fraction expansion (see Section 2.9.1 for the derivation of this equation):

$$\bar{y}(t) = h_{\text{dc}} + \sum_{i=1}^{N} \frac{r_i}{\rho - p_i}\delta(t), \tag{2.5}$$

where

$$p_i = \begin{cases} \lambda_{\frac{i+1}{2}} & , \quad i = 1, 3, \cdots, 2M_{\text{OSC}} - 1 \\ (p_{i-1})^* & , \quad i = 2, 4, \cdots, 2M_{\text{OSC}} \\ \lambda_{i-M_{\text{OSC}}} & , \quad i = 2M_{\text{OSC}} + 1, 2M_{\text{OSC}} + 2, \cdots, N \end{cases} \tag{2.6}$$

$$r_i = \begin{cases} \frac{1}{2}A_{\frac{i+1}{2}}\mathrm{e}^{j\varphi_{\frac{i+1}{2}}} & , \quad i = 1, 3, \cdots, 2M_{\text{OSC}} - 1 \\ (r_{i-1})^* & , \quad i = 2, 4, \cdots, 2M_{\text{OSC}} \\ A_{i-M_{\text{OSC}}} & , \quad i = 2M_{\text{OSC}} + 1, 2M_{\text{OSC}} + 2, \cdots, N \end{cases} \tag{2.7}$$

$$N = M + M_{\text{osc}} \tag{2.8}$$

and $(\cdot)^*$ denotes conjugate. It is important to observe that, by means of equations (2.6) and (2.7), modal parameters in (2.1) are directly related with the partial fractions' residues $\{r_i\}$ and poles $\{p_i\}$ in (2.5). In this sense, each oscillatory mode in (2.1) is represented by two complementary partial fractions in (2.5). It is also important to remark ρ denotes the

so-called differentiation operator, which makes any pair of generic functions $G(\rho)$ and $x(t)$ to satisfy

$$G(\rho)x(t) = \mathcal{L}^{-1}\left\{G(s)X(s)\right\}, \tag{2.9}$$

where $X(s)$ represents the Laplace transform of $x(t)$, whereas $\mathcal{L}^{-1}\{\cdot\}$ represents the inverse Laplace transform operator.

Based on representation (2.5), one can indirectly estimate oscillatory and purely exponential components of a generic ringdown signal $y(t)$ by formulating the least-squares problem

$$\begin{aligned} \hat{\gamma} &= \arg\min_{\gamma} \sum_{k=0}^{K-1} \left(y(kT) - \bar{y}(kT)\right)^2, \\ &= \arg\min_{\gamma} \sum_{k=0}^{K-1} \left(y(kT) - \left(h_{\mathrm{dc}} + \sum_{i=1}^{N} \frac{r_i}{\rho - p_i}\delta(kT)\right)\right)^2, \end{aligned} \tag{2.10}$$

where $\hat{\gamma}$ represents an estimate for parameter vector

$$\gamma = \left[\begin{array}{ccccccc} h_{\mathrm{dc}} & r_1 & \cdots & r_N & p_1 & \cdots & p_N \end{array}\right]^{\mathrm{T}}, \tag{2.11}$$

with $(\cdot)^{\mathrm{T}}$ being the transpose operator.

Estimating γ via (2.10) constitutes a *nonlinear* optimization problem, once poles $\{p_i\}$ appear in the denominator of $\bar{y}(t)$. In this sense, one can observe that, if poles $\{p_i\}$ are assumed to be known beforehand, (2.10) reduces itself to a *linear* least-squares problem, since only coefficients $\{r_i\}$ and h_{dc} remain unknown. Unfortunately, prior knowledge about these poles is usually not available.

In what follows, we address the problem of estimating all parameters in γ (including poles $\{p_i\}$) by means of the 'single-signal ringdown time-domain Vector Fitting' (single-signal RTD-VF) method proposed in (SCHUMACHER; OLIVEIRA; KUIAVA, 2018). As a VF approach, single-signal RTD-VF is based on transforming the nonlinear least-squares problem in (2.10) into a sequence of *linear* least-squares problems where coefficient sets are estimated via pre-specified update-dependent poles.

2.2 Single-signal RTD-VF

VF approaches estimate pole sets by means of alternative OE model structures (SCHUMACHER; OLIVEIRA, 2017; GRIVET-TALOCIA; GUSTAVSEN, 2016; DESCHRIJVER; HAEGEMAN; DHAENE, 2007). When it comes to the ringdown context introduced in Section 2.1 of this thesis, one can use the two auxiliary transfer functions in equations (2.13) and (2.14) in order to define the alternative structure shown in equation (2.12).

$$\begin{aligned} \hat{y}(t) &= h_{\mathrm{dc}} + \frac{B(\rho)}{F(\rho)}\delta(t), \\ &= h_{\mathrm{dc}} + \frac{\displaystyle\sum_{i=1}^{N} \frac{c_i}{\rho - \bar{p}_i}}{1 + \displaystyle\sum_{i=1}^{N} \frac{d_i}{\rho - \bar{p}_i}}\delta(t); \end{aligned} \tag{2.12}$$

$$\frac{B(\rho)}{\hat{F}(\rho)} = \sum_{i=1}^{N} \frac{c_i}{\rho - \bar{p}_i}; \tag{2.13}$$

$$\frac{F(\rho)}{\hat{F}(\rho)} = 1 + \sum_{i=1}^{N} \frac{d_i}{\rho - \bar{p}_i}; \tag{2.14}$$

where $\{\bar{p}_i\}$ is assumed to be a set of pre-specified (known) poles. In these equations, $\hat{F}(\rho)$ denotes the known monic polynomial whose roots are $\{\bar{p}_i\}$, i.e.,

$$\hat{F}(\rho) = (\rho - \bar{p}_1)(\rho - \bar{p}_2)\cdots(\rho - \bar{p}_N). \tag{2.15}$$

Meanwhile, $B(\rho)$ and $F(\rho)$ denote polynomials whose roots are, respectively, the zeros of (2.13) and (2.14).

Now, by defining parameter vector

$$\theta = \begin{bmatrix} h_{\mathrm{dc}} & c_1 & \cdots & c_N & d_1 & \cdots & d_N \end{bmatrix}^{\mathrm{T}}, \tag{2.16}$$

the following objective function can be formulated:

$$J(\theta) = \sum_{k=0}^{K-1} e^2(kT), \tag{2.17}$$

where $e(kT)$ is the scalar error

$$e(kT) = y(kT) - \hat{y}(kT) \tag{2.18}$$

that, based on equation (2.12), also reads

$$e(kT) = \frac{F(\rho)}{F(\rho)} y(kT) - \left(h_{\text{dc}} + \frac{B(\rho)}{F(\rho)} \delta(kT) \right). \tag{2.19}$$

As a VF approach (GRIVET-TALOCIA; GUSTAVSEN, 2016), one can consider approximation $e(kT) \approx \tilde{e}(kT)$, where

$$\begin{aligned} \tilde{e}(kT) &= \frac{F(\rho)}{\hat{F}(\rho)} y(kT) - \left(h_{\text{dc}} + \frac{B(\rho)}{\hat{F}(\rho)} \delta(kT) \right) && (2.20) \\ &= \left(1 + \sum_{i=1}^{N} \frac{d_i}{\rho - \bar{p}_i} \right) y(kT) - \left(h_{\text{dc}} + \sum_{i=1}^{N} \frac{c_i}{\rho - \bar{p}_i} \delta(kT) \right) && (2.21) \end{aligned}$$

or, equivalently,

$$\tilde{e}(kT) = y(kT) - \mathbf{m}^{\text{T}}(kT)\theta, \tag{2.22}$$

being

$$\mathbf{m}(kT) = \begin{bmatrix} 1 & \tilde{\mathbf{u}}^{\text{T}}(kT) & -\tilde{\mathbf{y}}^{\text{T}}(kT) \end{bmatrix}^{\text{T}}; \tag{2.23}$$

$$\tilde{\mathbf{y}}(kT) = \begin{bmatrix} \frac{1}{\rho - \bar{p}_i} & \cdots & \frac{1}{\rho - \bar{p}_N} \end{bmatrix}^{\text{T}} y(kT); \tag{2.24}$$

$$\tilde{\mathbf{u}}(kT) = \begin{bmatrix} \frac{1}{\rho - \bar{p}_i} & \cdots & \frac{1}{\rho - \bar{p}_N} \end{bmatrix}^{\text{T}} \delta(kT). \tag{2.25}$$

By approximating $e(kT)$ by $\tilde{e}(kT)$ in equation (2.17), the *nonlinear* problem of minimizing objective function $J(\theta)$ (in terms of θ) is transformed into an approximated but *linearized* least-squares problem whose solution can be written as follows

$$\hat{\theta} = \arg\min_{\theta} \sum_{k=0}^{K-1} \tilde{e}^2(kT) \tag{2.26}$$

$$= \arg\min_{\theta} \sum_{k=0}^{K-1} \Big(y(kT) - \mathbf{m}^{\mathrm{T}}(kT)\theta\Big)^2 \tag{2.27}$$

$$= \Big[\mathbf{M}^{\mathrm{T}}\mathbf{M}\Big]^{-1}\mathbf{M}^{\mathrm{T}}\mathbf{y}, \tag{2.28}$$

where $\hat{\theta}$ can be considered as an estimate for $\theta^\star$ obtained for a given set of pre-specified poles $\{\bar{p}_i\}$, being $\theta^\star$ the global minimum of $J(\theta)$. In (2.28), matrices $\mathbf{M}$ and $\mathbf{y}$ are defined as follows

$$\mathbf{M} = \left[\begin{array}{cc} \widetilde{\mathbf{U}} & -\widetilde{\mathbf{Y}} \end{array}\right]; \tag{2.29}$$

$$\mathbf{y} = \left[\begin{array}{ccc} y[0] & \cdots & y[K-1] \end{array}\right]^{\mathrm{T}}; \tag{2.30}$$

where

$$\widetilde{\mathbf{Y}} = \left[\begin{array}{ccc} \tilde{\mathbf{y}}[0] & \cdots & \tilde{\mathbf{y}}[K-1] \end{array}\right]^{\mathrm{T}}; \tag{2.31}$$

$$\widetilde{\mathbf{U}} = \left[\begin{array}{ccc} 1 & \cdots & 1 \\ \tilde{\mathbf{u}}[0] & \cdots & \tilde{\mathbf{u}}[K-1] \end{array}\right]^{\mathrm{T}}. \tag{2.32}$$

Throughout this thesis, we may sometimes use terminology $x(kT) = x[k]$ to simplify notation.

Once θ has been estimated via (2.28), one can try to make the approximate error $\tilde{e}(kT)$ in (2.20) closer to the original error $e(kT)$ in (2.19) by considering the obtained polynomial $F(\rho)$ as a possibly more refined estimate for polynomial $\hat{F}(\rho)$. In terms of roots, this means that roots of $F(\rho)$, which can be determined based on the estimated coefficients $\{d_i\}$ in θ (see equation (2.14)), are to be considered as a more refined estimate for the N pre-specified poles $\bar{p}_1, \cdots, \bar{p}_N$. Based on this novel set of poles $\{\bar{p}_i\}$, one can reestimate θ via (2.28).

This procedure can be repeated (iterated) until $\hat{\theta}$ and $\{\bar{p}_i\}$ converge to fixed values $\hat{\theta}'$ and $\{\bar{p}'_i\}$. When convergence is achieved, it naturally follows that $F'(\rho) = \hat{F}'(\rho)$, where $F'(\rho)$ and $\hat{F}'(\rho)$ denote the values obtained for polynomials $F(\rho)$ and $\hat{F}(\rho)$ when $\bar{p}_i = \bar{p}'_i$ and $\hat{\theta} = \hat{\theta}'$. Consequently, the alternative modeling structure $\hat{y}(t)$ in (2.12) obtained after algorithm convergence fits exactly into the desired signal structure in (2.5):

$$\begin{aligned} \hat{y}'(t) &= h'_{\text{dc}} + \frac{B'(\rho)}{F'(\rho)}\delta(t) \\ &= h'_{\text{dc}} + \frac{B'(\rho)}{\hat{F}'(\rho)}\delta(t) \\ &= h'_{\text{dc}} + \sum_{i=1}^{N} \frac{c'_i}{\rho - \bar{p}'_i}\delta(t) \end{aligned} \tag{2.33}$$

Expression (2.33) reveals h'_{dc}, $c'_1, \cdots, c'_N$ and $\bar{p}'_1, \cdots, \bar{p}'_N$ are our final estimates for h_{dc}, $r_1, \cdots, r_N$ and $p_1, \cdots, p_N$. Since $F'(\rho) = \hat{F}'(\rho)$, one can observe that, at convergence, equation (2.14) becomes

$$\frac{F'(\rho)}{\hat{F}'(\rho)} = 1 + \sum_{i=1}^{N} \frac{d'_i}{\rho - \bar{p}'_i} \tag{2.34}$$

$$= 1. \tag{2.35}$$

This means that the converged coefficients $\{d'_i\}$ no longer affect the resulting modeling signal $\hat{y}'(t)$, as shown in (2.33).

2.2.1 Step by step procedure for implementing single-signal RTD-VF

Step 1. Given a ringdown response $y(t)$ sampled at $t = kT$, with $k = 0, \cdots, K-1$, one must define the number of iterations and a set of starting poles $\{\bar{p}_i\}$, $i = 1, \cdots, N$.

Comment: As emphasized in (SCHUMACHER; OLIVEIRA; KUIAVA, 2018; GRIVET-TALOCIA; GUSTAVSEN, 2016), starting poles can be chosen as weakly attenuated complex conjugate pairs (for instance, with $\Re\text{e}(\bar{p}_i) = -0.01 \times |\Im\text{m}(\bar{p}_i)|$) with imaginary parts linearly distributed over a frequency band of interest $[0, \omega_{\text{max}}]$. Since electromechanical modes in power systems usually have an imaginary part which is not

higher than 3 Hz, one can simply define staring poles as follows:

$$\bar{p}_i = \begin{cases} \bar{p}_{i+1}^* & , \quad i = 1, 3, \cdots, N-1 \\ i(-0.01 + j)\omega_{\max}/N & , \quad i = 2, 4, \cdots, N \end{cases} \tag{2.36}$$

where $\omega_{\max} = 2\pi \times 3$. If N is an odd number, then one can additionally define $\bar{p}_N = \Re\mathrm{e}(\bar{p}_{N-1})$, meaning $\bar{p}_N$ is not defined without occurrence of its corresponding conjugate.

Step 2. Construct matrices $\mathbf{M}$ and $\mathbf{y}$ based on (2.29)–(2.32). In these equations, vectors $\tilde{\mathbf{y}}[k]$ and $\tilde{\mathbf{u}}[k]$ can be approximated, for $k = 1, \cdots, K-1$, by recursive use of the following state-space discretizations of equations (2.24) and (2.25) (see Section 2.9.2 for the derivation):

$$\tilde{\mathbf{y}}[k] \approx \mathbf{A}_\mathrm{d}\tilde{\mathbf{y}}[k-1] + \mathbf{B}_\mathrm{d} y[k-1], \quad \tilde{\mathbf{y}}[0] = \mathbf{0} \tag{2.37}$$

$$\tilde{\mathbf{u}}[k] \approx \mathbf{A}_\mathrm{d}\tilde{\mathbf{u}}[k-1], \quad \tilde{\mathbf{u}}[0] = \mathbf{B} \tag{2.38}$$

where

$$\mathbf{A}_\mathrm{d} = \mathrm{e}^{\mathbf{A}T}; \quad \mathbf{B}_\mathrm{d} = \mathbf{A}^{-1}(\mathbf{A}_\mathrm{d} - \mathbf{I})\mathbf{B} \tag{2.39}$$

$$\mathbf{A} = \begin{bmatrix} \bar{p}_1 & 0 & \cdots & 0 \\ 0 & \bar{p}_2 & \cdots & 0 \\ \vdots & \vdots & \ddots & \vdots \\ 0 & 0 & \cdots & \bar{p}_N \end{bmatrix}; \quad \mathbf{B} = \begin{bmatrix} 1 \\ 1 \\ \vdots \\ 1 \end{bmatrix}_{N\times 1} \tag{2.40}$$

and $\mathbf{I}$ denotes the $N \times N$ identity matrix.

Step 3. Obtain a least-squares estimate for parameter vector θ via (2.28).

Comment: As shown in (GRIVET-TALOCIA; GUSTAVSEN, 2016; SCHUMACHER; OLIVEIRA; KUIAVA, 2018), it is possible to ensure that the partial fraction residues c_i and c_{i+1} are always estimated in perfect conjugate pairs ($c_{i+1} = c_i^*$) whenever $\bar{p}_{i+1} = \bar{p}_i^*$.

As evidenced in equation (2.41), if $\bar{p}_i$ and $\bar{p}_{i+1}$ constitute a complex conjugate pair, then the corresponding basic partial fractions $1/(s-\bar{p}_i)$ and $1/(s-\bar{p}_i^*)$ in (2.12) can be substituted by $(1/(s-\bar{p}_i)+1/(s-\bar{p}_i^*))$ and $(j/(s-\bar{p}_i)-j/(s-\bar{p}_i^*))$, respectively. In the corresponding state-space representation, this modification is implemented by simply replacing submatrices

$$\begin{bmatrix} \bar{p}_i & 0 \\ 0 & \bar{p}_{i+1} \end{bmatrix} \quad \text{and} \quad \begin{bmatrix} 1 \\ 1 \end{bmatrix}$$

within matrices $\mathbf{A}$ and $\mathbf{B}$ in (2.40) by, respectively,

$$\begin{bmatrix} \Re\mathrm{e}(\bar{p}_i) & \Im\mathrm{m}(\bar{p}_i) \\ -\Im\mathrm{m}(\bar{p}_i) & \Re\mathrm{e}(\bar{p}_i) \end{bmatrix} \quad \text{and} \quad \begin{bmatrix} 2 \\ 0 \end{bmatrix}.$$

Such a substitution can be regarded as a modal transformation (CHEN, 1999) and it is also performed in classical frequency-domain VF (GUSTAVSEN; SEMLYEN, 1999). As it can be observed through equation (2.41), it has the effect that the corresponding residues in the solution vector θ become equal to $\Re\mathrm{e}(c_i)$ and $\Im\mathrm{m}(c_i)$.

$$\begin{bmatrix} \dfrac{1}{s-\bar{p}_i} & \dfrac{1}{s-\bar{p}_i^*} \end{bmatrix} \begin{bmatrix} c_i \\ c_i^* \end{bmatrix} = \begin{bmatrix} \dfrac{1}{s-\bar{p}_i}+\dfrac{1}{s-\bar{p}_i^*} & \dfrac{j}{s-\bar{p}_i}-\dfrac{j}{s-\bar{p}_i^*} \end{bmatrix} \begin{bmatrix} \Re\mathrm{e}(c_i) \\ \Im\mathrm{m}(c_i) \end{bmatrix}. \tag{2.41}$$

Step 4. Update $\{\bar{p}_i\}$ with the roots of polynomial $F(\rho)$.

Comment: Since the roots of polynomial $F(\rho)$ naturally equal the zeros of transfer function $F(\rho)/\hat{F}(\rho)$, defined in (2.14), one can update $\{\bar{p}_i\}$ by calculating the eigenvalues of matrix $(\mathbf{A}-\mathbf{B}\mathbf{D}^{-1}\mathbf{C})$ (see (GRIVET-TALOCIA; GUSTAVSEN, 2016) for a proof), with $(\mathbf{A},\mathbf{B},\mathbf{C},\mathbf{D})$ being the state-space realization for $F(\rho)/\hat{F}(\rho)$ in which $\mathbf{A}$ and $\mathbf{B}$ satisfy (2.40) while

$$\mathbf{C} = \begin{bmatrix} d_1 & \cdots & d_n \end{bmatrix} \quad \text{and} \quad \mathbf{D} = 1. \tag{2.42}$$

To ensure model stability, a usual practice in continuous-time VF implementations (GRIVET-TALOCIA; GUSTAVSEN, 2016) is the one which consists of inverting the sign of poles with positive real parts if they occur while adopting

$$\{\bar{p}_i\} \leftarrow \text{eig}\left(\mathbf{A} - \mathbf{B}\mathbf{D}^{-1}\mathbf{C}\right). \tag{2.43}$$

It is also interesting to remark that, if the modal transformation commented in **Step 3** has been applied to a pole set $\{\bar{p}_i\}$ formed only by real-valued numbers and complex conjugate pairs, then $\mathbf{A}$, $\mathbf{B}$ and consequently θ are real-valued, meaning (2.43) returns a novel pole set which is also formed only by real-valued numbers and complex conjugate pairs.

Comment: Throughout iterations, we might also want to observe how our current set of poles $\{\bar{p}_i\}$ performs in structure (2.5). In this case, its coefficients $\{r_i\}$ can be estimated in the linear least-squares sense via (2.28) by simply redefining $\mathbf{M} = \widetilde{\mathbf{U}}$. In this context, the associated root mean square (RMS) error of modeling signal $\bar{y}(t)$ is a metric which can be observed, being its definition given as follows

$$\text{RMS error} = \sqrt{\frac{1}{K}\sum_{k=0}^{K-1}\left(y[k] - \bar{y}[k]\right)^2}. \tag{2.44}$$

Step 5. Repeat steps 2 to 4 until the number of iterations is achieved.

Step 6. The resulting modal components of the estimated ringdown signal $\bar{y}(t)$ are obtained through relations described in (2.6) and (2.7).

Comment: It is straightforward to reorganize partial fractions' real and complex conjugate poles (and their corresponding residues) in case they do not come directly organized in the order presumed by equations (2.6) and (2.7).

2.3 Numerical results using single-signal RTD-VF

In this section, three case studies are used to validate single-signal RTD-VF. In particular, single-signal RTD-VF is compared with the worldwide recognized Prony (HAUER; DEMEURE; SCHARF, 1990) and Matrix Pencil (CROW; SINGH, 2005) techniques as well as with the emerging Curve-Fitting (HWANG; LIU, 2017) and 'ringdown frequency-domain Vector Fitting' (RFD-VF) (PAPADOPOULOS *et al.*, 2016) approches, being the latter the frequency-domain counterpart method of RTD-VF. We remark that most results exposed in this section have been first presented in (SCHUMACHER; OLIVEIRA; KUIAVA, 2018).

The first case study presented in this section aims to identify a synthetic test signal formed by known modal parameters. In particular, this case study shows RTD-VF is less sensitive to additive white Gaussian noise when compared to RFD-VF.

The other two case studies of this section consider actual ringdown data sets extracted from North American Eastern Interconnection (NAEI) (YE; LIU, 2012; HWANG; LIU, 2014; HWANG; LIU, 2017) and Brazilian Interconnected Power (BIP) (MEDFASEE, 2017) systems. In these two case studies, the modal parameters of the measured signals are not known beforehand. Therefore, the so-called R^2 coefficient of determination is also used during comparisons. The R^2 coefficient of determination is defined by

$$\mathrm{R}^2 = \left(1 - \frac{\sum_{k=0}^{K-1} (y[k] - \bar{y}[k])^2}{\sum_{k=0}^{K-1} (y[k] - \check{y})^2} \right) \times 100\%, \tag{2.45}$$

where $\check{y}$ represents the mean value of the ringdown data set $y[k], k = 0, \cdots, K-1$. Note that $\mathrm{R}^2 = 100\%$ indicates a perfect fit for each sample $y[k]$.

We remark that a small improvement has been incorporated into the original RFD-VF (PAPADOPOULOS *et al.*, 2016) so that it can also estimate a non-zero dc component h_{dc}. Lastly, we also remark that all simulations were performed in an Intel(R) Core(TM) i5 2.2GHz 8GB RAM laptop.

Table 1 – Modal estimates for the synthetic signal.

method	l	σ_l [s^{-1}]	ω_l [rad/s]	A_l [ ]	φ_l [rad]
RFD-VF	1	−0.1697	1.4351	0.9962	−2.5087
	2	−0.8166	3.9264	1.3242	1.8864
	3	−1.8230	6.4751	1.1263	0.3067
RTD-VF	1	−0.1697	1.4351	1.0000	−2.5133
	2	−0.8150	3.9270	1.3200	1.8850
	3	−1.8230	6.4654	1.1300	0.3142

2.3.1 Synthetic signal with known modal parameters

This first case study aims to identify the modal components of the synthetic test signal defined by equation (2.46). As also performed in (PAPADOPOULOS *et al.*, 2016), such a test signal is discretized with a sampling time $T = 0.01s$ and assuming a total observation time of 30s.

$$\begin{aligned} y_0(t) = & \underbrace{1.00 \times \mathrm{e}^{-0.1697t} \cos(1.4351t - 2.5133)}_{\text{mode \#1 } (l=1)} + \\ & \underbrace{1.32 \times \mathrm{e}^{-0.8150t} \cos(3.9270t + 1.8850)}_{\text{mode \#2 } (l=2)} + \\ & \underbrace{1.13 \times \mathrm{e}^{-1.8230t} \cos(6.4654t + 0.3142)}_{\text{mode \#3 } (l=3)} . \end{aligned} \tag{2.46}$$

We first consider that the obtained discretized noise-free sequence $y_0[k]$ is available for direct measurement, so that estimation data are given by $y[k] = y_0[k]$. Fig. 4 compares such estimation data with curves fitted via RFD-VF and RTD-VF, considering $N = 6$ poles for both techniques. Table 1 shows the resulting estimated modal components. Although Fig. 4 shows that both fitted curves satisfactorily match with $y[k]$, Table 1 reveals that RTD-VF gives more precise estimates for the true modal components of $y_0(t)$ in (2.46).

We now consider sequence $y_0[k]$ is no longer available for direct measurement, being $y[k]$ now assumed to be contaminated by a sequence of additive white Gaussian noise $n[k]$ with zero mean and variance 0.05^2, so that measurements are actually given by $y[k] = y_0[k] + n[k]$. RTD-VF and RFD-VF are ran for 1000 different generations of noise sequence $n[k]$. All estimated modal parameters obtained with both RFD-VF and RTD-VF during these 1000 generations are represented by their normalized estimated probability

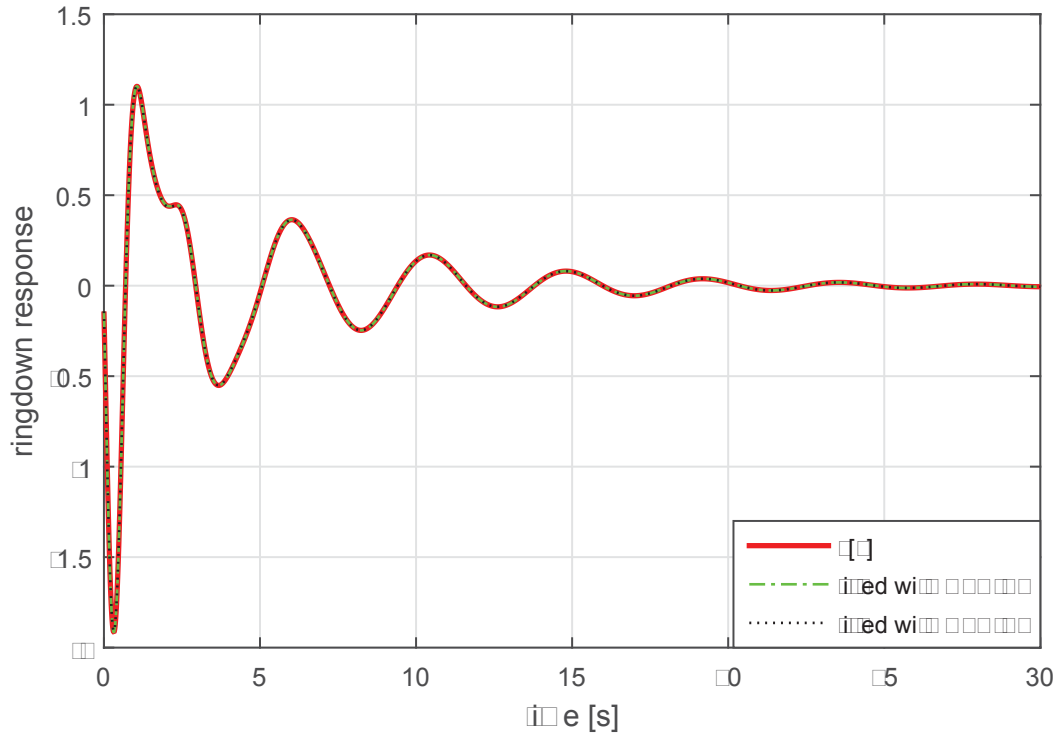

Figure 4 – Comparison between the noise-free synthetic signal and fitted responses.

density functions in Fig. 5. In this figure, dotted vertical lines represent the true values for the modal parameters of the synthetic signal $y_0(t)$ in (2.46). From Fig. 5, it is observed that only RTD-VF is able to provide concise estimates around the true modal parameters, whereas RFD-VF presents a clear bias for most modal components.

The average simulation time per simulation (i.e., per noise generation) is shown in Table 2. It is observed that time is not an issue for both algorithms, although RTD-VF is faster than RFD-VF. This was already expected since RFD-VF relies on performing additional computations such as DFT of ringdown signal $y[k]$.

Table 2 – Average simulation time in seconds.

RFD-VF	RTD-VF
0.8191	0.4435

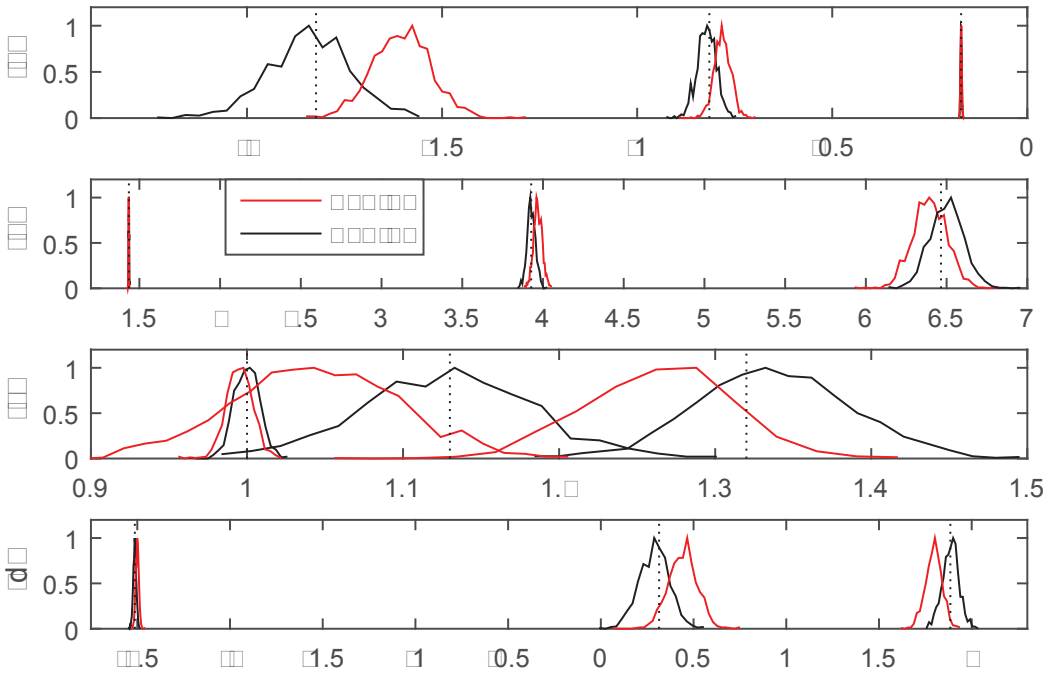

Figure 5 – Estimated normalized probability density functions for (a) attenuations σ_l; (b) frequencies ω_l; (c) amplitudes A_l; (d) phases φ_l. Vertical dotted lines represent the true values for σ_l, ω_l, A_l, φ_l, found in (2.46).

2.3.2 NAEI system

Due to severe weather conditions, an event occurred in the NAEI system on April 27, 2011 (HWANG; LIU, 2017). This event caused the Northern and Southern areas from the system to oscillate with decreasing dc components. Oscillations were measured by two Frequency Disturbance Recorders (FDRs) (one located in Maine and the other in Florida) with a sampling time of $T = 0.1$s. Fig. 6 (top) depicts the recorded data sets normalized at the nominal frequency $f_0 = 60$Hz. Fig. 6 (top) also reveals that the difference sequence 'Maine–Florida' (signal Maine *minus* signal Florida) has a constant dc component. In (HWANG; LIU, 2017), the $K = 201$ samples extracted from such a difference sequence (after a specified start time of 5.6s) are considered to form the measured ringdown sequence $y[k]$ (see Fig. 6 (bottom)). Here, for a fair comparison between RTD-VF and the Curve-Fitting method proposed in (HWANG; LIU, 2017), the same sequence $y[k]$ is considered, although we remark that RTD-VF can also be naturally applied to ringdown sequences with increasing/decreasing dc components (this is clearly shown, for instance,

Table 3 – Modal estimates in the NAEI system.

method	l	σ_l [s^{-1}]	ω_l [rad/s]	A_l [Hz]	φ_l [rad]	R^2 [%]
Curve-Fitting	1	−0.2290	1.2758	0.0415	−1.6713	88.1367
	2	−0.1384	2.1016	0.0210	−1.3531	
Prony	1	−0.2317	1.2261	0.0396	−1.3663	92.5183
	2	−0.1517	2.0874	0.0221	−1.1534	
Matrix Pencil	1	−0.1973	1.2441	0.0340	−1.4031	94.3820
	2	−0.2074	2.2010	0.0290	−1.4981	
RFD-VF	1	−0.1916	1.2502	0.0321	−1.4520	94.3697
	2	−0.2264	2.1852	0.0307	−1.4755	
RTD-VF	1	−0.2028	1.2522	0.0345	−1.4612	94.5728
	2	−0.2279	2.1819	0.0311	−1.4448	

in the case study of Section 2.3.3).

Fig. 6 (bottom) depicts the fitted ringdown responses obtained with RTD-VF and RFD-VF (considering $N = 4$ for both techniques). Table 3 shows their corresponding modal components. Fig. 6 (bottom) and Table 3 also show the results obtained with the Curve-Fitting and Prony methods (such results are available in (HWANG; LIU, 2017)). Results for the Matrix Pencil method (CROW; SINGH, 2005) are also provided. From Table 3 it is observed RTD-VF presents a higher R^2 coefficient of determination when compared to the other methods. This suggests that the modal estimates obtained via RTD-VF are more likely to be closer to the true modal parameters of the NAEI system.

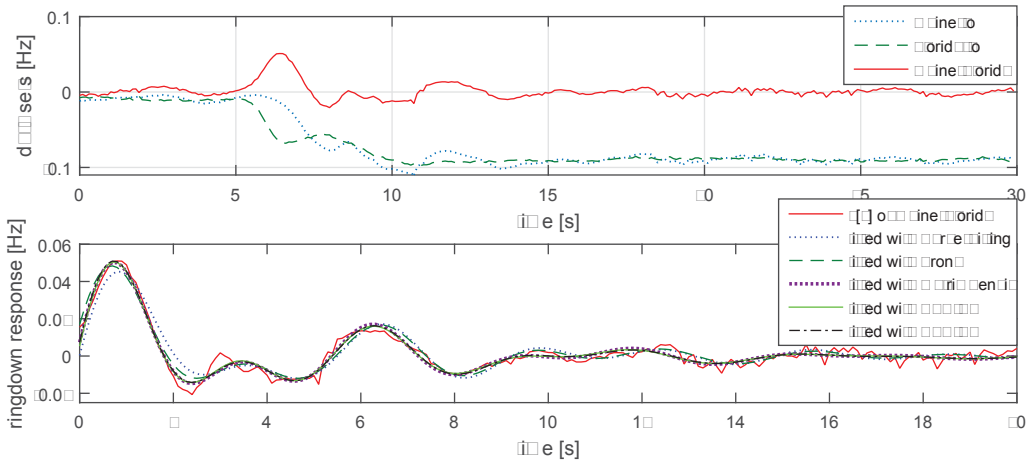

Figure 6 – Data sets (top) and ringdown responses (bottom). Since a difference sequence has been used in this case study as estimation data, RTD-VF and RFD-VF fitted small constant dc components of $h_{\text{dc}} = -0.0005$ and $h_{\text{dc}} = -0.0004$, respectively.

2.3.3 BIP system

The Itaipu Hydroelectric was disconnected from the rest of the BIP system on September 02, 2011, at 19h43m40.3s UTC, due to an electrical bushing explosion (ONS, 2011). The Itaipu Hydroelectric was reconnected to the BIP system 27m49.7s later (ONS, 2011). Both disconnection and reconnection events caused the Southern, Northern, Southeastern and Northeastern areas from the system to oscillate against each other with varying dc components. As already presented in Fig. 3 of this thesis, oscillatory and purely exponential dynamics were measured by a FDR located at the Federal University of Santa Catarina, with a sampling time of $T = (1/60)$s. Fig. 7 (top) depicts the data set recorded during the Itaipu Hydroelectric reconnection. For modal identification purposes, the $K = 901$ samples extracted from such data set (after a specified start time of 1.5s) are considered to form ringdown sequence $y[k]$.

The main objective of this case study is to show RTD-VF presents is more suitable than RFD-VF for modeling ringdown sequences with increasing dc components. From Fig. 7 (bottom) it is observed that the fitted ringdown response obtained with RTD-VF matches with $y[k]$, whereas RFD-VF presents a clear mismatch for the exponential component of $y[k]$. Table 4 shows the resulting modal components for both techniques (note that in both methods a model order $N = 7$ has been selected). Fig. 7 (bottom) and Table 4 also show results for the Matrix Pencil method.

Lastly, it is also interesting to remark that the angular frequencies observed in Table 4 for the RTD-VF and RFD-VF methods correspond to typical values found in the Brazilian literature (JEREMIAS *et al.*, 2012) for interarea oscillations between South-Southeast (usually around $2\pi \times 0.70$rad/s), North-Northeast ($2\pi \times 0.58$rad/s) and North-South ($2\pi \times 0.39$rad/s) areas.

2.4 Multi-signal modeling: Fundamentals

As mentioned in Chapter 1 of this thesis, since it is based on modeling ringdown signals independently, i.e., one at a time, single-signal RTD-VF generates modal estimates that are naturally more related with the particular section of the power system in which

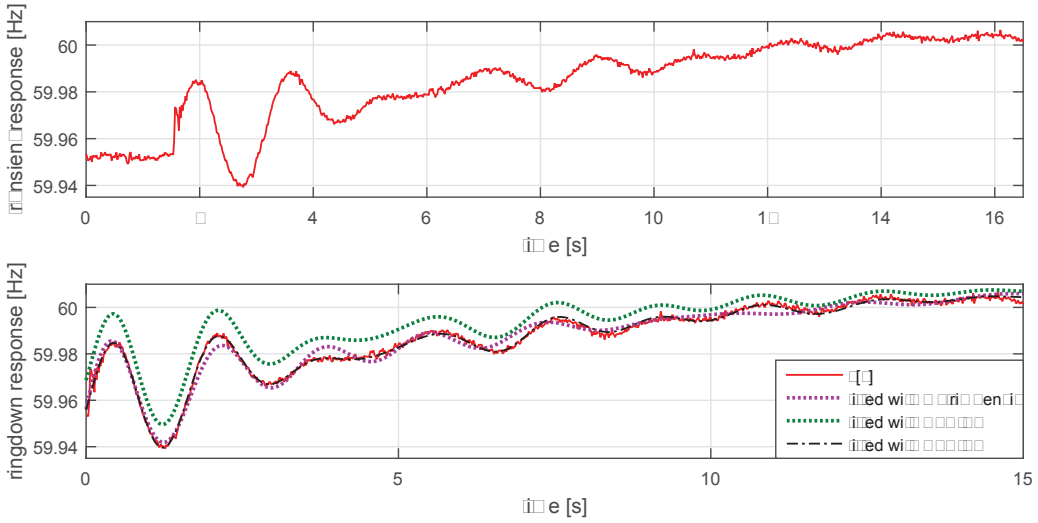

Figure 7 – Data set (top) and ringdown responses (bottom). In this case study, RTD-VF, RFD-VF and Matrix Pencil fitted constant dc components of $h_{\mathrm{dc}} = 60.0188$, $h_{\mathrm{dc}} = 60.0177$ and $h_{\mathrm{dc}} = 46.6979$, respectively.

Table 4 – Modal estimates in the BIP system.

method	l	σ_l [s^{-1}]	ω_l [rad/s]	A_l [Hz]	φ_l [rad]	R^2 [%]
RFD-VF	1	−0.3865	4.3631	0.0149	−2.2510	75.5845
	2	−0.1722	3.6059	0.0136	−1.6151	
	3	−0.1806	2.3556	0.0092	0.5522	
	4	−0.1029	–	−0.0469	–	
RTD-VF	1	−0.3837	4.3713	0.0145	−2.2833	99.2988
	2	−0.1729	3.6016	0.0129	−1.6350	
	3	−0.1862	2.3578	0.0091	0.4951	
	4	−0.0993	–	−0.0603	–	
Matrix Pencil	1	−0.3691	3.6594	0.0305	−1.5419	97.1401
	2	−0.0731	2.6180	0.0030	−0.7084	
	3	−0.2404	–	−0.0346	–	
	4	0.0004	–	12.8365	–	
	5	−0.0085	–	0.4531	–	

the signal under modeling has been measured. In this context, one can expect more realistic estimates for the entire system if multiple signals distributed over different locations are simultaneously used during modal estimation (TRUDNOWSKI; JOHNSON; HAUER, 1999; DOSIEK; PIERRE, 2012; DOSIEK; PIERRE, 2013; KHAZAEI *et al.*, 2016).

In this section, by redefining some variables initially defined in Sections 2.1 and 2.2, we establish fundamentals of multi-signal modeling based on ringdown data. Such fundamentals are then used in Section 2.5 for transforming single-signal RTD-VF into the

generalized multi-signal RTD-VF approach proposed in (SCHUMACHER; OLIVEIRA; KUIAVA, 2019), which is capable of generating modal estimates by processing multiple ringdown signals simultaneously.

As already discussed in this thesis, oscillatory as well as purely exponential dynamics are induced in power system signals (power flows, system frequency, etc) when transient (ringdown) events occur. In this context, one can assume a finite number of V signals to be considerably affected due to a particular ringdown event.

$$y_{(v)}(t); \quad v = 1, \cdots, V. \tag{2.47}$$

The phenomenon aforementioned is exemplified through Fig. 8, which depicts five sets of ringdown measurements simultaneously extracted during a reconnection of the Itaipu Hydroelectric to the BIP system. Differently from Figs. 3 and 7, which depicts measurements observed only in Federal University of Santa Catarina (UFSC), Fig. 8 depicts measurements observed also in other four different universities. Each university is located in one of the five regions of Brazil: North, Northeast, Central-West, Southeast and South.

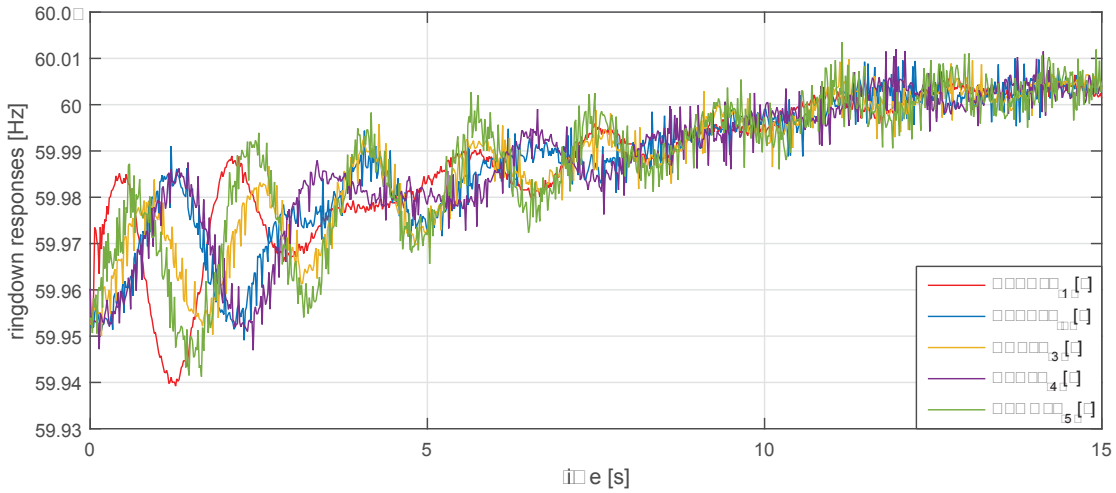

Figure 8 – Example of a typical set of ringdown responses which have been measured simultaneously. Measurements represent system frequency and have been recorded by five different FDRs installed within the following Brazilian universities: Federal University of Santa Catarina (UFSC); Federal University of Pará (UFPA); University of Brasília (UNB); Federal University of Ceará (UFC); Federal University of Minas Gerais (UFMG).

Approximating signals $\{y_{(v)}(t)\}$ is possible by means of the following set of modeling signal structures:

$$\bar{y}_{(v)}(t) = h_{\rm dc}^{(v)} + \sum_{l=1}^{M_{\rm OSC}} A_l^{(v)} {\rm e}^{\sigma_l t} \cos(\omega_l t + \varphi_l^{(v)}) + \sum_{l=M_{\rm OSC}+1}^{M} A_l^{(v)} {\rm e}^{\sigma_l t}, \quad v = 1, \cdots, V. \quad (2.48)$$

In this equation, each modeling signal $\bar{y}_{(v)}(t)$ has a particular dc component $h_{\rm dc}^{(v)}$ and also its own set of mode amplitudes $\{A_l^{(v)}\}$ and phases $\{\varphi_l^{(v)}\}$. Nonetheless, all V ringdown signals in (2.48) are modeled based on a common set of complex-valued eigenvalues $\lambda_l = \sigma_l + j\omega_l$, $l = 1, \cdots, M_{\rm OSC}$ and real-valued eigenvalues $\lambda_l = \sigma_l$, $l = M_{\rm OSC}+1, \cdots, M$.

A similar derivation to the one presented in Section 2.9.1 can be used to alternatively express each v-th signal $\bar{y}_{(v)}(t)$ in (2.48) as follows:

$$\bar{y}_{(v)}(t) = h_{\rm dc}^{(v)} + \sum_{i=1}^{N} \frac{r_i^{(v)}}{\rho - p_i} \delta(t), \quad (2.49)$$

where

$$p_i = \begin{cases} \lambda_{\frac{i+1}{2}} & , \quad i = 1, 3, \cdots, 2M_{\rm OSC} - 1 \\ (p_{i-1})^* & , \quad i = 2, 4, \cdots, 2M_{\rm OSC} \\ \lambda_{i-M_{\rm OSC}} & , \quad i = 2M_{\rm OSC}+1, 2M_{\rm OSC}+2, \cdots, N \end{cases} \quad (2.50)$$

$$r_i^{(v)} = \begin{cases} \frac{1}{2} A_{\frac{i+1}{2}}^{(v)} {\rm e}^{j\varphi_{\frac{i+1}{2}}^{(v)}} & , \quad i = 1, 3, \cdots, 2M_{\rm OSC} - 1 \\ (r_{i-1}^{(v)})^* & , \quad i = 2, 4, \cdots, 2M_{\rm OSC} \\ A_{i-M_{\rm OSC}}^{(v)} & , \quad i = 2M_{\rm OSC}+1, 2M_{\rm OSC}+2, \cdots, N \end{cases} \quad (2.51)$$

Based on representation (2.49) and assuming signals $\{y_{(v)}(t)\}$ have all been measured over the same set of K discrete-time instants $t = kT$, $k = 0, \cdots, K-1$, one can formulate the following least-squares problem for indirectly estimating oscillatory and

purely exponential components of these signals:

$$\begin{aligned}\hat{\gamma} &= \arg\min_{\gamma} \sum_{v=1}^{V}\sum_{k=0}^{K-1}\Big(y_{(v)}(kT) - \bar{y}_{(v)}(kT)\Big)^2 \\ &= \arg\min_{\gamma} \sum_{v=1}^{V}\sum_{k=0}^{K-1}\left(y_{(v)}(kT) - \left(h_{\mathrm{dc}}^{(v)} + \sum_{i=1}^{N}\frac{r_i^{(v)}}{\rho - p_i}\delta(kT)\right)\right)^2\end{aligned} \tag{2.52}$$

where $\hat{\gamma}$ can be considered to be an estimate for parameter vector γ that, as shown by equation (2.53), concatenates the parameters of all modeling signals $\{\bar{y}_{(v)}(t)\}$, $v = 1, \cdots, V$.

$$\gamma = \left[\begin{array}{cccccccccccc} h_{\mathrm{dc}}^{(1)} & r_1^{(1)} & \cdots & r_N^{(1)} & \cdots & h_{\mathrm{dc}}^{(V)} & r_1^{(V)} & \cdots & r_N^{(V)} & p_1 & \cdots & p_N \end{array}\right]^{\mathrm{T}}. \tag{2.53}$$

As in the single-signal modeling context described in Section 2.1, estimating γ via (2.52) constitutes a nonlinear optimization problem, since poles $\{p_i\}$ appear in the denominator of $\bar{y}_{(v)}(t)$.

2.5 Multi-signal RTD-VF

In order to formulate a generalizing multi-signal RTD-VF approach for estimating γ in (2.53), we shall here use the two auxiliary transfer functions shown in equations (2.55) and (2.56) to define the following alternative structure:

$$\begin{aligned}\hat{y}_{(v)}(t) &= h_{\mathrm{dc}}^{(v)} + \frac{B^{(v)}(\rho)}{F(\rho)}\delta(t); \\ &= h_{\mathrm{dc}}^{(v)} + \frac{\displaystyle\sum_{i=1}^{N}\frac{c_i^{(v)}}{\rho - \bar{p}_i}}{1 + \displaystyle\sum_{i=1}^{N}\frac{d_i}{\rho - \bar{p}_i}}\delta(t);\end{aligned} \tag{2.54}$$

$$\frac{B^{(v)}(\rho)}{\hat{F}(\rho)} = \sum_{i=1}^{N}\frac{c_i^{(v)}}{\rho - \bar{p}_i}; \tag{2.55}$$

$$\frac{F(\rho)}{\hat{F}(\rho)} = 1 + \sum_{i=1}^{N}\frac{d_i}{\rho - \bar{p}_i}. \tag{2.56}$$

As in single-signal RTD-VF, $\{\bar{p}_i\}$ is assumed to be a set of pre-specified (known) poles.

The related parameter vector is now defined by

$$\theta = \left[\begin{array}{cccccccccccc} h_{\mathrm{dc}}^{(1)} & c_1^{(1)} & \cdots & c_N^{(1)} & \cdots & h_{\mathrm{dc}}^{(V)} & c_1^{(V)} & \cdots & c_N^{(V)} & d_1 & \cdots & d_N \end{array} \right]^{\mathrm{T}}, \tag{2.57}$$

and the following objective function can be here formulated:

$$J(\theta) = \sum_{v=1}^{V} \sum_{k=0}^{K-1} e_{(v)}^2(kT), \tag{2.58}$$

where $e_{(v)}(kT)$ is the scalar error

$$e_{(v)}(kT) = y_{(v)}(kT) - \hat{y}_{(v)}(kT) \tag{2.59}$$

that, based on equation (2.54), also reads

$$e_{(v)}(kT) = \frac{F(\rho)}{F(\rho)} y_{(v)}(kT) - \left(h_{\mathrm{dc}}^{(v)} + \frac{B^{(v)}(\rho)}{F(\rho)} \delta(kT) \right). \tag{2.60}$$

As a VF approach, one can consider approximation $e_{(v)}(kT) \approx \tilde{e}_{(v)}(kT)$, where

$$\begin{aligned} \tilde{e}_{(v)}(kT) &= \frac{F(\rho)}{\hat{F}(\rho)} y_{(v)}(kT) - \left(h_{\mathrm{dc}}^{(v)} + \frac{B^{(v)}(\rho)}{\hat{F}(\rho)} \delta(kT) \right) && (2.61) \\ &= \left(1 + \sum_{i=1}^{N} \frac{d_i}{\rho - \bar{p}_i} \right) y_{(v)}(kT) - \left(h_{\mathrm{dc}}^{(v)} + \sum_{i=1}^{N} \frac{c_i^{(v)}}{\rho - \bar{p}_i} \delta(kT) \right) && (2.62) \end{aligned}$$

or, equivalently,

$$\tilde{e}_{(v)}(kT) = y_{(v)}(kT) - \mathbf{m}_{(v)}^{\mathrm{T}}(kT)\theta, \tag{2.63}$$

being now

$$\mathbf{m}_{(v)}(kT) = \left[\begin{array}{ccccc} \mathbf{0}_{1\times(N+1)(v-1)} & 1 & \tilde{\mathbf{u}}^{\mathrm{T}}(kT) & \mathbf{0}_{1\times(N+1)(V-v)} & -\tilde{\mathbf{y}}_{(v)}^{\mathrm{T}}(kT) \end{array} \right]^{\mathrm{T}}; \tag{2.64}$$

$$\widetilde{\mathbf{y}}_{(v)}(kT) = \left[\begin{array}{ccc} \dfrac{1}{\rho - \bar{p}_i} & \cdots & \dfrac{1}{\rho - \bar{p}_N} \end{array} \right]^{\mathrm{T}} y_{(v)}(kT); \tag{2.65}$$

$$\widetilde{\mathbf{u}}(kT) = \left[\begin{array}{ccc} \dfrac{1}{\rho - \bar{p}_i} & \cdots & \dfrac{1}{\rho - \bar{p}_N} \end{array} \right]^{\mathrm{T}} \delta(kT). \tag{2.66}$$

Comparison between equations (2.23) and (2.64) reveal multi-signal RTD-VF require terms $\mathbf{0}_{i\times j}$ to be defined in order to make expression (2.63) valid for $v = 1, \cdots, V$. In this thesis, $\mathbf{0}_{i\times j}$ terms represent matrices of zeros with i rows and j columns. Nonetheless, from now on, we may sometimes use $\mathbf{0}$ to omit dimensions and simplify notation.

By approximating $e_{(v)}(kT)$ by $\tilde{e}_{(v)}(kT)$ in equation (2.58), the *nonlinear* problem of minimizing objective function $J(\theta)$ is transformed into an approximated but *linearized* least-squares problem whose solution can be written as follows

$$\begin{aligned} \hat{\theta} &= \arg\min_{\theta} \sum_{v=1}^{V} \sum_{k=0}^{K-1} \tilde{e}^2_{(v)}(kT) && (2.67)\\ &= \arg\min_{\theta} \sum_{v=1}^{V} \sum_{k=0}^{K-1} \left(y_{(v)}(kT) - \mathbf{m}^{\mathrm{T}}_{(v)}(kT)\theta \right)^2 && (2.68)\\ &= \left[\mathbf{M}^{\mathrm{T}}\mathbf{M} \right]^{-1} \mathbf{M}^{\mathrm{T}}\mathbf{y}, && (2.69) \end{aligned}$$

where $\hat{\theta}$ can be considered as an estimate for $\theta^\star$ obtained for a given set of pre-specified poles $\{\bar{p}_i\}$, being $\theta^\star$ the global minimum of $J(\theta)$. In (2.69), matrices $\mathbf{M}$ and $\mathbf{y}$ are defined as follows

$$\mathbf{M} = \left[\begin{array}{cc} \widetilde{\mathbf{U}} & -\widetilde{\mathbf{Y}} \end{array} \right]; \tag{2.70}$$

$$\mathbf{y} = \left[\begin{array}{ccccccc} y_{(1)}[0] & \cdots & y_{(1)}[K-1] & \cdots & y_{(V)}[0] & \cdots & y_{(V)}[K-1] \end{array} \right]^{\mathrm{T}}; \tag{2.71}$$

where

$$\widetilde{\mathbf{Y}} = \left[\begin{array}{ccccccc} \widetilde{\mathbf{y}}_{(1)}[0] & \cdots & \widetilde{\mathbf{y}}_{(1)}[K-1] & \cdots & \widetilde{\mathbf{y}}_{(V)}[0] & \cdots & \widetilde{\mathbf{y}}_{(V)}[K-1] \end{array} \right]^{\mathrm{T}}; \tag{2.72}$$

$$\widetilde{\mathbf{U}} = \begin{bmatrix} \widetilde{\mathbf{U}}'_{(1)} & \mathbf{0} & \cdots & \mathbf{0} \\ \mathbf{0} & \widetilde{\mathbf{U}}'_{(2)} & \cdots & \mathbf{0} \\ \cdots & \cdots & \cdots & \cdots \\ \mathbf{0} & \mathbf{0} & \cdots & \widetilde{\mathbf{U}}'_{(V)} \end{bmatrix}^{\mathrm{T}} \quad ; \quad \widetilde{\mathbf{U}}'_{(v)} = \begin{bmatrix} 1 & \cdots & 1 \\ \tilde{\mathbf{u}}[0] & \cdots & \tilde{\mathbf{u}}[K-1] \end{bmatrix} \tag{2.73}$$

Comparison between equations (2.29)–(2.32) and (2.70)–(2.73) shows multi-signal RTD-VF effectively generalize single-signal RTD-VF, since, if $V = 1$ (meaning measurements only from a single ringdown response are being considered during modal estimation), these two sets of equations equal each other.

Once θ has been estimated via (2.69), one can try to make the approximate error $\tilde{e}_{(v)}(kT)$ in (2.61) closer to the original error $e_{(v)}(kT)$ in (2.60) by considering the obtained polynomial $F(\rho)$ as a possibly more refined estimate for polynomial $\hat{F}(\rho)$. In terms of roots, this means that roots of $\hat{F}(\rho)$, which can be determined based on the estimated coefficients $\{d_i\}$ in θ (see equation (2.56)), are to be considered as a more refined estimate for the N pre-specified poles $\bar{p}_1, \cdots, \bar{p}_N$. Based on this novel set of poles $\{\bar{p}_i\}$, one can reestimate θ via (2.69).

As in single-signal RTD-VF, this procedure can be repeated (iterated) until $\hat{\theta}$ and $\{\bar{p}_i\}$ converge to fixed values $\hat{\theta}'$ and $\{\bar{p}'_i\}$. When convergence is achieved, it naturally follows that $F'(\rho) = \hat{F}'(\rho)$, where $F'(\rho)$ and $\hat{F}'(\rho)$ denote the values obtained for polynomials $F(\rho)$ and $\hat{F}(\rho)$ when $\bar{p}_i = \bar{p}'_i$ and $\hat{\theta} = \hat{\theta}'$. Consequently, all V alternative modeling structures $\hat{y}_{(v)}(t)$ in (2.54) obtained after algorithm convergence fits exactly into the desired signal structure in (2.49):

$$\begin{aligned} \hat{y}'_{(v)}(t) &= h_{\mathrm{dc}}^{\prime(v)} + \frac{B'^{(v)}(\rho)}{F'(\rho)}\delta(t) \\ &= h_{\mathrm{dc}}^{\prime(v)} + \frac{B'^{(v)}(\rho)}{\hat{F}'(\rho)}\delta(t) \\ &= h_{\mathrm{dc}}^{\prime(v)} + \sum_{i=1}^{N} \frac{c_i^{\prime(v)}}{\rho - \bar{p}'_i}\delta(t) \end{aligned} \tag{2.74}$$

Expression (2.74) reveals $h_{\mathrm{dc}}^{\prime(v)}$, $c_1^{\prime(v)}, \cdots, c_N^{\prime(v)}$ and $\bar{p}'_1, \cdots, \bar{p}'_N$ are our final estimates for $h_{\mathrm{dc}}^{(v)}$, $r_1^{(v)}, \cdots, r_N^{(v)}$ and $p_1, \cdots, p_N$. Since $F'(\rho) = \hat{F}'(\rho)$, one can observe that, at

convergence, equation (2.56) becomes

$$\frac{F'(\rho)}{\hat{F}'(\rho)} = 1 + \sum_{i=1}^{N} \frac{d'_i}{\rho - \bar{p}'_i} \tag{2.75}$$

$$= 1. \tag{2.76}$$

This means that the converged coefficients $\{d'_i\}$ no longer affect the resulting modeling signals $\hat{y}'_{(v)}(t)$, as shown in (2.74).

2.5.1 Step by step procedure for implementing multi-signal RTD-VF

As one may expect, the step by step procedure for implementing multi-signal RTD-VF is very similar to the one used for implementing its single-signal version (presented in Section 2.2.1). In fact, the major difference between these two approaches comes from the fact that multi-signal RTD-VF naturally relies on additional computations, since possibly multiple ringdown sequences are simultaneously used for processing modal estimates.

The complete procedure for implementing multi-signal RTD-VF is described in the following.

Step 1. Given a set of ringdown responses $\{y_{(v)}(t)\}$, $v = 1, \cdots, V$ sampled at $t = kT$, with $k = 0, \cdots, K-1$, one must define the number of iterations and a set of starting poles $\{\bar{p}_i\}$, $i = 1, \cdots, N$.

Comment: As emphasized in (SCHUMACHER; OLIVEIRA; KUIAVA, 2018; GRIVET-TALOCIA; GUSTAVSEN, 2016), starting poles can be chosen as weakly attenuated complex conjugate pairs (for instance, with $\Re\mathrm{e}(\bar{p}_i) = -0.01 \times |\Im\mathrm{m}(\bar{p}_i)|$) with imaginary parts linearly distributed over a frequency band of interest $[0, \omega_{\max}]$. Since electromechanical modes in power systems usually have an imaginary part which is not higher than 3 Hz, one can simply define staring poles as follows:

$$\bar{p}_i = \begin{cases} \bar{p}^*_{i+1} & , \quad i = 1, 3, \cdots, N-1 \\ i(-0.01 + j)\omega_{\max}/N & , \quad i = 2, 4, \cdots, N \end{cases} \tag{2.77}$$

where $\omega_{\max} = 2\pi \times 3$. If N is an odd number, then one can additionally define $\bar{p}_N = \Re\mathrm{e}(\bar{p}_{N-1})$, meaning $\bar{p}_N$ is not defined without occurrence of its corresponding conjugate.

Step 2. Construct matrices $\mathbf{M}$ and $\mathbf{y}$ based on (2.70)–(2.73). In these equations, vectors $\widetilde{\mathbf{y}}_{(v)}[k]$ and $\widetilde{\mathbf{u}}[k]$ can be approximated, for $k = 1, \cdots, K-1$, by recursive use of the following state-space discretizations of equations (2.65) and (2.66)[2] :

$$\widetilde{\mathbf{y}}_{(v)}[k] \approx \mathbf{A}_{\mathrm{d}}\widetilde{\mathbf{y}}_{(v)}[k-1] + \mathbf{B}_{\mathrm{d}}y_{(v)}[k-1], \quad \widetilde{\mathbf{y}}_{(v)}[0] = \mathbf{0} \tag{2.78}$$

$$\widetilde{\mathbf{u}}[k] \approx \mathbf{A}_{\mathrm{d}}\widetilde{\mathbf{u}}[k-1], \quad \widetilde{\mathbf{u}}[0] = \mathbf{B} \tag{2.79}$$

where

$$\mathbf{A}_{\mathrm{d}} = \mathrm{e}^{\mathbf{A}T}; \quad \mathbf{B}_{\mathrm{d}} = \mathbf{A}^{-1}(\mathbf{A}_{\mathrm{d}} - \mathbf{I})\mathbf{B} \tag{2.80}$$

$$\mathbf{A} = \begin{bmatrix} \bar{p}_1 & 0 & \cdots & 0 \\ 0 & \bar{p}_2 & \cdots & 0 \\ \vdots & \vdots & \ddots & \vdots \\ 0 & 0 & \cdots & \bar{p}_N \end{bmatrix}; \quad \mathbf{B} = \begin{bmatrix} 1 \\ 1 \\ \vdots \\ 1 \end{bmatrix}_{N\times 1} \tag{2.81}$$

and $\mathbf{I}$ denotes the $N \times N$ identity matrix.

Step 3. Obtain a least-squares estimate for parameter vector θ via (2.69).

Comment: As shown in (GRIVET-TALOCIA; GUSTAVSEN, 2016; SCHUMACHER; OLIVEIRA; KUIAVA, 2018), it is possible to ensure that the partial fraction residues $c_i^{(v)}$ and $c_{i+1}^{(v)}$ are always estimated in perfect conjugate pairs $c_{i+1}^{(v)} = (c_i^{(v)})^*$ whenever $\bar{p}_{i+1} = \bar{p}_i^*$. As evidenced in equation (2.82), if $\bar{p}_i$ and $\bar{p}_{i+1}$ constitute a complex conjugate pair, then the corresponding basic partial fractions $1/(s-\bar{p}_i)$ and $1/(s-\bar{p}_i^*)$ in (2.54) can be substituted by $(1/(s-\bar{p}_i) + 1/(s-\bar{p}_i^*))$ and $(j/(s-\bar{p}_i) - j/(s-\bar{p}_i^*))$, respectively. In

[2] Derivation of equations (2.78)–(2.80) would follow the same steps presented in Section 2.9.2 for single-signal RTD-VF.

the corresponding state-space representation, this modification is implemented by simply replacing submatrices

$$\begin{bmatrix} \bar{p}_i & 0 \\ 0 & \bar{p}_{i+1} \end{bmatrix} \quad \text{and} \quad \begin{bmatrix} 1 \\ 1 \end{bmatrix}$$

within matrices $\mathbf{A}$ and $\mathbf{B}$ in (2.81) by, respectively,

$$\begin{bmatrix} \Re\mathrm{e}(\bar{p}_i) & \Im\mathrm{m}(\bar{p}_i) \\ -\Im\mathrm{m}(\bar{p}_i) & \Re\mathrm{e}(\bar{p}_i) \end{bmatrix} \quad \text{and} \quad \begin{bmatrix} 2 \\ 0 \end{bmatrix}.$$

Such a substitution can be regarded as a modal transformation (CHEN, 1999) and it is also performed in classical frequency-domain VF (GUSTAVSEN; SEMLYEN, 1999). As it can be observed through equation (2.82), it has the effect that the corresponding residues in the solution vector θ become equal to $\Re\mathrm{e}(c_i^{(v)})$ and $\Im\mathrm{m}(c_i^{(v)})$.

$$\begin{bmatrix} \dfrac{1}{s-\bar{p}_i} & \dfrac{1}{s-\bar{p}_i^*} \end{bmatrix} \begin{bmatrix} c_i^{(v)} \\ (c_i^{(v)})^* \end{bmatrix} = \begin{bmatrix} \dfrac{1}{s-\bar{p}_i} + \dfrac{1}{s-\bar{p}_i^*} & \dfrac{j}{s-\bar{p}_i} - \dfrac{j}{s-\bar{p}_i^*} \end{bmatrix} \begin{bmatrix} \Re\mathrm{e}(c_i^{(v)}) \\ \Im\mathrm{m}(c_i^{(v)}) \end{bmatrix}. \tag{2.82}$$

Step 4. Update $\{\bar{p}_i\}$ with the roots of polynomial $F(\rho)$.

Comment: Since the roots of polynomial $F(\rho)$ equal the zeros of transfer function $F(\rho)/\hat{F}(\rho)$, defined in (2.56), one can update $\{\bar{p}_i\}$ by calculating the eigenvalues of matrix $(\mathbf{A} - \mathbf{B}\mathbf{D}^{-1}\mathbf{C})$ (see (GRIVET-TALOCIA; GUSTAVSEN, 2016) for a proof), with $(\mathbf{A}, \mathbf{B}, \mathbf{C}, \mathbf{D})$ being the state-space realization for $F(\rho)/\hat{F}(\rho)$ in which $\mathbf{A}$ and $\mathbf{B}$ satisfy (2.40) while

$$\mathbf{C} = \begin{bmatrix} d_1 & \cdots & d_n \end{bmatrix}; \quad \mathbf{D} = 1. \tag{2.83}$$

To ensure model stability, a usual practice in continuous-time VF implementations (GRIVET-TALOCIA; GUSTAVSEN, 2016) is the one which consists of inverting the

sign of poles with positive real parts if they occur while adopting

$$\{\bar{p}_i\} \leftarrow \text{eig}\left(\mathbf{A} - \mathbf{B}\mathbf{D}^{-1}\mathbf{C}\right). \tag{2.84}$$

It is also interesting to remark that, if the modal transformation commented in **Step 3** has been applied to a pole set $\{\bar{p}_i\}$ formed only by real-valued numbers and complex conjugate pairs, then $\mathbf{A}$, $\mathbf{B}$ and consequently θ are real-valued, meaning (2.84) returns a novel pole set which is also formed only by real-valued numbers and complex conjugate pairs.

Comment: Throughout iterations, we might also want to observe how our current set of poles $\{\bar{p}_i\}$ performs in structure (2.49). In this case, coefficients $\{r_i^{(v)}\}$ can be estimated in the linear least-squares sense via (2.69) by simply redefining $\mathbf{M} = \widetilde{\mathbf{U}}$. In this context, the associated root mean square (RMS) error of each v-th modeling signal $\bar{y}_{(v)}(t)$ is a metric which can be observed, being its definition given as follows

$$\text{RMS error}^{(v)} = \sqrt{\frac{1}{K}\sum_{k=0}^{K-1}\left(y_{(v)}[k] - \bar{y}_{(v)}[k]\right)^2}. \tag{2.85}$$

Step 5. Repeat steps 2 to 4 until the number of iterations is achieved.

Step 6. Resulting modal components of estimated ringdown signals are obtained through relations in (2.50) and (2.51).

Comment: It is straightforward to reorganize the refined real and complex conjugate poles (and their corresponding residues) in case they do not come directly organized in the order presumed by equations (2.50) and (2.51).

In the following section of this thesis, we present a multi-signal IV-based RTD-VF method which can be applied for further refining modal estimates generated by regular multi-signal RTD-VF. Both techniques are then compared and validated in Section 2.7.

2.6 Multi-signal IV-RTD-VF

It is well known regular VF implementations are extremely popular within system identification since they usually provide satisfactory estimates for transfer function poles (GRIVET-TALOCIA; GUSTAVSEN, 2016). In the particular case of RTD-VF, for instance, Section 2.3 of this thesis (which exposes the same results presented in (SCHUMACHER; OLIVEIRA; KUIAVA, 2018)) has shown it can provide superior fitting performance over the worldwide recognized Prony (HAUER; DEMEURE; SCHARF, 1990) and Matrix Pencil (CROW; SINGH, 2005) techniques as well as over the emerging Curve-Fitting (HWANG; LIU, 2017) and RFD-VF (PAPADOPOULOS *et al.*, 2016) approches.

Nonetheless, it is also well known regular VF implementations do not guarantee their converged solutions are local (or the global) optimums of their corresponding nonlinear objective functions. In Section 2.7 of this thesis, we show that even a very simple example leads the RTD-VF converged solution $\hat{\theta}'$ to not satisfy the necessary gradient condition for local/global optimality

$$\left.\frac{\partial J}{\partial \theta}\right|_{\theta=\hat{\theta}'} = \mathbf{0}. \tag{2.86}$$

In this section, we extend multi-signal RTD-VF to the instrumental variable (IV)-based context proposed in (SCHUMACHER; OLIVEIRA; KUIAVA, 2019). Through theorem 2.6.1, we also prove such an extension guarantees its solutions after algorithm convergence do satisfy (2.86).

From equations (2.54) and (2.57)–(2.59), it follows that (see Section 2.9.3 for the derivation of this equation)

$$\frac{\partial}{\partial \theta} J(\theta) = -2 \begin{bmatrix} \sum_{k=0}^{K-1} \mathbf{i}_{(1)}(kT)\ e_{(1)}(kT) \\ \cdots \\ \sum_{k=0}^{K-1} \mathbf{i}_{(V)}(kT)\ e_{(V)}(kT) \\ \sum_{v=1}^{V} \sum_{k=0}^{K-1} \mathbf{i}'_{(v)}(kT)\ e_{(v)}(kT) \end{bmatrix}, \tag{2.87}$$

where $\mathbf{i}_{(v)}(kT)$ and $\mathbf{i}'_{(v)}(kT)$ correspond to the following instrument vectors:

$$\mathbf{i}_{(v)}(kT) = \left[\begin{array}{cccc} \dfrac{\partial}{\partial h_{\mathrm{dc}}^{(v)}} & \dfrac{\partial}{\partial c_1^{(v)}} & \cdots & \dfrac{\partial}{\partial c_N^{(v)}} \end{array} \right]^{\mathrm{T}} \hat{y}_{(v)}(kT); \tag{2.88}$$

$$\mathbf{i}'_{(v)}(kT) = \left[\begin{array}{ccc} \dfrac{\partial}{\partial d_1} & \cdots & \dfrac{\partial}{\partial d_N} \end{array} \right]^{\mathrm{T}} \hat{y}_{(v)}(kT). \tag{2.89}$$

Similarly to the linearization performed in the regular multi-signal RTD-VF approach of Section 2.5, one can use approximation $e_{(v)}(kT) \approx \tilde{e}_{(v)}(kT)$ to transform the local optimality condition $\dfrac{\partial J}{\partial \theta} = \mathbf{0}$ into the approximated problem

$$\left[\begin{array}{c} \displaystyle\sum_{k=0}^{K-1} \mathbf{i}_{(1)}(kT)\ \tilde{e}_{(1)}(kT) \\ \cdots \\ \displaystyle\sum_{k=0}^{K-1} \mathbf{i}_{(V)}(kT)\ \tilde{e}_{(V)}(kT) \\ \displaystyle\sum_{v=1}^{V} \sum_{k=0}^{K-1} \mathbf{i}'_{(v)}(kT)\ \tilde{e}(kT) \end{array} \right] = \mathbf{0} \tag{2.90}$$

or, equivalently, by means of equation (2.63),

$$\sum_{k=0}^{K-1} \left[\begin{array}{cccc} \mathbf{i}_{(1)}[k] & \mathbf{0} & \cdots & \mathbf{0} \\ \mathbf{0} & \mathbf{i}_{(2)}[k] & \cdots & \mathbf{0} \\ \cdots & \cdots & \cdots & \cdots \\ \mathbf{0} & \mathbf{0} & \cdots & \mathbf{i}_{(V)}[k] \\ \mathbf{i}'_{(1)}[k] & \mathbf{i}'_{(2)}[k] & \cdots & \mathbf{i}'_{(V)}[k] \end{array} \right] \left[\left[\begin{array}{c} y_{(1)}[k] \\ \cdots \\ y_{(V)}[k] \end{array} \right] - \left[\begin{array}{c} \mathbf{m}_{(1)}^{\mathrm{T}}[k] \\ \cdots \\ \mathbf{m}_{(V)}^{\mathrm{T}}[k] \end{array} \right] \hat{\theta}_{\mathrm{IV}} \right] = \mathbf{0}. \tag{2.91}$$

Finally, by defining

$$\Psi = \begin{bmatrix} \mathbf{i}_{(1)}[0] & \cdots & \mathbf{i}_{(1)}[K-1] & \mathbf{0} & \cdots & \mathbf{0} & \cdots & \mathbf{0} & \cdots & \mathbf{0} \\ \mathbf{0} & \cdots & \mathbf{0} & \mathbf{i}_{(2)}[0] & \cdots & \mathbf{i}_{(2)}[K-1] & \cdots & \mathbf{0} & \cdots & \mathbf{0} \\ \cdots & \cdots & \cdots & \cdots & \cdots & \cdots & \cdots & \cdots & \cdots & \cdots \\ \mathbf{0} & \cdots & \mathbf{0} & \mathbf{0} & \cdots & \mathbf{0} & \cdots & \mathbf{i}_{(V)}[0] & \cdots & \mathbf{i}_{(V)}[K-1] \\ \mathbf{i}'_{(1)}[0] & \cdots & \mathbf{i}'_{(1)}[K-1] & \mathbf{i}'_{(2)}[0] & \cdots & \mathbf{i}'_{(2)}[K-1] & \cdots & \mathbf{i}'_{(V)}[0] & \cdots & \mathbf{i}'_{(V)}[K-1] \end{bmatrix}^{\mathrm{T}} \tag{2.92}$$

one can rewrite (2.91) into the matrix form

$$\Psi^{\mathrm{T}} \left(\mathbf{y} - \mathbf{M}\hat{\theta}_{\mathrm{IV}} \right) = \mathbf{0}, \tag{2.93}$$

so that

$$\hat{\theta}_{\mathrm{IV}} = \left[\Psi^{\mathrm{T}} \mathbf{M} \right]^{-1} \Psi^{\mathrm{T}} \mathbf{y}. \tag{2.94}$$

2.6.1 Approximation of instruments $\mathbf{i}_{(v)}(kT)$ and $\mathbf{i}'_{(v)}(kT)$

From Equations (2.54)–(2.57) and (2.66), it follows that instrument vectors in equations (2.88) and (2.89) can be rewritten as

$$\mathbf{i}_{(v)}(kT) = \begin{bmatrix} 1 \\ \dfrac{\hat{F}(\rho)}{F(\rho)} \tilde{\mathbf{u}}(kT) \end{bmatrix}; \quad \mathbf{i}'_{(v)}(kT) = -\left(\frac{\hat{F}(\rho)}{F(\rho)} \right)^2 \mathbf{y}'_{(v)}(kT), \tag{2.95}$$

where

$$\mathbf{y}'_{(v)}(kT) = \begin{bmatrix} \dfrac{1}{\rho - \bar{p}_1} & \cdots & \dfrac{1}{\rho - \bar{p}_N} \end{bmatrix}^{\mathrm{T}} y'_{(v)}(kT), \tag{2.96}$$

$$y'_{(v)}(kT) = \begin{bmatrix} c_1^{(v)} & \cdots & c_N^{(v)} \end{bmatrix} \tilde{\mathbf{u}}(kT). \tag{2.97}$$

The problem of computing these instruments via equations (2.95)–(2.97) is described in the following.

Equations (2.56) and (2.97) clearly show $\mathbf{i}_{(v)}(kT)$ and $\mathbf{i}'_{(v)}(kT)$ (and, as a consequence, matrix Ψ) are functions of coefficients $\{c_i^{(v)}\}$ and $\{d_i\}$, which are estimated via vector $\hat{\theta}_{\text{IV}}$ in (2.94). This means (2.94) cannot be used for directly finding $\hat{\theta}_{\text{IV}}$, since right-hand side of this equation is also function of $\hat{\theta}_{\text{IV}}$.

On the one hand, computing $\mathbf{i}_{(v)}(kT)$ and $\mathbf{i}'_{(v)}(kT)$ based on the values found for $\{c_i^{(v)}\}$ and $\{d_i\}$ during the previous iteration of the algorithm indeed makes it possible to use (2.94) for finding an estimated $\hat{\theta}_{\text{IV}}$. On the other hand, however, some specific values for $\{d_i\}$ can lead roots of polynomial $F(\rho)$ to become unstable poles in (2.95). To cope with this issue, one can assume that $\mathbf{i}_{(v)}(kT) \approx \tilde{\mathbf{i}}_{(v)}(kT)$ and $\mathbf{i}'_{(v)}(kT) \approx \tilde{\mathbf{i}}'_{(v)}(kT)$ are both valid considerations, with

$$\tilde{\mathbf{i}}_{(v)}(kT) = \begin{bmatrix} 1 \\ \tilde{\mathbf{u}}(kT) \end{bmatrix}; \quad \tilde{\mathbf{i}}'_{(v)}(kT) = -\tilde{\mathbf{y}}'_{(v)}(kT), \tag{2.98}$$

where $\tilde{\mathbf{y}}'_{(v)}(kT)$ represents the values found for $\mathbf{y}'_{(v)}(kT)$ in (2.96) when $y'_{(v)}(kT)$ in (2.97) has its coefficients $\{c_i^{(v)}\}$ replaced with their estimates obtained during the previous algorithm iteration.

When it comes to matrix Ψ, approximations in (2.98) leads to

$$\Psi \approx \begin{bmatrix} \widetilde{\mathbf{U}} & -\widetilde{\mathbf{Y}}' \end{bmatrix}, \tag{2.99}$$

where $\widetilde{\mathbf{U}}$ is given as shown in (2.73) and

$$\widetilde{\mathbf{Y}}' = \begin{bmatrix} \tilde{\mathbf{y}}'_{(1)}[0] & \cdots & \tilde{\mathbf{y}}'_{(1)}[K-1] & \cdots & \tilde{\mathbf{y}}'_{(V)}[0] & \cdots & \tilde{\mathbf{y}}'_{(V)}[K-1] \end{bmatrix}^{\text{T}}. \tag{2.100}$$

2.6.2 Practical implementation of multi-signal IV-RTD-VF

The same implementation steps used for regular multi-signal RTD-VF (described in Section 2.5.1) can also be used for implementing multi-signal IV-RTD-VF. To do so,

one must iteratively solve (2.94) instead of (2.69) during **Step 3**, with matrix Ψ being approximated as describes equation (2.99).

Due to the necessity of computing vectors $\widetilde{\mathbf{y}}'_{(v)}(kT)$ based on the values found for $\{c_i^{(v)}\}$ during the previous algorithm iteration, approximation of matrix Ψ via (2.99) makes IV-RTD-VF to rely on an initial estimate for these coefficients. In general, a satisfactory initial estimate can be obtained by running the regular RTD-VF solution (2.69) during a specific number of iterations. Then, by adopting the estimated values for $\{c_i^{(v)}\}$, one can naturally migrate to the IV iterations.

Lastly, we remark a (2.78)-like state-space discretization can also be used for estimating each v-th vector $\widetilde{\mathbf{y}}'_{(v)}[k]$ for $k = 1, \cdots, K-1$. Comparison between (2.65) and (2.96) reveals such a state-space discretization is given by:

$$\widetilde{\mathbf{y}}'_{(v)}[k] \approx \mathbf{A}_{\mathrm{d}}\widetilde{\mathbf{y}}'_{(v)}[k-1] + \mathbf{B}_{\mathrm{d}}y'_{(v)}[k-1], \quad \widetilde{\mathbf{y}}'_{(v)}[0] = \mathbf{0}. \tag{2.101}$$

2.6.3 Optimal property of multi-signal IV-RTD-VF converged solutions

Differently from regular multi-signal RTD-VF, the presented multi-signal IV-RTD-VF method allows us to guarantee that the solution after its convergence is indeed a local optimum of the nonlinear objective function $J(\theta)$, defined in (2.58). Such an important proposition is proved to be true by means of the following theorem.

Theorem 2.6.1. *Let $\overline{\mathbf{p}}^t$ denote the set of pre-specified poles $\overline{\mathbf{p}} = \begin{bmatrix} \bar{p}_1 & \cdots & \bar{p}_N \end{bmatrix}^T$ used for obtaining $\hat{\theta}^t_{IV}$, where $t \in \mathbb{N}$ emphasizes the iteration number in which $\hat{\theta}_{IV}$ has been computed. If $\hat{\theta}^t_{IV}$ and $\overline{\mathbf{p}}^t$ converge to fixed values $\hat{\theta}'_{IV}$ and $\overline{\mathbf{p}}'$ at a specific iteration $t = t_c$, then $\hat{\theta}^{t_c}_{IV} = \hat{\theta}'_{IV}$ is a local (if not the global) optimum of the nonlinear objective function $J(\theta)$.*

Proof. See Section 2.9.4 for the proof of theorem 2.6.1.

□

2.7 Numerical results using both multi-signal RTD-VF and multi-signal IV-RTD-VF

This section explores two numerical examples to validate the multi-signal RTD-VF and IV-RTD-VF techniques presented in Sections 2.5 and 2.6.

The first example considers actual ringdown data sets extracted from NAEI (YE; LIU, 2012; HWANG; LIU, 2014; HWANG; LIU, 2017) and BIP (MEDFASEE, 2017) systems. In this example, we demonstrate multi-signal RTD-VF may provide superior fitting performance when compared to its single-signal version, in which ringdown signals are modeled independently. Besides, we also show IV-RTD-VF can be used to further refine solutions provided by regular RTD-VF.

The second example uses a single synthetic signal with known modal parameters to demonstrate IV-RTD-VF also overcomes regular RTD-VF when estimation data are corrupted by colored noise. In this example, a statistical analysis is provided.

We remark that most results exposed in this section have been first presented in (SCHUMACHER; OLIVEIRA; KUIAVA, 2019).

2.7.1 NAEI and BIP systems

As already discussed in the example of Section 2.3.2, due to severe weather conditions, an event occurred in the NAEI system on April 27, 2011 (HWANG; LIU, 2017). In Section 2.3.2, modal estimates for NAEI system have been obtained by submitting the difference sequence 'Maine–Florida' (signal Maine *minus* signal Florida) to single-signal estimating methods such as single-signal RTD-VF. In this section, by considering that signals Maine and Florida form the ringdown sequences $y_{(v)}[k]$, $v = 1, 2$, we show both regular multi-signal RTD-VF as well as multi-signal IV-RTD-VF can be alternatively used for simultaneously estimating these signals. Resulting fitted curves considering $N = 8$ poles are shown in Fig. 9. Such a value for N has been found to be the 'dominant order' of signals Florida and Maine and has been calculated by using the mode selection approach described in (TRUDNOWSKI *et al.*, 2008).

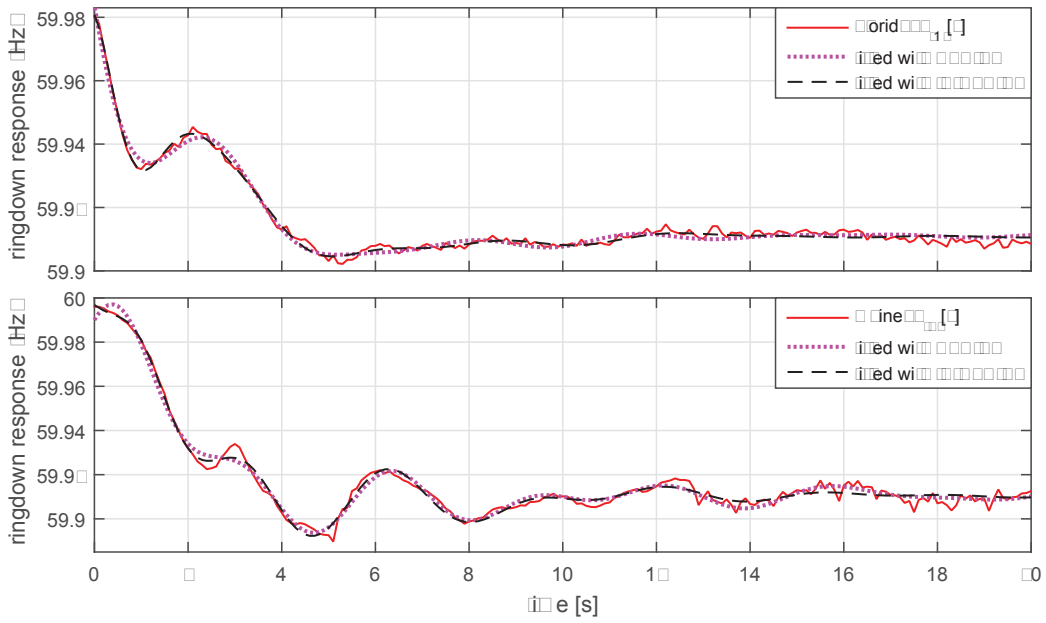

Figure 9 – NAEI system response and fitted ringdown responses obtained when modeling Florida and Maine curves *simultaneously*, i.e., via multi-signal (IV-)RTD-VF.

Fig. 10 depicts the corresponding RMS error (through iterations) for each modeling signal (RMS errors obtained at iteration #50 are emphasized in the right-hand side of this figure). Fig. 10 reveals the strategy adopted for initializing IV-RTD-VF: regular RTD-VF is used for the first twenty iterations to generate an initial estimate for the IV-RTD-VF technique, which is then used for more thirty iterations to obtain further refinement of modal estimates. Although RTD-VF and IV-RTD-VF techniques were both capable of satisfactory estimating Florida and Maine ringdown responses (see Fig. 9), Fig. 10 reveals regular RTD-VF presents higher RMS errors after convergence. Overall simulation time for both techniques is shown in Table 5. Although IV-RTD-VF is slower (since it relies on computing the additional matrix Ψ (see, for instance, equation (2.94)), the time difference of about 0.6 second is not significant.

Table 5 – Overall simulation time in seconds.

RTD-VF	IV-RTD-VF
4.428	5.021

Table 6 shows the resulting eigenvalue estimates $\lambda_l = \sigma_l + j\omega_l$ for the RTD-VF and

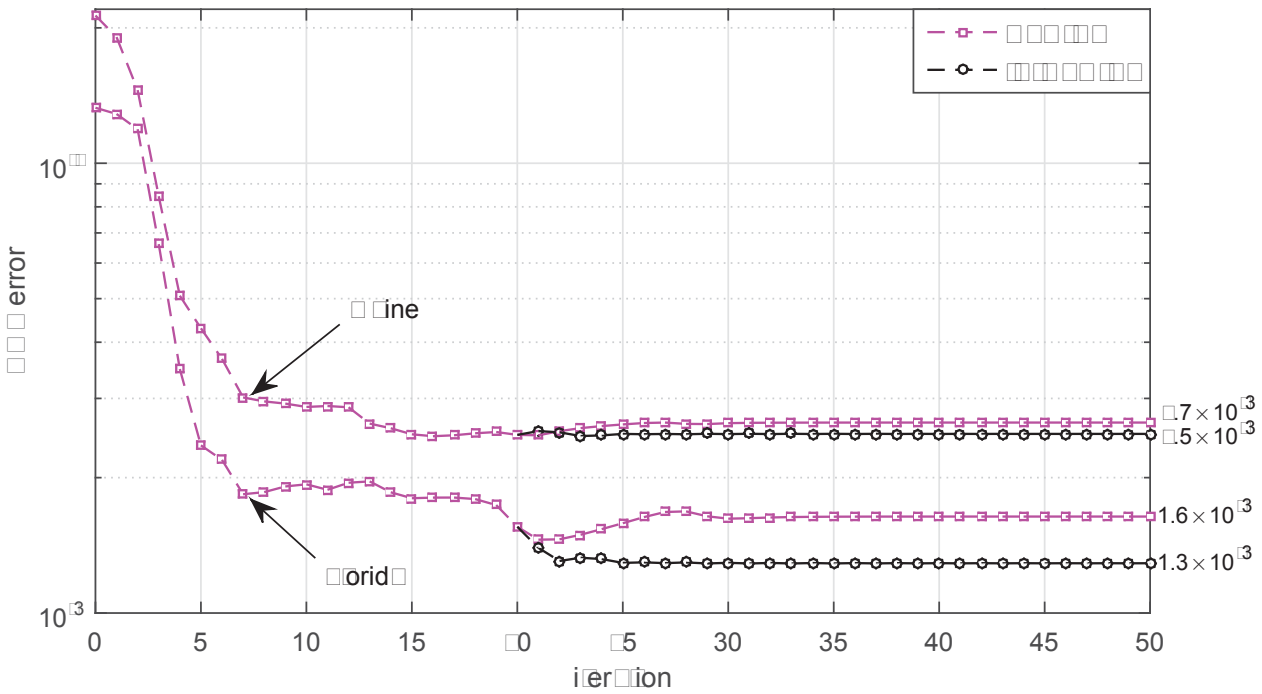

Figure 10 – Fitting error through iterations when modeling Florida and Maine curves with $N = 8$.

IV-RTD-VF techniques. Resulting RMS errors and results for the Matrix Pencil (CROW; SINGH, 2005) and ringdown frequency-domain Vector Fitting (RFD-VF) (PAPADOPOULOS *et al.*, 2016) methods are also provided in this table. In the case of Matrix Pencil and RFD-VF, a multi-signal analysis is formulated based on the average energy approach described in (KONTIS *et al.*, 2018a). As it can be observed through Table 6, the proposed IV-RTD-VF technique presents superior fitting performance (smaller RMS errors) when compared to Matrix Pencil, RFD-VF and RTD-VF. Through Table 6 it is also observed that the estimated eigenvalues λ_1, λ_2 and λ_3 are arguably similar for all methods. On the other hand, estimates for $\lambda_4 = \sigma_4 + j\omega_4$ vary significantly, meaning this mode can be either spurious or weakly observable at Florida and Maine signals. Indeed, as shown in Table 7, by repeating the identification procedure with a reduced model order $N = 6$, one can obtain more consistent estimates for the most strongly observable eigenvalues (λ_1, λ_2 and λ_3). In this particular case, a higher RMS error presented by IV-RTD-VF for Maine signal (when compared to RTD-VF and RFD-VF) is somewhat compensated by a smaller RMS error presented by this same technique for Florida signal. Such a behavior can also be observed in Fig. 11, which depicts the corresponding RMS errors (through iterations)

Table 6 – Comparison between eigenvalue estimates and RMS errors in NAEI system when using $N = 8$.

method	σ_1; σ_2; σ_3; σ_4 [1/s]	ω_1; ω_2; ω_3; ω_4 [rad/s]	RMS error Florida	RMS error Maine
Matrix Pencil	-0.161; -0.245; 0.073; -0.049	2.107; 1.317; 0.919; 4.240	1.1×10^{-2}	1.1×10^{-2}
RFD-VF	-0.151; -0.214; -0.396; -0.209	2.109; 1.328; 0.312; 4.055	2.0×10^{-3}	2.6×10^{-3}
RTD-VF	-0.157; -0.391; -0.398; -0.035	2.075; 1.355; 0.303; 1.302	1.6×10^{-3}	2.7×10^{-3}
IV-RTD-VF	-0.223; -0.221; -0.341; -1.090	2.077; 1.215; 0.462; 2.918	1.3×10^{-3}	2.5×10^{-3}

Table 7 – Comparison between eigenvalue estimates and RMS errors in NAEI system when using $N = 6$.

method	σ_1; σ_2; σ_3 [1/s]	ω_1; ω_2; ω_3 [rad/s]	RMS error Florida	RMS error Maine
Matrix Pencil	-0.140; -0.217; 0.048	2.140; 1.367; 0.731	1.2×10^{-2}	1.3×10^{-2}
RFD-VF	-0.144; -0.219; -0.404	2.131; 1.337; 0.260	2.1×10^{-3}	2.9×10^{-3}
RTD-VF	-0.193; -0.217; -0.372	2.069; 1.311; 0.296	2.0×10^{-3}	2.9×10^{-3}
IV-RTD-VF	-0.199; -0.293; -0.406	2.066; 1.321; 0.253	1.8×10^{-3}	3.0×10^{-3}

for both RTD-VF and IV-RTD-VF.

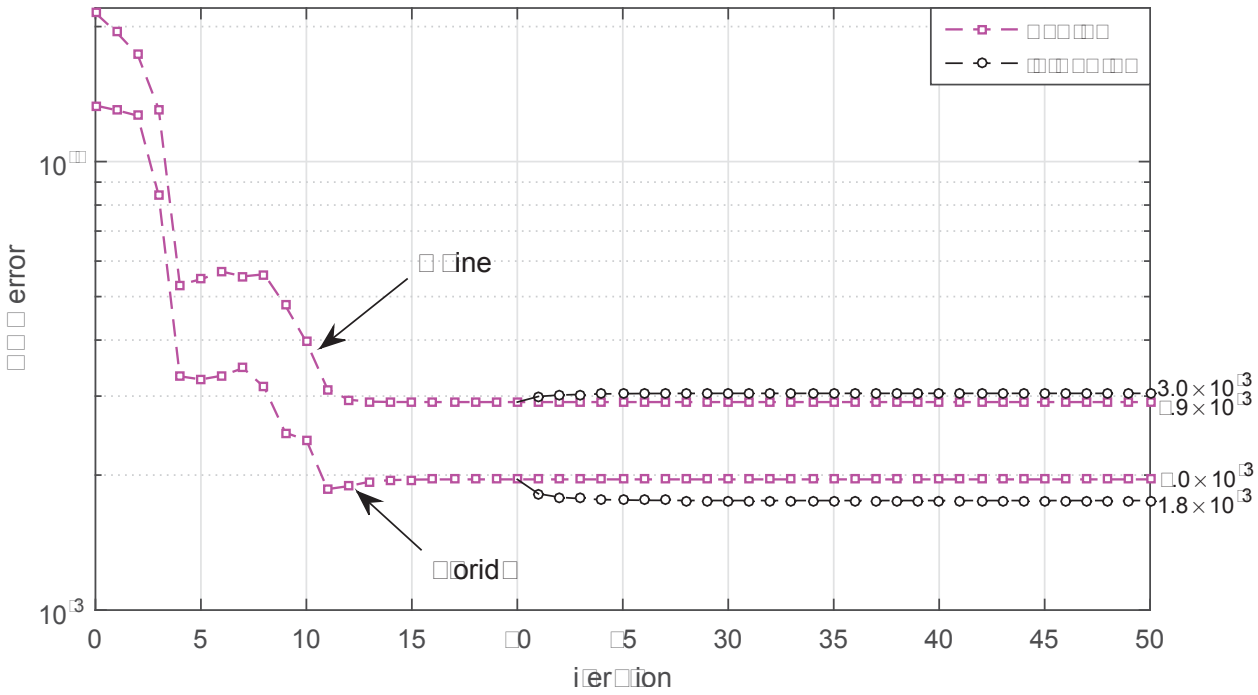

Figure 11 – Fitting error through iterations when modeling Florida and Maine curves with $N = 6$.

One can also consider a scenario where Florida and Maine curves are modeled *independently*, i.e., one at a time, via single-signal IV-RTD-VF, with $N = 6$ dedicated poles

Table 8 – Averaged eigenvalue estimates obtained via single-signal IV-RTD-VF.

method	$\sigma_1;\ \sigma_2;\ \sigma_3$ [1/s]	$\omega_1;\ \omega_2;\ \omega_3$ [rad/s]	RMS error Florida	RMS error Maine
IV-RTD-VF	-0.158; -0.243; -0.394	2.119; 1.352; 0.389	2.0×10^{-3}	3.2×10^{-3}

for each curve (resulting in a total of 12 estimated poles). In this scenario, single-signal IV-RTD-VF presented a RMS error of 1.6×10^{-3} for the Florida signal and a RMS error of 2.7×10^{-3} for the Maine signal. Since here each curve has its own set of 6 estimated poles, such RMS error values are naturally smaller than those presented in Table 7 for the multi-signal scenario, where 6 poles have been used for modeling both Maine and Florida signals simultaneously. A fairer comparison with the multi-signal results of Table 7 can be obtained by averaging both sets of poles estimated through single-signal IV-RTD-VF with the average energy approach described in (KONTIS *et al.*, 2018a). The results are presented in Table 8. This table also shows the corresponding RMS errors for each curve (obtained based on the averaged poles). As it can be observed, pole estimates obtained directly via multi-signal IV-RTD-VF result in better approximations when compared to those obtained indirectly via single-signal IV-RTD-VF.

We now analyze the BIP system case study from Fig. 8, in which five sets of $K = 901$ ringdown response samples are available for modal estimation. In this case study, as already mentioned in this thesis, data sets (which are now all depicted separately through Fig. 12) represent system frequency observed during a reconnection of Itaipu Hydroelectric to the BIP system. Each one of these signals has been measured with a sampling time of $T = (1/60)$s in one of the five regions of Brazil: North, Northeast, Central-West, Southeast and South[3].

Curves fitted via regular multi-signal RTD-VF and multi-signal IV-RTD-VF (considering $N = 7$) are depicted in Fig. 12, whereas Fig. 13 shows their resulting eigenvalue estimates $\lambda_l = \sigma_l + j\omega_l$ in the complex plane. Fig. 13 also shows the eigenvalue estimates obtained when data sets are independently modeled via single-signal (IV-)RTD-VF, also

[3] The website link referred in (MEDFASEE, 2017) exposes a diagram with real-time monitoring data of the BIP system. Such a diagram locates the five universities (UFPA, UNB, UFC, UFSC, UFMG) from which ringdown measurements used in this case study have been extracted.

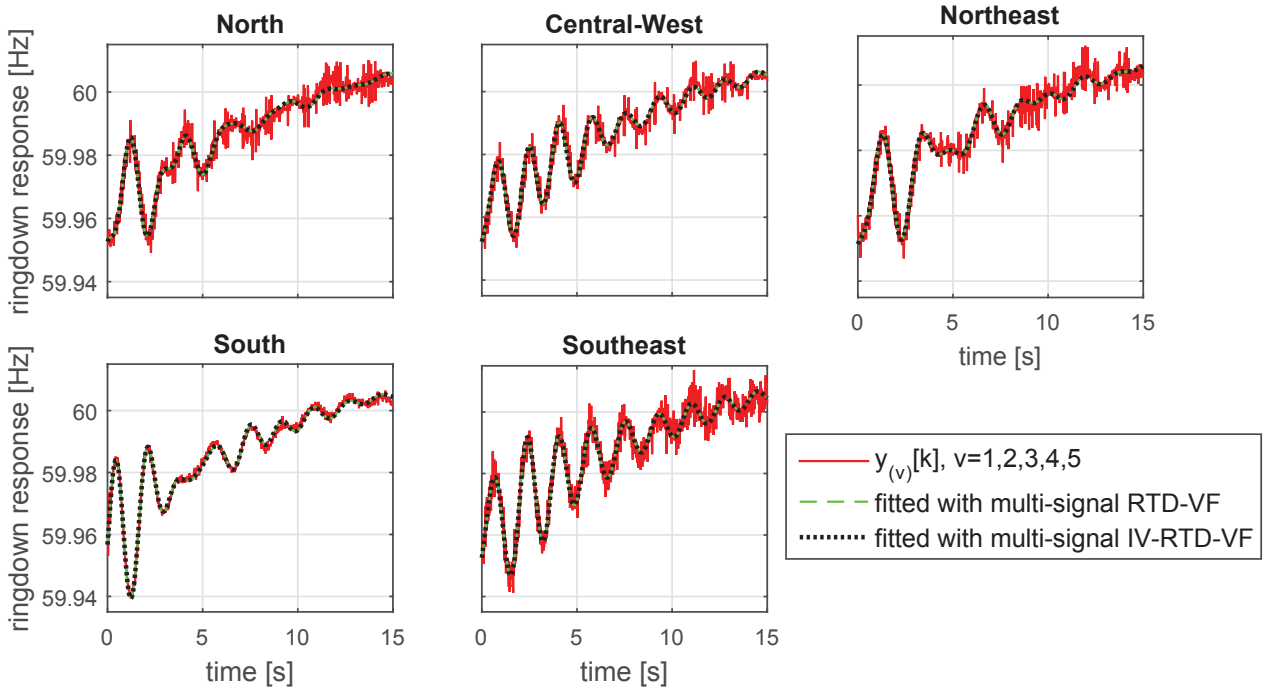

Figure 12 – BIP system response and fitted ringdown responses obtained via multi-signal (IV-)RTD-VF.

with $N = 7$. By using the same model order for both single- and multi-signal methods, it becomes possible to observe that most estimates provided by single-signal (IV-)RTD-VF are in the vicinity of estimates provided by multi-signal (IV-)RTD-VF. In principle, one can argue multi-signal (IV-)RTD-VF generates estimates that tend to represent a wider part of the BIP system, since multiple signals distributed over its five different regions are simultaneously approximated by means of a common set of eigenvalues. Meanwhile, single-signal (IV-)RTD-VF generates estimates that are naturally more related with the particular sections of the system in which each signal under modeling has been measured.

Now, by means of Fig. 14, we analyze sensitivity of multi-signal methods when five different data lengths are considered during modal estimation: $K = \begin{bmatrix} 501 & 601 & 701 & 801 & 901 \end{bmatrix}$. As it can be observed, eigenvalue estimates provided by Matrix Pencil and RFD-VF are more widely spread in the complex plane when compared to those obtained via RTD-VF and IV-RTD-VF. In fact, the latter present estimates concentrated in certain well-delimited regions despite changes in data length, being therefore less susceptible to variations in this parameter. We also remark that estimates observed in Fig. 14 present angular fre-

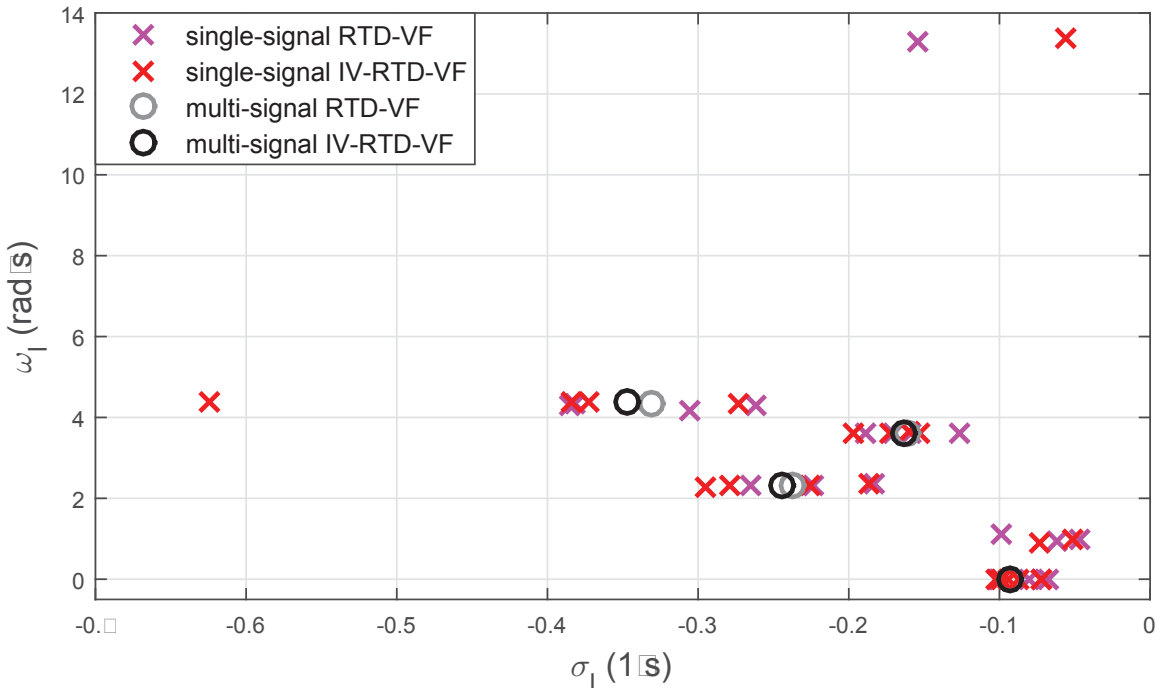

Figure 13 – Eigenvalue estimates obtained when BIP system is modeled with single- and multi-signal RTD-VF as well as with single- and multi-signal IV-RTD-VF.

quencies (ω_l values) which are very close to typical values found in the Brazilian literature (JEREMIAS *et al.*, 2012) for inter-area oscillations between South-Southeast (usually around $2\pi \times 0.70$rad/s), North-Northeast ($2\pi \times 0.58$rad/s) and North-South ($2\pi \times 0.39$rad/s) regions.

2.7.2 Single synthetic signal corrupted by colored noise

This second example directly compares IV-RTD-VF with the single-signal version of regular RTD-VF, which has been originally proposed in (SCHUMACHER; OLIVEIRA; KUIAVA, 2018). In particular, we show this IV formulation can also provide superior fitting performance than regular RTD-VF even when ringdown data samples are corrupted by colored noise, once it guarantees an optimal solution at convergence.

As in the example of Section 2.3.1, the synthetic three-mode signal to be identified is defined in equation (2.102). Such a test signal is discretized with a rate of 100 samples/s

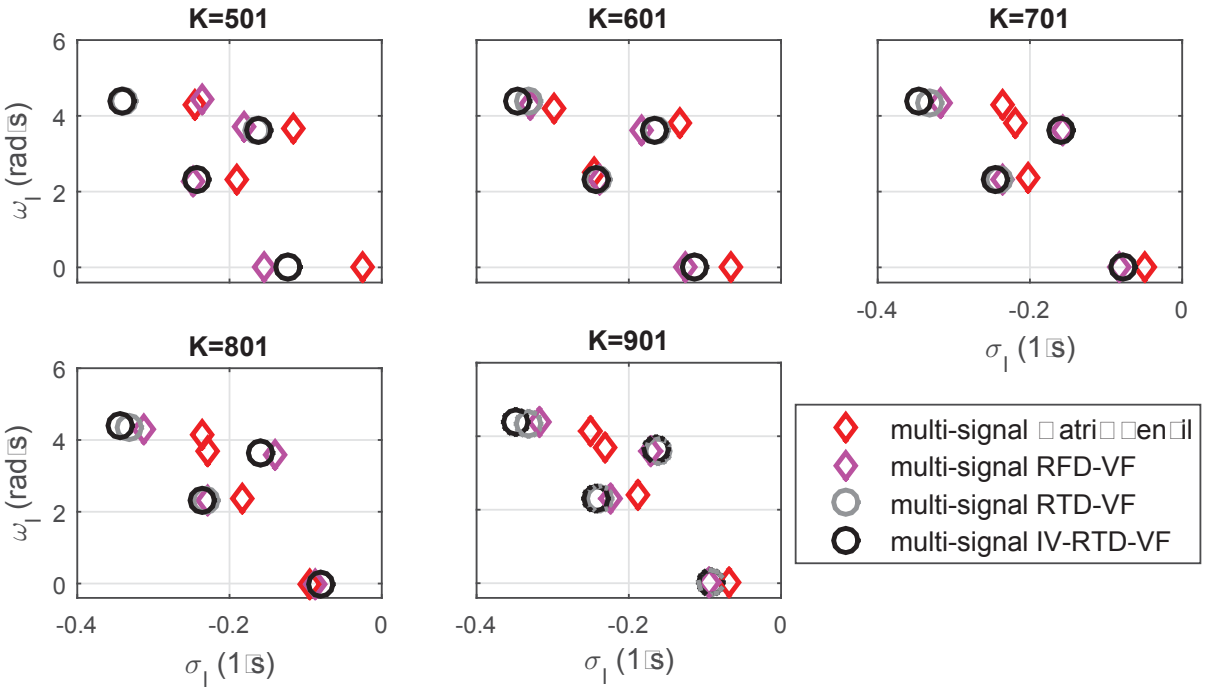

Figure 14 – Comparison between multi-signal methods when five different data lengths are considered during modal estimation.

and assuming a total observation time of 30s.

$$\begin{aligned} y(t) = &\underbrace{1.00 \times \mathrm{e}^{-0.1697t}\cos(1.4351t - 2.5133)}_{\text{mode \#1 } (l=1)} + \\ &\underbrace{1.32 \times \mathrm{e}^{-0.8150t}\cos(3.9270t + 1.8850)}_{\text{mode \#2 } (l=2)} + \\ &\underbrace{1.13 \times \mathrm{e}^{-1.8230t}\cos(6.4654t + 0.3142)}_{\text{mode \#3 } (l=3)}. \end{aligned} \tag{2.102}$$

Here, differently from what has been performed in Section 2.3.1, by defining the following two different sequences of white Gaussian noise of zero mean and variances 0.05^2 and 0.25^2, i.e.,

$$n_0[k] \sim \mathcal{N}(0, 0.05^2), \tag{2.103}$$

$$n_0'[k] \sim \mathcal{N}(0, 0.25^2), \tag{2.104}$$

one can consider each ringdown measurement $y_{(1)}[k]$ to be defined as

$$y_{(1)}[k] = y[k] + n_{\text{meas}}[k] + n_{\text{amb}}[k], \tag{2.105}$$

so that $y_{(1)}[k]$ is contaminated by a measurement noise component $n_{\text{meas}}[k] = n_0[k]$ as well as by an ambient noise component $n_{\text{amb}}[k]$, which is obtained by filtering sequence $n_0'[k]$ by the system dynamics described in (2.102). The resulting signal-to-noise ratios due to measurement and ambient noise are, respectively, 15.59 dB and 17.69 dB. Estimation data are depicted in Fig. 15 (top).

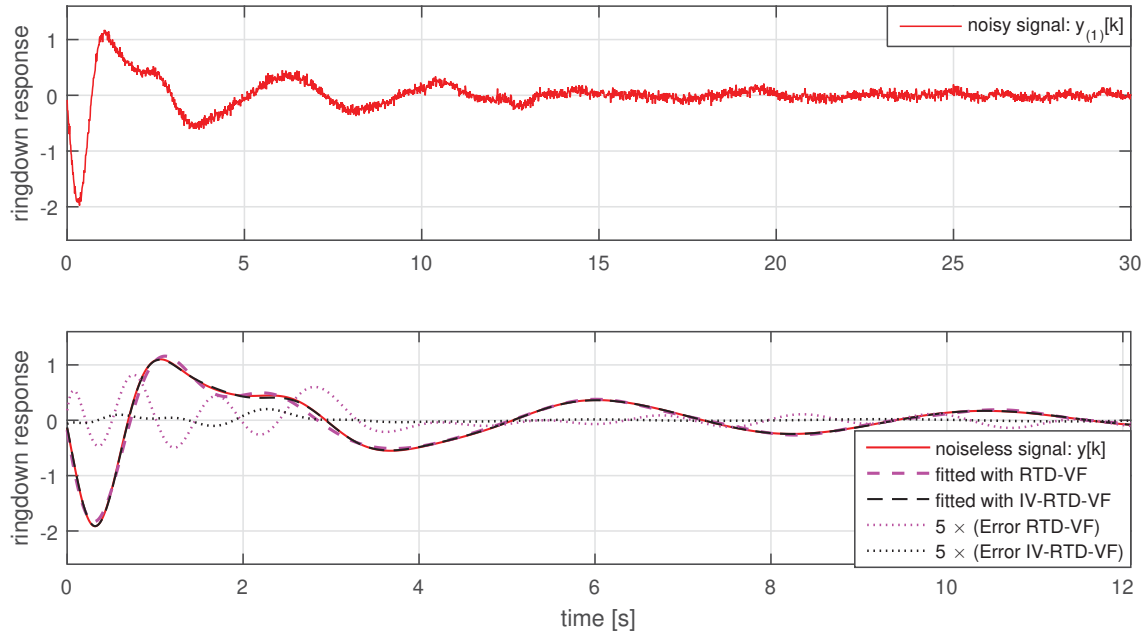

Figure 15 – Noisy measurements (top) and comparison between noise-free samples $y[k]$ and fitted responses (bottom).

Fig. 16 depicts the RMS error (through iterations) for each fitted ringdown response, considering $N = 6$ poles. Similarly to the previous example of Section 2.7.1, regular RTD-VF is used during the first twenty iterations to generate an initial estimate for the IV-RTD-VF technique, which is then used for more twenty iterations to improve modal estimates. Fig. 16 shows that RTD-VF presents a higher RMS error at convergence. Such a result is in agreement with Fig. 15 (bottom), which shows that RTD-VF presents a greater error with respect to the noise-free samples $y[k]$ during first transients (the errors

Table 9 – Gradient of the nonlinear objective function $J(\theta)$ at iteration #40.

	RTD-VF	IV-RTD-VF
$\partial J/\partial h_{\text{dc}}^{(1)}$	0.084×10^{-6}	-0.082×10^{-10}
$\partial J/\partial c_1^{(1)}; \partial J/\partial c_2^{(1)}$	$-0.045\times10^{-5}; -0.010\times10^{-5}$	$0.072\times10^{-10}; 0.134\times10^{-10}$
$\partial J/\partial c_3^{(1)}; \partial J/\partial c_4^{(1)}$	$-0.241\times10^{-5}; -0.298\times10^{-5}$	$-0.286\times10^{-10}; -0.028\times10^{-10}$
$\partial J/\partial c_5^{(1)}; \partial J/\partial c_6^{(1)}$	$0.046\times10^{-5}; -0.017\times10^{-5}$	$-0.007\times10^{-10}; 0.067\times10^{-10}$
$\partial J/\partial d_1; \partial J/\partial d_2$	$-1.406;\ 0.581$	$-0.078\times10^{-10}; -0.036\times10^{-10}$
$\partial J/\partial d_3; \partial J/\partial d_4$	$-0.548;\ 0.890$	$0.049\times10^{-10}; -0.227\times10^{-10}$
$\partial J/\partial d_5; \partial J/\partial d_6$	$-1.105; -0.888$	$0.083\times10^{-10}; 0.218\times10^{-10}$

appear multiplied by 5 to make visualization easier).

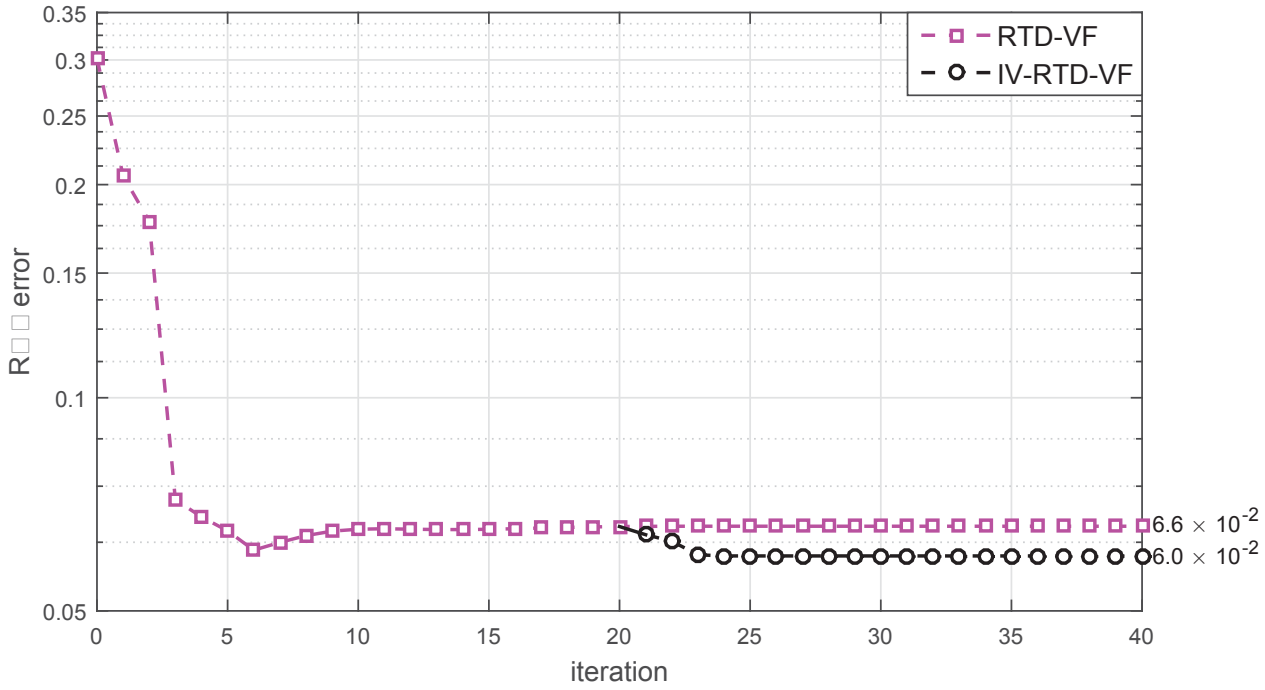

Figure 16 – Fitting error through iterations.

We now investigate the converged values obtained for $\hat{\theta}$ and $\hat{\theta}_{\text{IV}}$ at iteration #40, i.e., after algorithm convergence (see Fig. 16). Table 9 shows the associated gradient of the nonlinear objective function $J(\theta)$. One may consider that the IV formulation indeed converged to a local optimum of $J(\theta)$, since its partial derivatives are all highly close to zero. Meanwhile, regular RTD-VF did not converged to any local optimum.

The results obtained in this case study vary for different realizations since $n_0[k]$ and $n_0'[k]$ are randomly generated sequences. Therefore, we shall repeat the experiment

described so far by considering 1000 different generations for $n_0[k]$ and $n_0'[k]$. The estimated modal parameters obtained from these 1000 generations are represented by their corresponding normalized estimated probability density functions in Fig. 17. In this figure, dotted vertical lines represent the true values for the modal parameters of the synthetic signal $y(t)$, found in (2.102). Concise estimates around all true modes are provided only by IV-RTD-VF. On the other hand, regular RTD-VF clearly presents biased estimates for most parameters. By applying Matrix Pencil and RFD-VF to this statistical analysis, it is verified these techniques also present significant biasing effects.

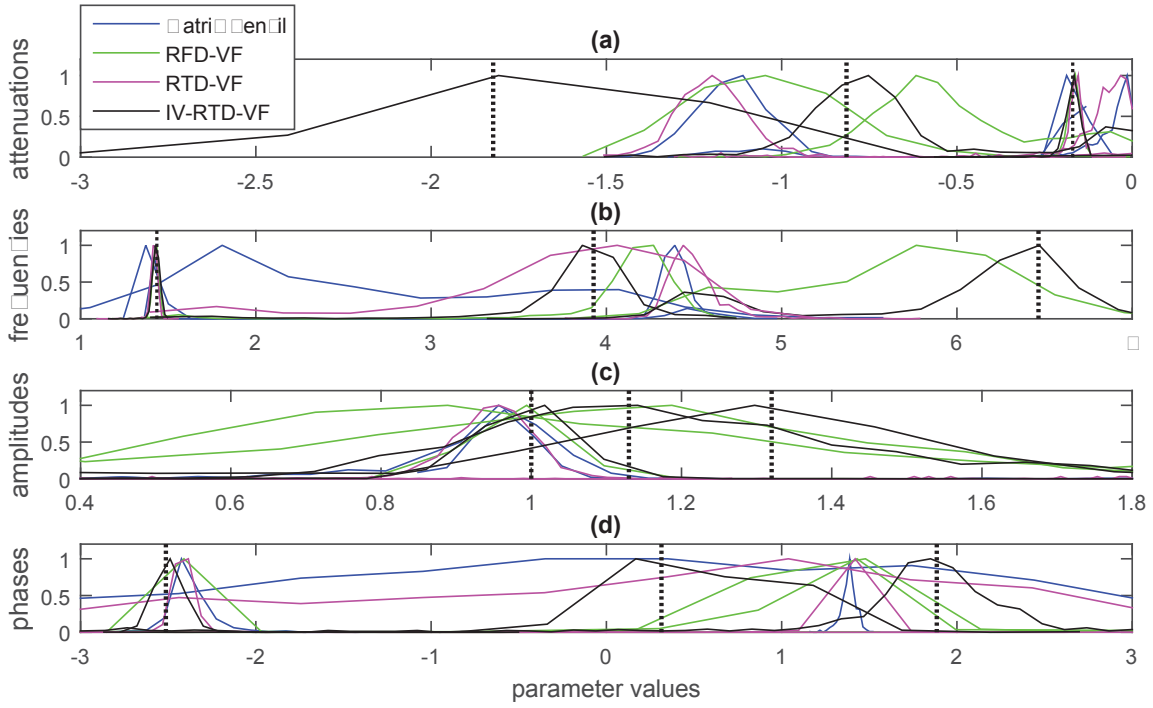

Figure 17 – Estimated normalized probability density functions for (a) attenuations σ_l; (b) frequencies ω_l; (c) amplitudes A_l; (d) phases φ_l. Vertical dotted lines represent the true values for σ_l, ω_l, A_l, φ_l, found in (2.102).

2.8 Final considerations of the chapter

In this chapter, it has been addressed the problem of formulating VF algorithms which are capable of estimating, based on transient (ringdown) data, oscillatory (as well as purely exponential) components of power system signals.

Firstly, based on fundamentals for single-signal modeling, it has been presented – from an objective function perspective – the 'single-signal ringdown time-domain Vector Fitting' (RTD-VF) method originally proposed in (SCHUMACHER; OLIVEIRA; KUIAVA, 2018), which can be considered as a natural extension of the regular TD-VF technique (GRIVET-TALOCIA, 2003) to the context of ringdown analysis. By adopting a suitable state-space discretization which enables an associated artificial unit impulse response to be easily calculated, it has been shown single-signal RTD-VF is capable of providing superior fitting performance over worldwide recognized techniques (such as Prony (HAUER; DEMEURE; SCHARF, 1990) and Matrix Pencil (CROW; SINGH, 2005)) as well as over its counterpart 'ringdown *frequency*-domain Vector Fitting' (RFD-VF) method previously proposed in (PAPADOPOULOS *et al.*, 2016). In particular, based on the results presented in Section 2.3.1, it has also been shown RTD-VF is less sensitive to additive white noise when compared to RFD-VF.

Subsequently, in Section 2.5, single-signal RTD-VF has been generalized into the multi-signal RTD-VF approach proposed in (SCHUMACHER; OLIVEIRA; KUIAVA, 2019), which may provide superior fitting performance than 'single-signal RTD-VF' since it is capable of generating modal estimates by simultaneously processing multiple ringdown signals possibly distributed over different locations of a power system.

Finally, this chapter has presented an IV version of multi-signal RTD-VF which is proved to guarantee local optimums after algorithm convergence. Such a 'multi-signal IV-RTD-VF' method has also been proposed in (SCHUMACHER; OLIVEIRA; KUIAVA, 2019) and may further refine solutions provided by regular multi-signal RTD-VF. Numerical results have also shown IV-RTD-VF may provide asymptotically unbiased estimates when modeling ringdown measurements corrupted by colored noise.

2.9 Chapter appendices

2.9.1 Appendix A: Derivation of equation (2.5)

Based on the well known Euler's formula $e^{jx} = \cos x + j \sin x$ and also on definition given by equation (2.4), one can rewrite (2.1) as follows

$$\bar{y}(t) = h_{\text{dc}} + \sum_{l=1}^{M_{\text{OSC}}} \left(\frac{A_l}{2} e^{j\varphi_l} e^{\lambda_l t} + \frac{A_l}{2} e^{-j\varphi_l} e^{\lambda_l^* t} \right) + \sum_{l=M_{\text{OSC}}+1}^{M} A_l e^{\lambda_l t}. \tag{2.106}$$

Since $\mathcal{L}\left\{ae^{bt}\right\} = a/(s-b)$, Laplace transform of (2.106) reads

$$\overline{Y}(s) = \frac{h_{\text{dc}}}{s} + \sum_{l=1}^{M_{\text{OSC}}} \left(\frac{\frac{1}{2}A_l e^{j\varphi_l}}{s-\lambda_l} + \frac{\frac{1}{2}A_l e^{-j\varphi_l}}{s-\lambda_l^*} \right) + \sum_{l=M_{\text{OSC}}+1}^{M} \frac{A_l}{s-\lambda_l}, \tag{2.107}$$

and can also be combined into a unique partial fraction expansion given by

$$\overline{Y}(s) = \frac{h_{\text{dc}}}{s} + \sum_{i=1}^{N} \frac{r_i}{s-p_i}, \tag{2.108}$$

where variables in this expression can be related to those in (2.107) as describes equations (2.6)–(2.8).

Finally, by considering $G(s) = \sum_{i=1}^{N} \frac{r_i}{s-p_i}$ and $X(s) = 1 = \mathcal{L}\{\delta(t)\}$ in (2.9), one can simply write the inverse Laplace transform of (2.108) as shown in (2.5).

2.9.2 Appendix B: Derivation of approximations in (2.37) and (2.38)

State equations which are capable of describing the dynamic behavior of single-input linear time-invariant systems usually take the form (CHEN, 1999)

$$\frac{d}{dt}\mathbf{x}(t) = \mathbf{A}\mathbf{x}(t) + \mathbf{B}u(t), \quad \mathbf{x}(0) = \mathbf{x}_0, \tag{2.109}$$

where $u(t)$ is the system input, $\mathbf{x}(t)$ is the so-called state vector, which contains N state variables, and $\mathbf{A}$ and $\mathbf{B}$ are constant matrices with dimensions $N \times N$ and $N \times 1$, respectively.

By applying the Laplace transform to equation (2.109), it follows that

$$s\mathbf{X}(s) - \mathbf{x}(0) = \mathbf{A}\mathbf{X}(s) + \mathbf{B}U(s), \tag{2.110}$$

$$s\mathbf{X}(s) - \mathbf{A}\mathbf{X}(s) = \mathbf{x}(0) + \mathbf{B}U(s), \tag{2.111}$$

$$(s\mathbf{I} - \mathbf{A})\mathbf{X}(s) = \mathbf{x}(0) + \mathbf{B}U(s), \tag{2.112}$$

$$\mathbf{X}(s) = (s\mathbf{I} - \mathbf{A})^{-1}\mathbf{x}(0) + (s\mathbf{I} - \mathbf{A})^{-1}\mathbf{B}U(s). \tag{2.113}$$

As shown through equations (2.114)–(2.116), by applying the inverse Laplace transform to (2.113), the analytic solution $\mathbf{x}(t)$ to state equation (2.109) can be written in terms of two different components: $\mathbf{x}_{\text{Zi}}(t)$ and $\mathbf{x}_{\text{ZS}}(t)$. Component $\mathbf{x}_{\text{Zi}}(t)$ is the so-called *zero-input response*, since it corresponds to the solution of (2.109) for $t \geq 0$ when the input $u(t)$ is identically zero for $t \geq 0$, meaning $\mathbf{x}(t)$ is excited exclusively by the initial state $\mathbf{x}(0)$. Meanwhile, component $\mathbf{x}_{\text{ZS}}(t)$ is the so-called *zero-state response*, since it corresponds to the solution of (2.109) for $t \geq 0$ when the initial state $\mathbf{x}(0)$ is zero, meaning $\mathbf{x}(t)$ is excited exclusively by $u(t), t \geq 0$.

$$\mathbf{x}(t) = \mathbf{x}_{\text{Zi}}(t) + \mathbf{x}_{\text{ZS}}(t), \tag{2.114}$$

where

$$\mathbf{x}_{\text{Zi}}(t) = \mathcal{L}^{-1}\left\{(s\mathbf{I} - \mathbf{A})^{-1}\right\}\mathbf{x}(0), \tag{2.115}$$

$$\mathbf{x}_{\text{ZS}}(t) = \mathcal{L}^{-1}\left\{(s\mathbf{I} - \mathbf{A})^{-1}\mathbf{B}U(s)\right\}. \tag{2.116}$$

Based on property in (2.9) and since, as proved in (CHEN, 1999),

$$\mathcal{L}^{-1}\left\{(s\mathbf{I}-\mathbf{A})^{-1}\right\} = \mathrm{e}^{\mathbf{A}t}, \tag{2.117}$$

one can also rewrite $\mathbf{x}_{\mathrm{zi}}(t)$ and $\mathbf{x}_{\mathrm{zs}}(t)$ as follows

$$\mathbf{x}_{\mathrm{zi}}(t) = \mathrm{e}^{\mathbf{A}t}\mathbf{x}(0), \tag{2.118}$$

$$\mathbf{x}_{\mathrm{zs}}(t) = (\rho\mathbf{I}-\mathbf{A})^{-1}\,\mathbf{B}\;u(t). \tag{2.119}$$

One can observe that computing the zero-state response $\mathbf{x}_{\mathrm{zs}}(t)$ analytically for $t \geq 0$ requires knowledge about input $u(t)$ for $t \geq 0$. Unfortunately, in several real-world applications, only a particular set of K measured samples for $u(t)$ is available, for instance, samples $u(kT) = u[k]$, $k = 0, \cdots, K-1$. In such cases, if $u(t)$ does not change significantly between adjacent samples, then, by choosing a sampling period T that respects Nyquist criterion, one can effectively approximate the state vector samples $\mathbf{x}(kT) = \mathbf{x}[k]$, $k = 1, \cdots, K-1$, by recursive use of the following state-space discretization of (2.109) (see (CHEN, 1999) for a proof):

$$\mathbf{x}[k] \approx \mathbf{A}_{\mathrm{d}}\mathbf{x}[k-1] + \mathbf{B}_{\mathrm{d}}u[k-1], \quad \mathbf{x}(0) = \mathbf{x}_0, \tag{2.120}$$

where

$$\mathbf{A}_{\mathrm{d}} = \mathrm{e}^{\mathbf{A}T}; \quad \mathbf{B}_{\mathrm{d}} = \mathbf{A}^{-1}(\mathbf{A}_{\mathrm{d}}-\mathbf{I})\mathbf{B}. \tag{2.121}$$

We now discuss how both approximations (2.37) and (2.38) (used during practical implementation of single-signal RTD-VF) have been formulated.

First, it is observed that the generic expression in (2.119) presents certain similarities with respect to equations in (2.24) and (2.25). In fact, by defining matrices $\mathbf{A}$ and $\mathbf{B}$ as in

equation (2.40), one can show (SCHUMACHER; OLIVEIRA, 2018)

$$(\rho\mathbf{I}-\mathbf{A})^{-1}\mathbf{B}=\left[\begin{array}{ccc}\dfrac{1}{\rho-\bar{p}_i} & \cdots & \dfrac{1}{\rho-\bar{p}_N}\end{array}\right]^{\mathrm{T}}. \tag{2.122}$$

This means that the continuous-time signals $\tilde{\mathbf{y}}(t)$ and $\tilde{\mathbf{u}}(t)$ are solutions for the following pair of state equations

$$\frac{d}{dt}\tilde{\mathbf{y}}(t)=\mathbf{A}\tilde{\mathbf{y}}(t)+\mathbf{B}y(t), \quad \tilde{\mathbf{y}}(0)=\mathbf{0}, \tag{2.123}$$

$$\frac{d}{dt}\tilde{\mathbf{u}}(t)=\mathbf{A}\tilde{\mathbf{u}}(t)+\mathbf{B}\delta(t), \quad \tilde{\mathbf{u}}(0)=\mathbf{0}. \tag{2.124}$$

When it comes to equation (2.123), application of a (2.120)-type discretization naturally leads to expression in (2.37). When it comes to equation (2.124), since its zero-input and zero-state responses read, respectively,

$$\begin{aligned}\tilde{\mathbf{u}}_{\mathrm{Zi}}(t) &= \mathrm{e}^{\mathbf{A}t}\tilde{\mathbf{u}}(0) && (2.125)\\ &= \mathrm{e}^{\mathbf{A}t}\mathbf{0} && (2.126)\\ &= \mathbf{0} && (2.127)\end{aligned}$$

and

$$\begin{aligned}\tilde{\mathbf{u}}_{\mathrm{ZS}}(t) &= \mathcal{L}^{-1}\left\{(s\mathbf{I}-\mathbf{A})^{-1}\mathbf{B}\mathcal{L}\left\{\delta(t)\right\}\right\} && (2.128)\\ &= \mathcal{L}^{-1}\left\{(s\mathbf{I}-\mathbf{A})^{-1}\mathbf{B}\right\} && (2.129)\\ &= \mathcal{L}^{-1}\left\{(s\mathbf{I}-\mathbf{A})^{-1}\right\}\mathbf{B} && (2.130)\\ &= \mathrm{e}^{\mathbf{A}t}\mathbf{B} && (2.131)\end{aligned}$$

the following analytic solution can be obtained:

$$\widetilde{\mathbf{u}}(t) = \widetilde{\mathbf{u}}_{\mathrm{Zi}}(t) + \widetilde{\mathbf{u}}_{\mathrm{ZS}}(t) \tag{2.132}$$

$$= \mathrm{e}^{\mathbf{A}t}\mathbf{B} \tag{2.133}$$

Equation (2.133) is also the analytic solution for the alternative state equation

$$\frac{d}{dt}\widetilde{\mathbf{u}}(t) = \mathbf{A}\widetilde{\mathbf{u}}(t), \quad \widetilde{\mathbf{u}}(0) = \mathbf{B}, \tag{2.134}$$

which can be readily discretized as shown in (2.38).

In principle, instead of using (2.38), one could use the analytical solution $\widetilde{\mathbf{u}}(t) = \mathrm{e}^{\mathbf{A}t}\mathbf{B}$ for computing the values of $\widetilde{\mathbf{u}}(t)$ at the discrete-time instants $t = kT$, $k = 1, \cdots, K-1$. However, as shown in (HIGHAM, 2005), practical evaluation of matrix exponentials demands for a significant number of mathematical computations. A second idea would be to apply the (2.120)-type discretization directly to (2.124). In this case, during evaluation of $\widetilde{\mathbf{u}}[1]$, the resulting state-space discretization would inconveniently require insertion of a well-defined quantity for $\delta(0)$.

2.9.3 Appendix C: Derivation of equation (2.87)

From (2.59) and (2.58), it follows

$$J(\theta) = \sum_{v=1}^{V} \sum_{k=0}^{K-1} \left(y_{(v)}(kT) - \hat{y}_{(v)}(kT) \right)^2 . \tag{2.135}$$

In addition, as it can be observed in equation (2.54), the v-th dc component $h_{\mathrm{dc}}^{(v)}$ and the v-th set of residues $\{c_i^{(v)}\}$ appear only at their corresponding v-th modeling signal

$\hat{y}_{(v)}(t)$. When it comes to (2.135), by also applying the so-called chain rule, this means

$$\begin{bmatrix} \dfrac{\partial}{\partial h_{\mathrm{dc}}^{(v)}} J(\theta) \\ \dfrac{\partial}{\partial c_1^{(v)}} J(\theta) \\ \cdots \\ \dfrac{\partial}{\partial c_N^{(v)}} J(\theta) \end{bmatrix} = -2 \sum_{k=0}^{K-1} \left(\begin{bmatrix} \dfrac{\partial}{\partial h_{\mathrm{dc}}^{(v)}} \\ \dfrac{\partial}{\partial c_1^{(v)}} \\ \cdots \\ \dfrac{\partial}{\partial c_N^{(v)}} \end{bmatrix} \hat{y}_{(v)}(kT) \right) \Big(y_{(v)}(kT) - \hat{y}_{(v)}(kT) \Big), \quad v = 1, \cdots, V \tag{2.136}$$

Meanwhile, modeling signals $\hat{y}_{(v)}(t)$, $v = 1, \cdots, V$, are all parametrized by the same set of residues $\{d_i\}$, so that

$$\begin{bmatrix} \dfrac{\partial}{\partial d_1} J(\theta) \\ \cdots \\ \dfrac{\partial}{\partial d_N} J(\theta) \end{bmatrix} = -2 \sum_{v=1}^{V} \sum_{k=0}^{K-1} \left(\begin{bmatrix} \dfrac{\partial}{\partial d_1} \\ \cdots \\ \dfrac{\partial}{\partial d_N} \end{bmatrix} \hat{y}_{(v)}(kT) \right) \Big(y_{(v)}(kT) - \hat{y}_{(v)}(kT) \Big). \tag{2.137}$$

Since parameters within θ are arranged as in (2.57), one can use definitions (2.88) and (2.89) in equations (2.136) and (2.137) to write $\dfrac{\partial}{\partial \theta} J(\theta)$ as shown in (2.87).

2.9.4 Appendix D: Proof of theorem 2.6.1

In order to prove theorem 2.6.1, we make explicit dependences on θ and $\overline{\mathbf{p}}$ that involved variables might have. One can identify if a specific variable depends on θ or $\overline{\mathbf{p}}$ by inspection of equations presented in Sections 2.5 and 2.6.

If $\hat{\theta}_{\mathrm{LO}}$ denotes a local optimum of $J(\theta)$, then it necessarily satisfies the local/global optimality condition $\left.\dfrac{\partial J}{\partial \theta}\right|_{\theta=\hat{\theta}_{\mathrm{LO}}} = \mathbf{0}$. Based on equation (2.87), this means

$$\begin{bmatrix} \displaystyle\sum_{k=0}^{K-1} \mathbf{i}_{(1)}(kT, \hat{\theta}_{\mathrm{LO}}, \overline{\mathbf{p}})\ e_{(1)}(kT, \hat{\theta}_{\mathrm{LO}}, \overline{\mathbf{p}}) \\ \cdots \\ \displaystyle\sum_{k=0}^{K-1} \mathbf{i}_{(V)}(kT, \hat{\theta}_{\mathrm{LO}}, \overline{\mathbf{p}})\ e_{(V)}(kT, \hat{\theta}_{\mathrm{LO}}, \overline{\mathbf{p}}) \\ \displaystyle\sum_{v=1}^{V} \sum_{k=0}^{K-1} \mathbf{i}'_{(v)}(kT, \hat{\theta}_{\mathrm{LO}}, \overline{\mathbf{p}})\ e_{(v)}(kT, \hat{\theta}_{\mathrm{LO}}, \overline{\mathbf{p}}) \end{bmatrix} = \mathbf{0}. \tag{2.138}$$

Meanwhile, when it comes to the IV-RTD-VF approach, approximations $e_{(v)}(kT,\theta,\overline{\mathbf{p}}) \approx \tilde{e}_{(v)}(kT,\hat{\theta}^t_{\mathrm{IV}},\overline{\mathbf{p}}^t)$, $\mathbf{i}_{(v)}(kT,\theta,\overline{\mathbf{p}}) \approx \tilde{\mathbf{i}}_{(v)}(kT,\overline{\mathbf{p}}^t)$ and $\mathbf{i}'_{(v)}(kT,\theta,\overline{\mathbf{p}}) \approx \tilde{\mathbf{i}}'_{(v)}(kT,\hat{\theta}^{t-1}_{\mathrm{IV}},\overline{\mathbf{p}}^t)$ make it possible to formulate the approximated problem:

$$\left[\begin{array}{c} \displaystyle\sum_{k=0}^{K-1} \tilde{\mathbf{i}}_{(1)}(kT,\overline{\mathbf{p}}^t)\ \tilde{e}_{(1)}(kT,\hat{\theta}^t_{\mathrm{IV}},\overline{\mathbf{p}}^t) \\ \cdots \\ \displaystyle\sum_{k=0}^{K-1} \tilde{\mathbf{i}}_{(V)}(kT,\overline{\mathbf{p}}^t)\ \tilde{e}_{(V)}(kT,\hat{\theta}^t_{\mathrm{IV}},\overline{\mathbf{p}}^t) \\ \displaystyle\sum_{v=1}^{V}\sum_{k=0}^{K-1} \tilde{\mathbf{i}}'_{(v)}(kT,\hat{\theta}^{t-1}_{\mathrm{IV}},\overline{\mathbf{p}}^t)\ \tilde{e}_{(v)}(kT,\hat{\theta}^t_{\mathrm{IV}},\overline{\mathbf{p}}^t), \end{array}\right] = \mathbf{0}, \tag{2.139}$$

where $\overline{\mathbf{p}}^t$ is specified so that polynomial $\hat{F}(\rho,\overline{\mathbf{p}})$ equals the estimate obtained for polynomial $F(\rho,\theta,\overline{\mathbf{p}})$ during the previous algorithm iteration, i.e, so that equation (2.140) is satisfied.

$$\hat{F}(\rho,\overline{\mathbf{p}}^t) = F(\rho,\hat{\theta}^{t-1}_{\mathrm{IV}},\overline{\mathbf{p}}^{t-1}). \tag{2.140}$$

Now, if there is a sufficiently small positive value ε and a sufficiently large iteration number t_c such that $\left|\hat{\theta}^{t_c}_{\mathrm{IV}} - \hat{\theta}^{t_c+j}_{\mathrm{IV}}\right| < \varepsilon$ and $|\overline{\mathbf{p}}^{t_c} - \overline{\mathbf{p}}^{t_c+j}| < \varepsilon$ for all $j \in \mathbb{N}$, then one can consider $\hat{\theta}^t_{\mathrm{IV}}$ and $\overline{\mathbf{p}}^t$ assume fixed values $\hat{\theta}'_{\mathrm{IV}}$ and $\overline{\mathbf{p}}'$ for any $t \geq t_c$.

For iteration $t = t_c + 1$, it follows from equation (2.140) that

$$\hat{F}(\rho,\overline{\mathbf{p}}^{t_c+1}) = F(\rho,\hat{\theta}^{t_c}_{\mathrm{IV}},\overline{\mathbf{p}}^{t_c}). \tag{2.141}$$

Once

$$\hat{\theta}^{t_c+1}_{\mathrm{IV}} = \hat{\theta}^{t_c}_{\mathrm{IV}} = \hat{\theta}'_{\mathrm{IV}} \quad \text{and} \quad \overline{\mathbf{p}}^{t_c+1} = \overline{\mathbf{p}}^{t_c} = \overline{\mathbf{p}}', \tag{2.142}$$

one can also rewrite (2.141) as

$$\hat{F}(\rho,\overline{\mathbf{p}}') = F(\rho,\hat{\theta}'_{\mathrm{IV}},\overline{\mathbf{p}}'), \quad \text{so that} \quad \hat{F}(\rho,\overline{\mathbf{p}}')/F(\rho,\hat{\theta}'_{\mathrm{IV}},\overline{\mathbf{p}}') = 1. \tag{2.143}$$

Based on these results, it becomes possible to rewrite equation (2.139) for iteration $t = t_c + 1$ as

$$\left[\begin{array}{c} \sum_{k=0}^{K-1} \mathbf{i}_{(1)}(kT, \hat{\theta}'_{\mathrm{IV}}, \overline{\mathbf{p}}')\ e_{(1)}(kT, \hat{\theta}'_{\mathrm{IV}}, \overline{\mathbf{p}}') \\ \cdots \\ \sum_{k=0}^{K-1} \mathbf{i}_{(V)}(kT, \hat{\theta}'_{\mathrm{IV}}, \overline{\mathbf{p}}')\ e_{(V)}(kT, \hat{\theta}'_{\mathrm{IV}}, \overline{\mathbf{p}}') \\ \sum_{v=1}^{V} \sum_{k=0}^{K-1} \mathbf{i}'_{(v)}(kT, \hat{\theta}'_{\mathrm{IV}}, \overline{\mathbf{p}}')\ e_{(v)}(kT, \hat{\theta}'_{\mathrm{IV}}, \overline{\mathbf{p}}') \end{array}\right] = \mathbf{0} \tag{2.144}$$

since, by means of definitions in (2.142)–(2.143), (2.60)–(2.61) and (2.95)–(2.98),

$$\begin{aligned} \tilde{e}_{(v)}(kT, \hat{\theta}^{t_c+1}_{\mathrm{IV}}, \overline{\mathbf{p}}^{t_c+1}) &= \tilde{e}_{(v)}(kT, \hat{\theta}'_{\mathrm{IV}}, \overline{\mathbf{p}}') \\ &= \frac{F(\rho, \hat{\theta}'_{\mathrm{IV}}, \overline{\mathbf{p}}')}{\hat{F}(\rho, \overline{\mathbf{p}}')} y_{(v)}(kT) - \left(h^{(v)}_{\mathrm{dc}} + \frac{B^{(v)}(\rho, \hat{\theta}'_{\mathrm{IV}}, \overline{\mathbf{p}}')}{\hat{F}(\rho, \overline{\mathbf{p}}')} \delta(kT) \right) \\ &= \frac{F(\rho, \hat{\theta}'_{\mathrm{IV}}, \overline{\mathbf{p}}')}{F(\rho, \hat{\theta}'_{\mathrm{IV}}, \overline{\mathbf{p}}')} y_{(v)}(kT) - \left(h^{(v)}_{\mathrm{dc}} + \frac{B^{(v)}(\rho, \hat{\theta}'_{\mathrm{IV}}, \overline{\mathbf{p}}')}{F(\rho, \hat{\theta}'_{\mathrm{IV}}, \overline{\mathbf{p}}')} \delta(kT) \right) \\ &= e_{(v)}(kT, \hat{\theta}'_{\mathrm{IV}}, \overline{\mathbf{p}}') \end{aligned} \tag{2.145}$$

$$\begin{aligned} \tilde{\mathbf{i}}_{(v)}(kT, \overline{\mathbf{p}}^{t_c+1}) &= \tilde{\mathbf{i}}_{(v)}(kT, \overline{\mathbf{p}}') \\ &= \left[\begin{array}{c} 1 \\ \tilde{\mathbf{u}}(kT, \overline{\mathbf{p}}') \end{array}\right] \\ &= \left[\begin{array}{c} 1 \\ \dfrac{\hat{F}(\rho, \overline{\mathbf{p}}')}{F(\rho, \hat{\theta}'_{\mathrm{IV}}, \overline{\mathbf{p}}')} \tilde{\mathbf{u}}(kT, \overline{\mathbf{p}}') \end{array}\right] \\ &= \mathbf{i}_{(v)}(kT, \hat{\theta}'_{\mathrm{IV}}, \overline{\mathbf{p}}') \end{aligned} \tag{2.146}$$

$$\begin{aligned} \tilde{\mathbf{i}}'_{(v)}(kT, \hat{\theta}^{t_c}_{\mathrm{IV}}, \overline{\mathbf{p}}^{t_c+1}) &= -\tilde{\mathbf{y}}'_{(v)}(kT, \hat{\theta}^{t_c}_{\mathrm{IV}}, \overline{\mathbf{p}}^{t_c+1}) \\ &= -\tilde{\mathbf{y}}'_{(v)}(kT, \hat{\theta}'_{\mathrm{IV}}, \overline{\mathbf{p}}') \\ &= -\left(\frac{\hat{F}(\rho, \overline{\mathbf{p}}')}{F(\rho, \hat{\theta}'_{\mathrm{IV}}, \overline{\mathbf{p}}')} \right)^2 \mathbf{y}'_{(v)}(kT, \hat{\theta}'_{\mathrm{IV}}, \overline{\mathbf{p}}') \\ &= \mathbf{i}'_{(v)}(kT, \hat{\theta}'_{\mathrm{IV}}, \overline{\mathbf{p}}') \end{aligned} \tag{2.147}$$

Expression (2.144) matches exactly with the local optimality condition in (2.138), meaning that $\hat{\theta}'_{\mathrm{IV}}$ is guaranteed a local (if not the global) optimum of $J(\theta)$.

3 FREQUENCY-DOMAIN SYSTEM IDENTIFICATION

In this chapter, it is addressed the problem of formulating VF algorithms for system identification based on frequency-domain (frequency response) data. Numerical examples exposed in this chapter focus mainly on frequency response data extracted from power and inductive potential transformers.

Firstly, it is formulated, in frequency-domain (FD), the problem of estimating linear models formed by rational basis function (RBF) expansions. In this context, it is also established a unifying FD-VF method for estimating these models. The terminology 'unifying' is used to emphasize that such a method can be similarly applied for estimating models formed either by continuous- or discrete-time RBFs, being compatible, for instance, with any RBF set listed in (SCHUMACHER; OLIVEIRA, 2018). Subsequently, this unifying FD-VF method is transformed into the instrumental variable (IV-)FD-VF iterations, originally proposed in (SCHUMACHER; OLIVEIRA, 2019). In fact, the IV-FD-VF approach proposed in this chapter consists of a multi-input multi-output (MIMO) generalization of the single-input single-output (SISO) approach proposed in (SCHUMACHER; OLIVEIRA, 2019). As will be shown, since it is proved to guarantee local optimums after algorithm convergence, IV-FD-VF may provide superior fitting performance when compared to standard FD-VF algorithms such as, for instance, *vectfit3* (PACKAGE, 2008), which is still one of the most popular implementations of standard FD-VF. Indeed, IV-FD-VF can be used for further refining solutions provided by *vectfit3* and can be regarded as a frequency-domain extension of the discrete time-domain IV-based approach in (SCHUMACHER; OLIVEIRA, 2017).

3.1 Problem statement and a unifying FD-VF method

A stable single-input single-output (SISO) linear time-invariant system can be described in terms of its scalar input $U_0(\alpha)$ and its scalar output $Y_0(\alpha)$ as

$$Y_0(\alpha) = G(\alpha)U_0(\alpha) + V(\alpha), \qquad \alpha = z \text{ or } s \tag{3.1}$$

where $V(\alpha)$ represents the additive disturbance at the system output, and α determines if the system is described either in continuous-time ($\alpha = s$) or discrete-time ($\alpha = z$).

Based on these definitions, one can establish the frequency-domain system identification problem of estimating a rational basis function (RBF) model for $G(\alpha)$ based on a set of noisy frequency response data samples $\{G'(\alpha_k), \alpha_k\}, k = 1, \cdots, N$, where each term α_k is associated with a frequency ω_k according to one of the following relations:

$$\alpha_k = \begin{cases} s_k = j\omega_k & \text{(continuous-time case)} \\ z_k = e^{j2\pi\omega_k/\omega_\mathrm{s}} & \text{(discrete-time case)} \end{cases} \tag{3.2}$$

where ω_s denotes sampling frequency. Note that an additive noise component $V_\mathrm{U}(\alpha_k)$ appears in the measured frequency response of system $G'(\alpha_k)$ due to the input-output relation in (3.1):

$$\frac{Y_0(\alpha_k)}{U_0(\alpha_k)} = G(\alpha_k) + V_\mathrm{U}(\alpha_k) = G'(\alpha_k), \tag{3.3}$$

where $V_\mathrm{U}(\alpha_k) = V(\alpha_k)/U_0(\alpha_k)$.

The desired RBF model must have a N-th order transfer function structure in the form

$$\bar{G}(\alpha) = r_0 + \sum_{i=1}^{N} r_i \Phi_i(\alpha, \mathbf{p}), \tag{3.4}$$

where $\{r_i\}$ are the unknown model structure coefficients and $\{\Phi_i(\alpha, \mathbf{p})\}$ denotes a set of N rational basis functions which are completely parametrized by the unknown poles of $\bar{G}(\alpha)$, here grouped into vector $\mathbf{p} = \begin{bmatrix} p_1 & \cdots & p_N \end{bmatrix}^\mathrm{T}$.

In this chapter, it is also assumed (3.4)-like model structures can be represented by a linear state-space realization given by

$$\begin{cases} \alpha\mathbf{X}(\alpha) &= \mathbf{A}\mathbf{X}(\alpha) + \mathbf{B}U_0(\alpha), \\ Y(\alpha) &= \begin{bmatrix} r_1 & \cdots & r_N \end{bmatrix}\mathbf{X}(\alpha) + r_0 U_0(\alpha), \end{cases} \tag{3.5}$$

which means that the pair of matrices $\mathbf{A} \in \mathbb{C}^{N\times N}$ and $\mathbf{B} \in \mathbb{C}^{N\times 1}$ must necessarily satisfy the well known state condition

$$\mathbf{\Phi}(\alpha) = \begin{bmatrix} \Phi_1(\alpha, \mathbf{p}) & \cdots & \Phi_N(\alpha, \mathbf{p}) \end{bmatrix}^{\mathrm{T}} = (\alpha\mathbf{I} - \mathbf{A})^{-1}\mathbf{B}, \tag{3.6}$$

From equation (3.6), it is clear matrices $\mathbf{A}$ and $\mathbf{B}$ define the RBF set used in the model structure. In principle, any continuous- or discrete-time set $\{\Phi_i(\alpha, \mathbf{p})\}$ that fits into definition (3.6) can be used as RBFs.

When it comes to continuous-time system identification, perhaps the most common choice is to use a set of partial fractions as RBFs (GRIVET-TALOCIA; GUSTAVSEN, 2016; GUSTAVSEN; SEMLYEN, 1999), i.e.,

$$\Phi_i(s, \mathbf{p}) = \frac{1}{s - p_i}, \quad i = 1, \cdots, N. \tag{3.7}$$

For this particular case, $\mathbf{A}$ and $\mathbf{B}$ are as follows

$$\mathbf{A} = \begin{bmatrix} p_1 & 0 & \cdots & 0 \\ 0 & p_2 & \cdots & 0 \\ \vdots & \vdots & \ddots & \vdots \\ 0 & 0 & \cdots & p_N \end{bmatrix}; \qquad \mathbf{B} = \begin{bmatrix} 1 \\ 1 \\ \vdots \\ 1 \end{bmatrix}. \tag{3.8}$$

Meanwhile, discrete-time approaches many times consider models formed by the so-called discrete-time Takenaka-Malmquist orthonormal basis functions (NOURI; ACHAR; NAKHLA, 2010; HEUBERGER; VAN DEN HOF; WAHLBERG, 2005)

$$\Phi_i(z, \mathbf{p}) = \frac{\sqrt{1 - |p_i|^2}}{z - p_i} \prod_{j=1}^{i-1} \left(\frac{1 - p_j^* z}{z - p_j} \right), \quad i = 1, \cdots, N \tag{3.9}$$

The corresponding state-space construction for the RBF set in (3.9) can be found, for instance, in (SCHUMACHER; OLIVEIRA, 2018). In fact, in (SCHUMACHER; OLIVEIRA, 2018) it is listed the corresponding state-space construction of several continuous- and discrete-time RBF sets for which (3.6) holds.

Now, from a broader perspective, instead of considering the identification of SISO systems only, one can consider the more general problem which consists of estimating all V transfer functions from a multi-input multi-output (MIMO) system simultaneously[1]:

$$G_{(v)}(\alpha) \approx \bar{G}_{(v)}(\alpha); \quad v = 1, \cdots, V, \tag{3.10}$$

where

$$\bar{G}_{(v)}(\alpha) = r_0^{(v)} + \sum_{i=1}^{N} r_i^{(v)} \Phi_i(\alpha, \mathbf{p}); \quad v = 1, \cdots, V. \tag{3.11}$$

As it can be observed through Equation (3.11), all V transfer functions from the MIMO system are here considered to be approximated with a unique set of poles $\mathbf{p}$, although each v-th modeling transfer function $\bar{G}_{(v)}(\alpha)$ has its own set of coefficients $\{r_i^{(v)}\}$, $i = 0, \cdots, N$.

If the MIMO system transfer functions are only known by means of the (possibly) noisy frequency response data samples $\{G'_{(v)}(\alpha_k), \alpha_k\}, k = 1, \cdots, K$, $v = 1, \cdots, V$, then estimating all V RBF models $\bar{G}_{(v)}(\alpha)$ in terms of their poles $\mathbf{p}$ and coefficients $\{r_i^{(v)}\}$ requires the definition of a certain estimation criterion. By means of the absolute weighted least-squares criterion, estimating $\mathbf{p}$ and $\{r_i^{(v)}\}$ becomes the following nonlinear optimization problem:

$$\begin{aligned} \hat{\gamma} &= \arg\min_{\gamma} \sum_{v=1}^{V} \sum_{k=1}^{K} \left| W_{(v)}(\alpha_k) \left(G'_{(v)}(\alpha_k) - \bar{G}_{(v)}(\alpha_k) \right) \right|^2 \\ &= \arg\min_{\gamma} \sum_{v=1}^{V} \sum_{k=1}^{K} \left| W_{(v)}(\alpha_k) \left(G'_{(v)}(\alpha_k) - \left(r_0^{(v)} + \sum_{i=1}^{N} r_i^{(v)} \Phi_i(\alpha_k, \mathbf{p}) \right) \right) \right|^2 \end{aligned} \tag{3.12}$$

[1] The set of transfer functions $G_{(v)}(\alpha), v = 1, \cdots, V$ are indeed elements of the system transfer matrix $\mathbf{G}$, which satisfies $\mathbf{y} = \mathbf{G}\mathbf{u}$, being $\mathbf{u}$ and $\mathbf{y}$ column vectors which concatenate the system inputs and outputs, respectively.

where $\hat{\gamma}$ can be considered to be an estimate for parameter vector γ, that, as shown by equation (3.13), concatenates the parameters of all modeling transfer functions $\{\bar{G}_{(v)}(\alpha)\}$, $v = 1, \cdots, V$. In (3.12), $W_{(v)}(\alpha_k)$ is a weighting function to be selected by the user. Choosing this weighting function goes beyond the scope of this chapter, although the interested reader is hereby referred to reference (PORDANJANI *et al.*, 2011), which analyses the adoption of different weighting functions in frequency-domain system identification.

$$\gamma = \left[\begin{array}{cccccccccc} r_0^{(1)} & \cdots & r_N^{(1)} & \cdots & r_0^{(V)} & \cdots & r_N^{(V)} & p_1 & \cdots & p_N \end{array} \right]^{\mathrm{T}}, \tag{3.13}$$

It is also important to remark that estimating γ via (3.12) constitutes a nonlinear optimization problem, since poles $\{p_i\}$ appear in the denominator of $\bar{G}_{(v)}(\alpha_k)$.

The main objective here is to present the IV-FD-VF iterations (SCHUMACHER; OLIVEIRA, 2019) from a MIMO system identification perspective. This means an optimal way for estimating the RBF model parameters $\{r_i^{(v)}\}$ and $\mathbf{p}$ is here addressed. In fact, IV-FD-VF may be considered as a unifying instrumental variable version of the standard FD-VF iterations (GRIVET-TALOCIA; GUSTAVSEN, 2016; DESCHRIJVER; HAEGEMAN; DHAENE, 2007; GUSTAVSEN, 2002; GUSTAVSEN; SEMLYEN, 1999), since it is also based on transforming (3.12) into a sequence of linear problems where coefficient sets are estimated by means of pre-specified update-dependent poles.

In what follows, we briefly introduce a formal and unifying definition for the standard FD-VF iterations. Such a unifying definition is then used in Section 3.2 for deriving the IV-FD-VF iterations (SCHUMACHER; OLIVEIRA, 2019).

The key idea of standard VF implementations is to replace the problem of estimating the pole set $\mathbf{p}$ within the original model structures in (3.11) by the equivalent problem of estimating the poles of the following alternative model structures (GRIVET-TALOCIA; GUSTAVSEN, 2016; DESCHRIJVER; HAEGEMAN; DHAENE, 2007; GUSTAVSEN;

SEMLYEN, 1999)

$$\begin{aligned}\hat{G}_{(v)}(\alpha) &= \frac{B^{(v)}(\alpha)}{F(\alpha)}, \\ &= \frac{c_0^{(v)} + \sum_{i=1}^{N} c_i^{(v)} \Phi_i(\alpha, \bar{\mathbf{p}})}{1 + \sum_{i=1}^{N} d_i \Phi_i(\alpha, \bar{\mathbf{p}})},\end{aligned} \tag{3.14}$$

$$\frac{B^{(v)}(\alpha)}{\hat{F}(\alpha)} = c_0^{(v)} + \sum_{i=1}^{N} c_i^{(v)} \Phi_i(\alpha, \bar{\mathbf{p}}), \tag{3.15}$$

$$\frac{F(\alpha)}{\hat{F}(\alpha)} = 1 + \sum_{i=1}^{N} d_i \Phi_i(\alpha, \bar{\mathbf{p}}), \tag{3.16}$$

where $\bar{\mathbf{p}} = \begin{bmatrix} \bar{p}_1 & \cdots & \bar{p}_N \end{bmatrix}^{\mathrm{T}}$ is assumed to be a set of pre-specified (known) poles. By rewriting (3.16) as a ratio between polynomials, one can observe that poles of $\hat{G}_{(v)}(\alpha)$ (roots of polynomial $F(\alpha)$) are function not only of the unknown coefficients $\{d_i\}$, but also of the RBF poles $\bar{\mathbf{p}}$ (roots of polynomial $\hat{F}(\alpha)$). However, by assuming $\bar{\mathbf{p}}$ to be a set of n specified (known) poles, poles of $\hat{G}_{(v)}(\alpha)$ naturally become function only of $\{d_i\}$.

Now, by defining the related parameter vector

$$\theta = \begin{bmatrix} c_0^{(1)} & \cdots & c_N^{(1)} & \cdots & c_0^{(V)} & \cdots & c_N^{(V)} & d_1 & \cdots & d_N \end{bmatrix}^{\mathrm{T}}, \tag{3.17}$$

the following objective function can be formulated:

$$J(\theta) = \sum_{v=1}^{V} \sum_{k=1}^{K} |e_{(v)}(\alpha_k)|^2, \tag{3.18}$$

where $e_{(v)}(\alpha_k)$ is the scalar error

$$e_{(v)}(\alpha_k) = W_{(v)}(\alpha_k) \left(G'_{(v)}(\alpha_k) - \hat{G}_{(v)}(\alpha_k) \right) \tag{3.19}$$

that, based on equation (3.14), also reads

$$e_{(v)}(\alpha_k) = \frac{F(\alpha_k)}{F(\alpha_k)} W_{(v)}(\alpha_k) G'_{(v)}(\alpha_k) - W_{(v)}(\alpha_k) \frac{B^{(v)}(\alpha_k)}{F(\alpha_k)}. \tag{3.20}$$

Note that, although the minimization of objective function $J(\theta)$ suggests an alternative way for estimating the original pole set $\mathbf{p}$ (by means of the roots of polynomial $F(\alpha)$), the optimization problem itself remains *nonlinear* with respect to coefficient vector θ, since polynomial $F(\alpha)$ (which is function of coefficients $\{d_i\}$ in θ) appears as transfer function denominator. To cope with this issue, one can first consider approximation $e_{(v)}(\alpha_k) \approx \tilde{e}_{(v)}(\alpha_k)$, where

$$\tilde{e}_{(v)}(\alpha_k) = \frac{F(\alpha_k)}{\hat{F}(\alpha_k)} W_{(v)}(\alpha_k) G'_{(v)}(\alpha_k) - W_{(v)}(\alpha_k) \frac{B^{(v)}(\alpha_k)}{\hat{F}(\alpha_k)} \tag{3.21}$$

$$= \left(1 + \sum_{i=1}^{N} d_i \Phi_i(\alpha_k, \bar{\mathbf{p}})\right) W_{(v)}(\alpha_k) G'_{(v)}(\alpha_k) - W_{(v)}(\alpha_k) \left(c_0^{(v)} + \sum_{i=1}^{N} c_i^{(v)} \Phi_i(\alpha_k, \bar{\mathbf{p}})\right) \tag{3.22}$$

or, equivalently,

$$\tilde{e}_{(v)}(\alpha_k) = W_{(v)}(\alpha_k) G'_{(v)}(\alpha_k) - \mathbf{m}_{(v)}^{\mathrm{T}}(\alpha_k)\theta, \tag{3.23}$$

being (see also Equation (3.6))

$$\mathbf{m}_{(v)}(\alpha_k) = W_{(v)}(\alpha_k) \begin{bmatrix} \mathbf{0}_{1\times(N+1)(v-1)} & 1 & \mathbf{\Phi}^{\mathrm{T}}(\alpha_k) & \mathbf{0}_{1\times(N+1)(V-v)} & -G'_{(v)}(\alpha_k)\mathbf{\Phi}^{\mathrm{T}}(\alpha_k) \end{bmatrix}^{\mathrm{T}} \tag{3.24}$$

As in chapter 2 of this thesis, $\mathbf{0}_{i\times j}$ terms represent matrices of zeros with i rows and j columns. Nonetheless, from now on, we may sometimes use $\mathbf{0}$ to omit dimensions and simplify notation.

By approximating $e_{(v)}(\alpha_k)$ by $\tilde{e}_{(v)}(\alpha_k)$ in equation (3.18), the *nonlinear* problem of minimizing objective function $J(\theta)$ (in terms of θ) is transformed into an approximated but *linearized* least-squares problem whose solution can be written as follows

$$\hat{\theta} = \arg\min_{\theta} \sum_{v=1}^{V} \sum_{k=1}^{K} \left| \tilde{e}_{(v)}(\alpha_k) \right|^2 \tag{3.25}$$

$$= \arg\min_{\theta} \sum_{v=1}^{V} \sum_{k=1}^{K} \left| W_{(v)}(\alpha_k) G'_{(v)}(\alpha_k) - \mathbf{m}^{\mathrm{T}}_{(v)}(\alpha_k)\theta \right|^2 \tag{3.26}$$

$$= \left[\mathbf{M}^{\mathrm{T}}\mathbf{M}\right]^{-1} \mathbf{M}^{\mathrm{T}}\mathbf{y}, \tag{3.27}$$

where $\hat{\theta}$ can be considered as an estimate for $\theta^\star$ obtained for a given set of pre-specified poles $\bar{\mathbf{p}}$, being $\theta^\star$ the global minimum of $J(\theta)$. In (3.27), matrices $\mathbf{M}$ and $\mathbf{y}$ are defined as follows

$$\mathbf{M} = \begin{bmatrix} \widetilde{\mathbf{U}} & -\widetilde{\mathbf{Y}} \end{bmatrix}, \tag{3.28}$$

$$\mathbf{y} = \begin{bmatrix} W_{(1)}(\alpha_1)G'_{(1)}(\alpha_1) \\ \vdots \\ W_{(1)}(\alpha_K)G'_{(1)}(\alpha_K) \\ \vdots \\ W_{(V)}(\alpha_1)G'_{(V)}(\alpha_1) \\ \vdots \\ W_{(V)}(\alpha_K)G'_{(V)}(\alpha_K) \end{bmatrix}, \tag{3.29}$$

with

$$\widetilde{\mathbf{Y}} = \begin{bmatrix} W_{(1)}(\alpha_1)G'_{(1)}(\alpha_1)\mathbf{\Phi}(\alpha_1) \\ \vdots \\ W_{(1)}(\alpha_K)G'_{(1)}(\alpha_K)\mathbf{\Phi}(\alpha_K) \\ \vdots \\ W_{(V)}(\alpha_1)G'_{(V)}(\alpha_1)\mathbf{\Phi}(\alpha_1) \\ \vdots \\ W_{(V)}(\alpha_K)G'_{(V)}(\alpha_K)\mathbf{\Phi}(\alpha_K) \end{bmatrix}, \tag{3.30}$$

$$\widetilde{\mathbf{U}} = \begin{bmatrix} \widetilde{\mathbf{U}}'_{(1)} & \mathbf{0} & \cdots & \mathbf{0} \\ \mathbf{0} & \widetilde{\mathbf{U}}'_{(2)} & \cdots & \mathbf{0} \\ \cdots & \cdots & \cdots & \cdots \\ \mathbf{0} & \mathbf{0} & \cdots & \widetilde{\mathbf{U}}'_{(V)} \end{bmatrix}^{\mathrm{T}}, \quad \widetilde{\mathbf{U}}'_{(v)} = \begin{bmatrix} W_{(v)}(\alpha_1) & \cdots & W_{(v)}(\alpha_K) \\ W_{(v)}(\alpha_1)\mathbf{\Phi}(\alpha_1) & \cdots & W_{(v)}(\alpha_K)\mathbf{\Phi}(\alpha_K) \end{bmatrix} \tag{3.31}$$

Instead of directly solving (3.27), however, one can guarantee that $\hat{\theta}$ always occurs as a vector of real-valued parameters by alternatively solving the real-valued equivalent problem

$$\hat{\theta} = \left[\widetilde{\mathbf{M}}^{\mathrm{T}}\widetilde{\mathbf{M}}\right]^{-1}\widetilde{\mathbf{M}}^{\mathrm{T}}\tilde{\mathbf{y}}, \tag{3.32}$$

where

$$\widetilde{\mathbf{M}} = \begin{bmatrix} \Re\mathrm{e}\{\mathbf{M}\} \\ \Im\mathrm{m}\{\mathbf{M}\} \end{bmatrix} \quad \text{and} \quad \tilde{\mathbf{y}} = \begin{bmatrix} \Re\mathrm{e}\{\mathbf{y}\} \\ \Im\mathrm{m}\{\mathbf{y}\} \end{bmatrix}. \tag{3.33}$$

Once $\hat{\theta}$ is obtained by solving (3.32), one can try to make the approximate error $\tilde{e}_{(v)}(\alpha_k)$ in (3.21) closer to the original error $e_{(v)}(\alpha_k)$ in (3.20) by considering the obtained polynomial $F(\alpha)$ as a possibly more refined estimate for polynomial $\hat{F}(\alpha)$. In terms of roots, this means that roots of $\hat{F}(\alpha)$, which can be determined based on the estimated coefficients $\{d_i\}$ in θ (see equation (3.16)), are to be considered as a more refined estimate for the N pre-specified poles in $\bar{\mathbf{p}}$. Based on this novel set of poles $\bar{\mathbf{a}}$, one can reestimate θ via (3.32).

This procedure can be repeated (iterated) until $\hat{\theta}$ and $\bar{\mathbf{p}}$ converge to fixed parameter vectors $\hat{\theta}'$ and $\bar{\mathbf{p}}'$. When convergence is achieved, it naturally follows that $F'(\alpha) = \hat{F}'(\alpha)$, where $F'(\alpha)$ and $\hat{F}'(\alpha)$ denote the values obtained for polynomials $F(\alpha)$ and $\hat{F}(\alpha)$ when $\hat{\theta} = \hat{\theta}'$ and $\bar{\mathbf{p}} = \bar{\mathbf{p}}'$. Consequently, since $F'(\alpha) = \hat{F}'(\alpha)$, the (3.14)-type RBF models obtained after algorithm convergence fits exactly into the desired model structure form in

(3.11):

$$\begin{aligned}\hat{G}'_{(v)}(\alpha) &= \frac{B'^{(v)}(\alpha)}{F'(\alpha)} \\ &= \frac{B'^{(v)}(\alpha)}{\hat{F}'(\alpha)} \\ &= c_0'^{(v)} + \sum_{i=1}^{N} c_i'^{(v)} \Phi_i(\alpha, \bar{\mathbf{p}}')\end{aligned} \tag{3.34}$$

Expression (3.34) reveals $c_0'^{(v)}, \cdots, c_N'^{(v)}$ and $\bar{\mathbf{p}}'$ are our final estimates for $r_0^{(v)}, \cdots, r_N^{(v)}$ and $\mathbf{p}$. Since $F'(\alpha) = \hat{F}'(\alpha)$, one can observe that, at convergence, equation (3.16) becomes

$$\frac{F(\alpha)}{\hat{F}(\alpha)} = 1 + \sum_{i=1}^{N} d_i' \Phi_i(\alpha, \bar{\mathbf{p}}') \tag{3.35}$$

$$= 1. \tag{3.36}$$

This means that the converged coefficients $\{d_i'\}$ no longer affect the resulting transfer functions $\hat{G}'_{(v)}(\alpha)$, as shown in (3.34).

3.1.1 Step by step procedure for implementing unifying FD-VF

Step 1. Given a set of (possibly) noisy frequency response data samples $\{G'_{(v)}(\alpha_k)\}$, $v = 1, \cdots, V$, sampled at $\{\alpha_k\}$, $k = 1, \cdots, K$, one must define the number of iterations, the weighting functions $W_{(v)}(\alpha_k)$, $v = 1, \cdots, V$, and a set of starting poles $\bar{\mathbf{p}} = \begin{bmatrix} \bar{p}_1 & \cdots & \bar{p}_N \end{bmatrix}^{\mathrm{T}}$. As shown in equation (3.2), definition for α_k depends if the RBF set chosen to the model structure is function of s (continuous-time) or z (discrete-time).

Comment: When it comes to FD-VF implementations based on continuous-time RBF sets, references (GRIVET-TALOCIA; GUSTAVSEN, 2016; GUSTAVSEN; SEMLYEN, 1999) recommend choosing starting poles as weakly attenuated complex conjugate pairs, with imaginary parts linearly distributed over a frequency band of interest $[0, \omega_{\max}]$. Meanwhile, in case of discrete-time models, a practical rule is the one which consists of choosing the $N = 2m$ initial poles as follows (GRIVET-TALOCIA; GUSTAVSEN, 2016):

$$\bar{a}_x = \rho e^{jx\pi/(m+1)}, \quad x = -m, \cdots, -1, 1, \cdots, m \tag{3.37}$$

with ρ being slightly smaller than unity, for instance, 0.99.

Step 2. Construct matrices $\widetilde{\mathbf{M}}$ and $\tilde{\mathbf{y}}$ in (3.33) based on equations (3.28)–(3.31).

Comment: Rational basis function vectors $\{\mathbf{\Phi}(\alpha_k)\}_{k=1}^{K}$ can be calculated, for instance, by varying α in equation (3.6) from α_1 to α_K.

Step 3. Obtain a least-squares estimate for parameter vector θ via (3.32).

Step 4. Update $\bar{\mathbf{p}}$ with the roots of polynomial $F(\alpha)$.

Comment: Since the roots of polynomial $F(\alpha)$ equal the zeros of transfer function $F(\alpha)/\hat{F}(\alpha)$, defined in (3.16), one can update $\bar{\mathbf{p}}$ by calculating the eigenvalues of matrix $(\mathbf{A}-\mathbf{B}\mathbf{D}^{-1}\mathbf{C})$ (see (GRIVET-TALOCIA; GUSTAVSEN, 2016) for a proof), with $(\mathbf{A},\mathbf{B},\mathbf{C},\mathbf{D})$ being the state-space realization for $F(\alpha)/\hat{F}(\alpha)$ in which $\mathbf{A}$ and $\mathbf{B}$ satisfy (3.6) and

$$\mathbf{C}=\left[\begin{array}{ccc} d_1 & \cdots & d_n \end{array}\right]; \quad \mathbf{D}=1. \tag{3.38}$$

If a continuous-time basis function set $\{\Phi(s,\mathbf{p})\}$ is being used as RBFs, it is possible to ensure model stability through iterations by simply inverting the sign of poles with positive real parts (if they occur while making $\bar{\mathbf{p}} \leftarrow \text{eig}(\mathbf{A}-\mathbf{B}\mathbf{D}^{-1}\mathbf{C})$). On the other hand, in case of discrete-time RBFs $\{\Phi(z,\mathbf{p})\}$, one can simply flip unstable poles back to the stable region $|z|<1$ by enforcing $\bar{p}_i \leftarrow \bar{p}_i/|\bar{p}_i|^2$.

Comment: Throughout iterations, we might also want to observe how our current set of estimated poles $\bar{\mathbf{p}}$ performs in model structures (3.11). In this case, coefficients $\{r_i^{(v)}\}$ can be estimated in the linear least-squares sense via (3.32) by simply redefining

$$\widetilde{\mathbf{M}}=\left[\begin{array}{c} \Re\mathrm{e}\{\widetilde{\mathbf{U}}\} \\ \Im\mathrm{m}\{\widetilde{\mathbf{U}}\} \end{array}\right]. \tag{3.39}$$

In this context, the associated root mean square (RMS) error of each v-th modeling transfer function $\hat{G}_{(v)}(\alpha_k)$ is a metric which can be observed, being its definition given as

follows

$$\text{RMS error}^{(v)} = \sqrt{\frac{1}{K}\sum_{k=1}^{K}\left|G'_{(v)}(\alpha_k) - \hat{G}_{(v)}(\alpha_k)\right|^2}. \tag{3.40}$$

Step 5. Repeat steps 2 to 4 until the number of iterations is achieved.

3.2 The IV-FD-VF iterations

FD-VF implementations are extremely popular within frequency-domain system identification since they usually provide satisfactory estimates for the RBF model parameters (GRIVET-TALOCIA; GUSTAVSEN, 2016).

However, although quite popular, it is also well known that standard FD-VF implementations do not guarantee their converged solutions are local (or the global) optimums of their corresponding nonlinear objective functions (NOFs). When it comes to the standard FD-VF method which consists of iteratively solving (3.32), this means the converged value $\hat{\theta}'$ is not necessarily a local optimum (or the global optimum $\theta^\star$) of the NOF $J(\theta)$, initially defined in (3.18). In fact, it is possible to verify through very simple examples that $\hat{\theta}'$ may not satisfy the necessary condition for local/global optimality

$$\left.\frac{\partial J}{\partial \theta}\right|_{\theta=\hat{\theta}'} = \mathbf{0}. \tag{3.41}$$

One of this examples is addressed in the results of this chapter (Section 3.3). In this section, we present an IV method for alternatively estimating the parameters of (3.11)-like RBF model structures. The method guarantees that its solutions after algorithm convergence necessarily satisfy (3.41).

From (3.18), it follows that (see Section 3.5.1 for the derivation of this equation)

$$\frac{\partial}{\partial\theta}J(\theta) = -2\sum_{k=1}^{K}\begin{bmatrix} \Re\mathrm{e}\left\{\mathbf{i}^{*}_{(1)}(\alpha_k)\ e_{(1)}(\alpha_k)\right\} \\ \cdots \\ \Re\mathrm{e}\left\{\mathbf{i}^{*}_{(V)}(\alpha_k)\ e_{(V)}(\alpha_k)\right\} \\ \sum_{v=1}^{V}\Re\mathrm{e}\left\{\mathbf{i}'^{*}_{(v)}(\alpha_k)\ e_{(v)}(\alpha_k)\right\} \end{bmatrix}, \tag{3.42}$$

where $\mathbf{i}_{(v)}(\alpha_k)$ and $\mathbf{i}'_{(v)}(\alpha_k)$ correspond to the following instrument vectors:

$$\mathbf{i}_{(v)}(\alpha_k) = W_{(v)}(\alpha_k)\begin{bmatrix} \dfrac{\partial}{\partial c_0^{(v)}} & \cdots & \dfrac{\partial}{\partial c_N^{(v)}} \end{bmatrix}^{\mathrm{T}}\hat{G}_{(v)}(\alpha_k); \tag{3.43}$$

$$\mathbf{i}'_{(v)}(\alpha_k) = W_{(v)}(\alpha_k)\begin{bmatrix} \dfrac{\partial}{\partial d_1} & \cdots & \dfrac{\partial}{\partial d_N} \end{bmatrix}^{\mathrm{T}}\hat{G}_{(v)}(\alpha_k). \tag{3.44}$$

Similarly to the linearization performed in the regular RTD-VF approach of Section 3.1, one can here use approximation $e_{(v)}(\alpha_k) \approx \tilde{e}_{(v)}(\alpha_k)$ to transform the local optimality condition $\dfrac{\partial J}{\partial\theta} = \mathbf{0}$ into the approximated problem

$$\sum_{k=1}^{K}\begin{bmatrix} \Re\mathrm{e}\left\{\mathbf{i}^{*}_{(1)}(\alpha_k)\ \tilde{e}_{(1)}(\alpha_k)\right\} \\ \cdots \\ \Re\mathrm{e}\left\{\mathbf{i}^{*}_{(V)}(\alpha_k)\ \tilde{e}_{(V)}(\alpha_k)\right\} \\ \sum_{v=1}^{V}\Re\mathrm{e}\left\{\mathbf{i}'^{*}_{(v)}(\alpha_k)\ \tilde{e}_{(v)}(\alpha_k)\right\} \end{bmatrix} = \mathbf{0}, \tag{3.45}$$

or, equivalently (see Section 3.5.2 for the derivation of this equation),

$$\widetilde{\Psi}^{\mathrm{T}}\left[\widetilde{\mathbf{y}} - \widetilde{\mathbf{M}}\hat{\theta}_{\mathrm{IV}}\right] = \mathbf{0}, \tag{3.46}$$

where $\hat{\theta}_{\mathrm{IV}}$ represents an IV estimate for $\theta^{\star}$, while

$$\widetilde{\Psi} = \begin{bmatrix} \Re\mathrm{e}\{\Psi\} \\ \Im\mathrm{m}\{\Psi\} \end{bmatrix} \tag{3.47}$$

and

$$\Psi = \begin{bmatrix} \mathbf{i}_{(1)}(\alpha_1) & \cdots & \mathbf{i}_{(1)}(\alpha_K) & \mathbf{0} & \cdots & \mathbf{0} & \cdots & \mathbf{0} & \cdots & \mathbf{0} \\ \mathbf{0} & \cdots & \mathbf{0} & \mathbf{i}_{(2)}(\alpha_1) & \cdots & \mathbf{i}_{(2)}(\alpha_K) & \cdots & \mathbf{0} & \cdots & \mathbf{0} \\ \cdots & \cdots & \cdots & \cdots & \cdots & \cdots & \cdots & \cdots & \cdots & \cdots \\ \mathbf{0} & \cdots & \mathbf{0} & \mathbf{0} & \cdots & \mathbf{0} & \cdots & \mathbf{i}_{(V)}(\alpha_1) & \cdots & \mathbf{i}_{(V)}(\alpha_K) \\ \mathbf{i}'_{(1)}(\alpha_1) & \cdots & \mathbf{i}'_{(1)}(\alpha_K) & \mathbf{i}'_{(2)}(\alpha_1) & \cdots & \mathbf{i}'_{(2)}(\alpha_K) & \cdots & \mathbf{i}'_{(V)}(\alpha_1) & \cdots & \mathbf{i}'_{(V)}(\alpha_K) \end{bmatrix}^{\mathrm{T}}. \tag{3.48}$$

Finally, by isolating coefficient vector $\hat{\theta}_{\mathrm{IV}}$ in (3.46), it follows that the IV-FD-VF method presented in this section consists of solving equation (3.49) iteratively.

$$\hat{\theta}_{\mathrm{IV}} = \left[\widetilde{\Psi}^{\mathrm{T}}\widetilde{\mathbf{M}}\right]^{-1}\widetilde{\Psi}^{\mathrm{T}}\widetilde{\mathbf{y}}. \tag{3.49}$$

3.2.1 Approximation of instrument vectors $\mathbf{i}_{(v)}(\alpha_k)$ and $\mathbf{i}'_{(v)}(\alpha_k)$

According to definitions in (3.6), (3.14)–(3.16), (3.43), (3.44), one can obtain

$$\begin{aligned} \mathbf{i}_{(v)}(\alpha_k) &= \begin{bmatrix} W_{(v)}(\alpha_k) \\ \dfrac{\hat{F}(\alpha_k)}{F(\alpha_k)} W_{(v)}(\alpha_k)\mathbf{\Phi}(\alpha_k) \end{bmatrix}, \\ \mathbf{i}'_{(v)}(\alpha_k) &= -W_{(v)}(\alpha_k)\left(\frac{\hat{F}(\alpha_k)}{F(\alpha_k)}\right)^2 \widetilde{G}'_{(v)}(\alpha_k)\mathbf{\Phi}(\alpha_k), \end{aligned} \tag{3.50}$$

where

$$\widetilde{G}'_{(v)}(\alpha_k) = \left(c_0^{(v)} + \sum_{i=1}^{N} c_i^{(v)}\Phi_i(\alpha_k, \bar{\mathbf{p}})\right). \tag{3.51}$$

The problem of computing these instruments via equations (3.50) and (3.51) is described in the following.

Equations (3.16) and (3.51) show $\mathbf{i}_{(v)}(\alpha_k)$ and $\mathbf{i}'_{(v)}(\alpha_k)$ (and, as a consequence, matrix Ψ) are functions of coefficients $\{c_i^{(v)}\}$ and $\{d_i\}$, which are estimated via vector $\hat{\theta}_{\mathrm{IV}}$ in (3.49). This means (3.49) cannot be used for directly finding $\hat{\theta}_{\mathrm{IV}}$, since right-hand side of this equation is also function of $\hat{\theta}_{\mathrm{IV}}$.

On the one hand, computing $\mathbf{i}_{(v)}(\alpha_k)$ and $\mathbf{i}'_{(v)}(\alpha_k)$ based on the values found for $\{c_i^{(v)}\}$ and $\{d_i\}$ during the previous iteration of the algorithm indeed makes it possible to use (3.49) for finding an estimated $\hat{\theta}_{\mathrm{IV}}$. On the other hand, however, some specific values for $\{d_i\}$ can lead roots of polynomial $F(\alpha)$ to become unstable poles in (3.50). To cope with this issue, one can assume $\mathbf{i}_{(v)}(\alpha_k) \approx \tilde{\mathbf{i}}_{(v)}(\alpha_k)$ and $\mathbf{i}'_{(v)}(\alpha_k) \approx \tilde{\mathbf{i}}'_{(v)}(\alpha_k)$ are both valid considerations, with

$$\begin{aligned} \tilde{\mathbf{i}}_{(v)}(\alpha_k) &= \begin{bmatrix} W_{(v)}(\alpha_k) \\ W_{(v)}(\alpha_k)\mathbf{\Phi}(\alpha_k) \end{bmatrix}, \\ \tilde{\mathbf{i}}'_{(v)}(\alpha_k) &= -W_{(v)}(\alpha_k)\widetilde{G}'_{(v)}(\alpha_k)\mathbf{\Phi}(\alpha_k). \end{aligned} \tag{3.52}$$

In (3.52), it is assumed coefficients $\{c_i^{(v)}\}$ are replaced with their estimates obtained during the previous algorithm iteration while constructing $\widetilde{G}'_{(v)}(\alpha_k)$ via (3.51).

When it comes to matrix Ψ (defined in Equation (3.48)), approximations in (3.52) lead to (see also (3.31))

$$\Psi \approx \begin{bmatrix} \widetilde{\mathbf{U}} & -\widetilde{\mathbf{Y}}' \end{bmatrix}, \tag{3.53}$$

where

$$\widetilde{\mathbf{Y}}' = \begin{bmatrix} W_{(1)}(\alpha_1)\widetilde{G}'_{(1)}(\alpha_1)\mathbf{\Phi}(\alpha_1) \\ \cdots \\ W_{(1)}(\alpha_K)\widetilde{G}'_{(1)}(\alpha_K)\mathbf{\Phi}(\alpha_K) \\ \cdots \\ W_{(V)}(\alpha_1)\widetilde{G}'_{(V)}(\alpha_1)\mathbf{\Phi}(\alpha_1) \\ \cdots \\ W_{(V)}(\alpha_K)\widetilde{G}'_{(V)}(\alpha_K)\mathbf{\Phi}(\alpha_K) \end{bmatrix}. \tag{3.54}$$

3.2.2 Step by step procedure for implementing IV-FD-VF

The same implementation steps used for standard FD-VF (described in Section 3.1.1) can also be used for implementing the IV-FD-VF iterations. To do so, one must

simply solve (3.49) instead of (3.32) during **Step 3**, with matrix Ψ being approximated as describes (3.53).

Due to necessity to compute terms $\widetilde{G}'_{(v)}(\alpha_k)$, $v = 1, \cdots, V$, such an approximation makes IV-FD-VF to rely on an initial estimate for coefficients $\{c_i^{(v)}\}$. In general, a satisfactory initial estimate can be obtained by running the standard FD-VF solution (3.32) during a specific number of iterations. Then, by adopting the estimated values for $\{c_i^{(v)}\}$, one can naturally migrate to IV-FD-VF.

3.2.3 Optimal property of IV-FD-VF converged solutions

Differently from the FD-VF iterations in (3.32), the IV-FD-VF iterations allow us to guarantee that the solution after their convergence is indeed a local optimum of the nonlinear objective function $J(\theta)$. Such an important proposition is formally confirmed by the following theorem.

Theorem 3.2.1. *Let $\bar{\mathbf{p}}^t$ denote the set of pre-specified poles $\bar{\mathbf{p}}$ used for obtaining $\hat{\theta}_{IV}^t$, where $t \in \mathbb{N}$ emphasizes the iteration number in which $\hat{\theta}_{IV}$ has been computed. If $\hat{\theta}_{IV}^t$ and $\bar{\mathbf{p}}^t$ converge to fixed values $\hat{\theta}'_{IV}$ and $\bar{\mathbf{p}}'$ at a specific iteration $t = t_c$, then $\hat{\theta}_{IV}^{t_c} = \hat{\theta}'_{IV}$ is a local (if not the global) optimum of the nonlinear objective function $J(\theta)$.*

Proof. See Section 3.5.3 for the proof of theorem 3.2.1.

□

3.3 Numerical results

In this section three numerical examples are used to compare IV-FD-VF with standard FD-VF. In the first case study, it is considered a continuous-time example where actual frequency-domain data samples were measured from two different power transformers, whereas the second and third case studies aim at identifying, respectively, a third order discrete-time system corrupted by colored noise and two inductive potential transformers (IPTs). Both IPTs are modeled as MIMO systems. The 'unifying' property of the presented FD-VF and IV-FD-VF algorithms is also explored here, since the first and

third examples consider system identification problems based on continuous-time models whereas the second one uses discrete-time models. All simulations were performed in an Intel(R) Core(TM) i5 2.2GHz 8GB RAM laptop.

We remark that most results exposed in this section have been first presented in (SCHUMACHER; OLIVEIRA, 2019).

3.3.1 Example I: Power transformer modeling

For analysis of power system electromagnetic transients, a power transformer is represented by a p-terminal symmetric admittance matrix $\mathbf{Y}$, as follows:

$$\mathbf{I}(\omega) \;=\; \mathbf{Y}(\omega)\,\mathbf{V}(\omega), \tag{3.55}$$

where the entries of vectors $\mathbf{I}(\omega)$ and $\mathbf{V}(\omega)$ represent, respectively, the power transformer current and voltage frequency responses at each terminal. Under certain terminal conditions, frequency responses of voltage ratios between terminals can be calculated based on the admittance matrix $\mathbf{Y}(\omega)$ (Gustavsen, 2004) or can be directly measured by using Sweep Frequency Response Analyser (SFRA)-type equipments (IEEE Std C57.149, 2012) such as FRAX-101 (FRAX-101, 2013).

Within this context, the case study of this section aims at comparing the IV-FD-VF algorithm with standard FD-VF by modeling two different power transformers. In particular, the results obtained with IV-FD-VF are compared to those obtained by the *vectfit3* algorithm (PACKAGE, 2008), which is one of the most popular open source implementations of FD-VF. We remark that the *vectfit3* algorithm, which has its theory described in (GUSTAVSEN; SEMLYEN, 1999; GUSTAVSEN, 2006; DESCHRIJVER *et al.*, 2008), is especially designed for estimating RBF models formed by continuous-time partial fractions. The main objective of this case study is to show that, due to the optimal property of its solution, the presented IV-FD-VF method can be used to further refine the model parameters provided by FD-VF.

The first power transformer modeled in this section consists of a single-phase 345/225 kV 225MVA transformer located in a Brazilian Hydroelectric power plant. Actual

measurements collected from this transformer in the field using a SFRA equipment are considered. Measurements have been extracted according to procedures and norms described in (IEEE Std C57.149, 2012). Such data are composed of 207 frequency response samples logarithmically spaced between 10 to 10^5 Hz and represent the voltage ratio between the high voltage terminal and the low voltage terminal. Fig. 18 depicts the corresponding magnitude and phase angle curves.

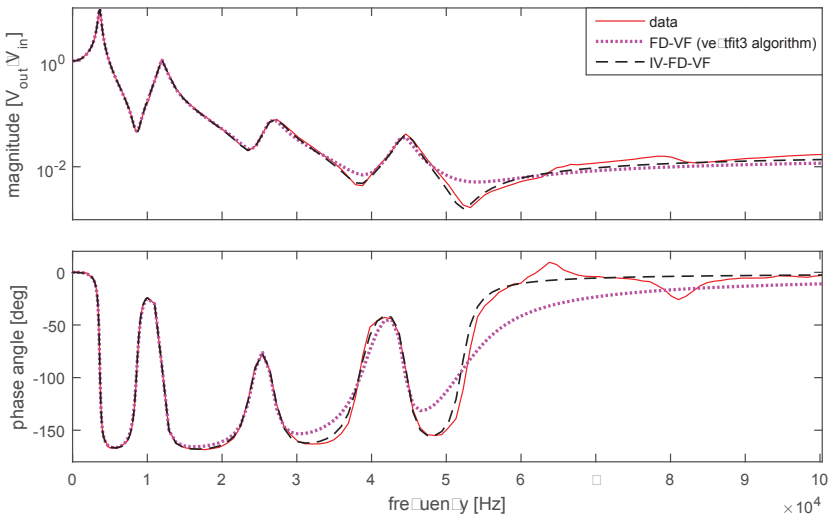

Figure 18 – Data extracted from a single-phase 345/225 kV 225MVA power transformer and resulting model frequency responses.

To model the curves presented in this figure, it is assumed models formed by 14 continuous-time partial fractions ($N = 14$) for both FD-VF and IV-FD-VF methods. The resulting fitted frequency responses are also depicted in Fig. 18. This figure clearly shows that the IV formulation presents a superior fitting to the data, especially for frequencies greater than 3×10^4 Hz.

Fig. 19 shows the RMS error (through iterations) for each RBF model. Fig. 20 provides a zoomed view with respect to the last iterations of Fig. 19. From Figs. 19 and 20 it can be observed the strategy used by the IV-FD-VF algorithm to refine the FD-VF solution: FD-VF is used for the first fourteen iterations to generate an initial estimate for the IV-FD-VF technique, which is then used for more eleven iterations to improve model fitness.

From Fig. 20, it is clearer that IV-FD-VF further refines the model parameters

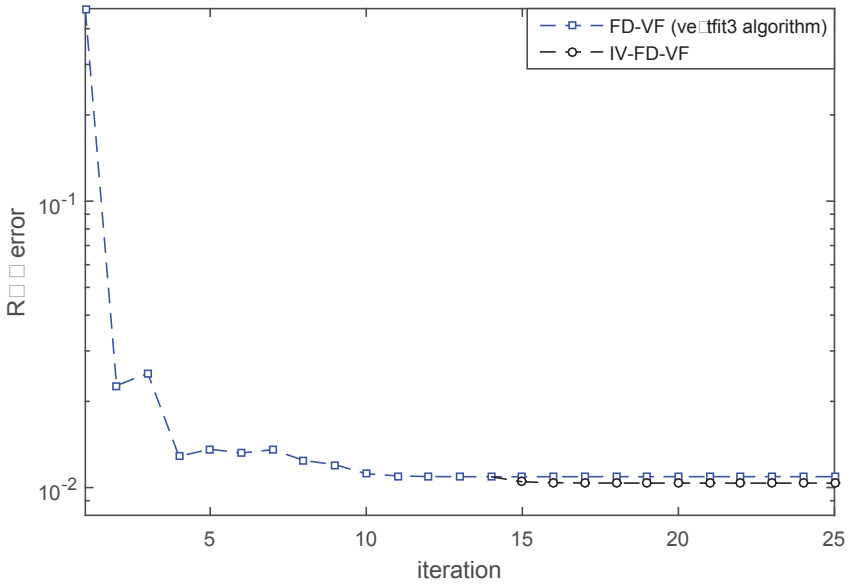

Figure 19 – RMS errors through iterations when modeling a single-phase 345/225 kV 225MVA power transformer.

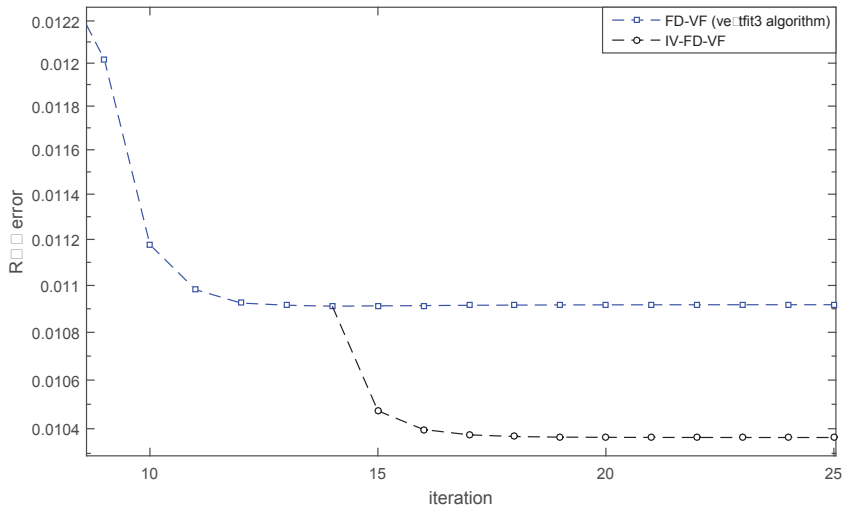

Figure 20 – Zoomed view with respect to the last iterations of Fig. 19.

provided by FD-VF. Note that results shown in this figure are in full agreement with the results provided by Fig. 18, where the biggest RMS error presented by FD-VF at iteration $t = 25$ is mainly due to the mismatch presented for frequencies greater than 3×10^4 Hz.

The second power transformer modeled in this section consists of a single-phase 525/18 kV 256 MVA transformer located in a gas-insulated substation. Fig. 21 depicts admittance data from this transformer (727 frequency response data samples) measured from 10 Hz up to approximately 2.8×10^6 Hz. Resulting fitted curves (assuming $N = 16$)

are also presented in Fig. 21, whereas Fig. 22 shows the corresponding RMS errors through iterations. In Fig. 22, the smaller RMS error presented by IV-FD-VF after convergence justifies its superior fitting performance for most data samples in Fig. 21. It is observed this example also confirms the applicability of IV-FD-VF for modeling resonance peaks of power transformers in high-frequency (> 50 kHz) measurements.

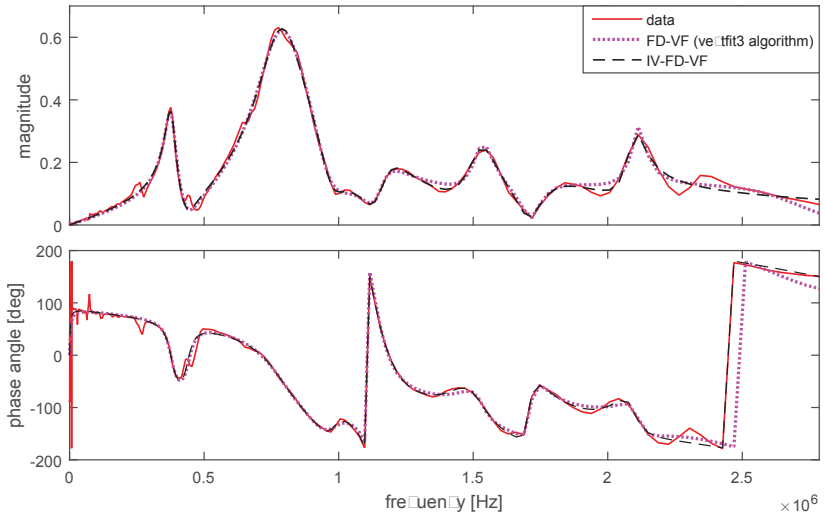

Figure 21 – Data extracted from a single-phase 525/18 kV 256 MVA power transformer and resulting model frequency responses.

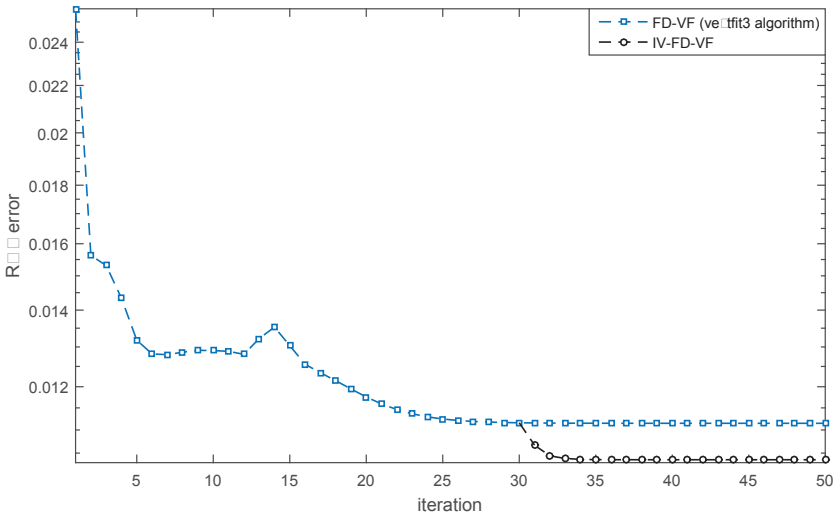

Figure 22 – RMS errors through iterations when modeling a single-phase 525/18 kV 256 MVA power transformer.

Finally, we remark that for both power transformers modeled in this section, gradient $\partial V/\partial\theta$ presented partial derivatives with values highly close to zero (in fact,

with absolute values smaller than 10^{-8}) at the last iteration of the IV-FD-VF algorithm, meaning that local optimums were obtained. In the next section of this chapter, we use a third order discrete-time system with known coefficients but corrupted by colored noise to further investigate this optimal property of IV-FD-VF.

3.3.2 Example II: Third order discrete-time system

In this second case study it is considered the identification of the 3$^{\text{rd}}$ order discrete-time system defined by (SCHUMACHER; OLIVEIRA, 2017)

$$G_0(z) = \frac{0.1389 + 0.4166z^{-1} + 0.4166z^{-2} + 0.1389z^{-3}}{1 + 0.4218z^{-1} + 0.2499z^{-2} - 0.5609z^{-3}}. \tag{3.56}$$

The data used to estimate $G_0(z)$ are formed by a set of 500 noisy frequency-domain data samples $\{G_0'(z_k = e^{j2\pi\omega_k/\omega_s}), \omega_k\}, k = 1, \cdots, 500$, with $\{\omega_k\}$ chosen linearly spaced between 0 and $(2\pi f_s/2)$ rad/s, with $f_s = 1$ Hz so that $z_k = e^{j\omega_k}$. In particular, the set $\{G_0'(j\omega_k)\}$ is assumed to be corrupted by additive colored noise, according to relation

$$G_0'(z_k) = G_0(z_k) + H_0(z_k)e(k), \quad k = 1, \cdots, 500, \tag{3.57}$$

where $e(k)$ is a sequence of independent random variables extracted from a Gaussian distribution of zero mean and variance 0.3^2, i.e.,

$$e(k) \sim \mathcal{N}(0, \sigma^2 = 0.3^2), \tag{3.58}$$

and the filter $H_0(z_k)$ is chosen to be equal to the system's frequency response $G_0(z_k)$ ($H_0(z_k) = G_0(z_k)$), so that each measurement $G_0'(z_k)$ has a noise component which is proportional to the magnitude of $G_0(z_k)$. Magnitude of the resulting estimation data samples is depicted in Fig. 23.

The main objective of this case study is to show that IV-FD-VF also provides superior fitting performance than regular FD-VF when estimation data are corrupted by colored noise, once it guarantees an optimal solution at convergence. Since $G_0(z)$ consists of a discrete-time system, instead of using simple continuous-time partial fractions as

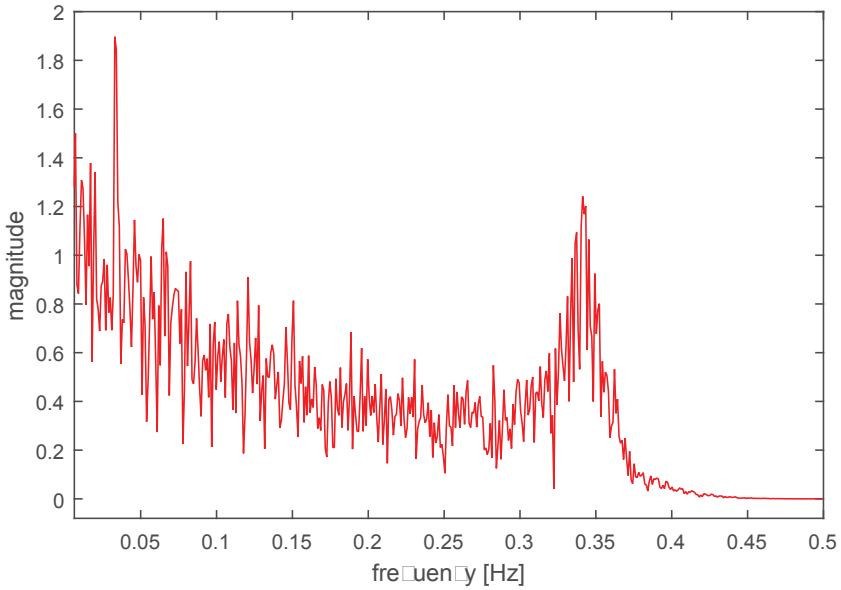

Figure 23 – Magnitude of the resulting estimation data samples used in Example II.

RBFs, in this case study it is considered for both FD-VF and IV-FD-VF methods models formed by the so-called discrete-time Takenaka-Malmquist Orthonormal Basis functions (see (SCHUMACHER, 2017) for details). Particularly, it is considered models with $N = 3$, that is, with 3 rational functions.

Fig. 24 depicts the RMS error (through iterations) for each fitted RBF model. Similarly to the first example, FD-VF is used for the first two iterations to generate an initial estimate for the IV-FD-VF technique, which is then used for more thirteen iterations to improve model fitness. Clearly, it is observed from Fig. 24 that the IV formulation presents a better model accuracy when compared with its standard method (FD-VF), since its solution has a significantly smaller error at iteration $t = 15$ and it converges with fewer iterations. Total simulation time for both methods is shown in Table 10. Although FD-VF is faster, the time difference of about 0.5 second (observed in a standard laptop) is not significant. Such an increase in simulation time was expected since the IV iterations rely on computing an additional matrix $\widetilde{\Psi}$.

Table 10 – Simulation time in seconds.

FD-VF	IV-FD-VF
2.321	2.731

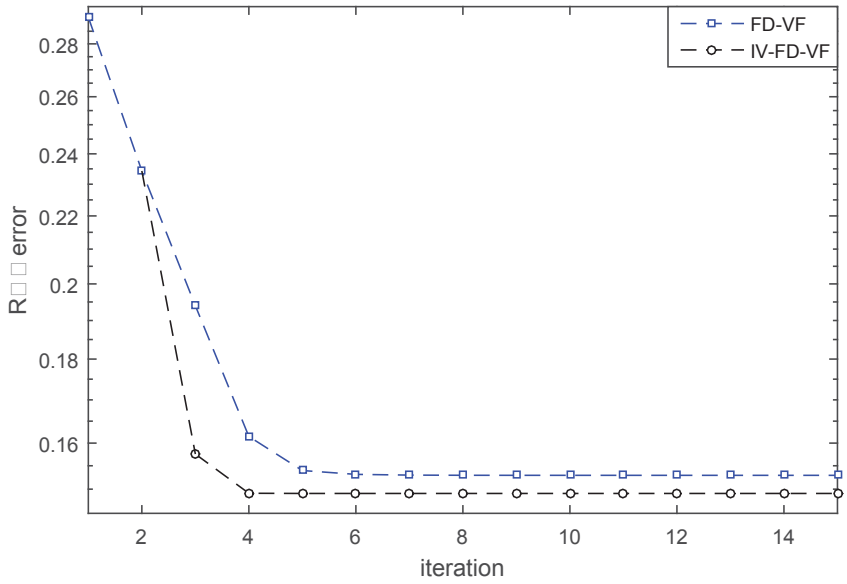

Figure 24 – RMS errors through iterations.

We now investigate the converged solutions $\hat{\theta}$ and $\hat{\theta}_{\text{IV}}$ obtained at $t = 15$. Table 11 shows the gradient of the nonlinear objective function $V(\theta)$ for both FD-VF and IV-FD-VF methods. It is observed that FD-VF converged to a non-optimal solution, whereas IV-FD-VF indeed converged to a local optimum of $V(\theta)$. A direct comparison with the coefficients of $G_0(z)$ given in (3.56) can be performed by converting the resulting RBF model state-space representations into transfer functions. Equations (3.59) and (3.60) show the equivalent models obtained for the IV-FD-VF and FD-VF methods, respectively. Note that the coefficient estimates provided by the IV-FD-VF are significantly closer to the coefficients of $G_0(z)$.

$$\bar{G}(z, \hat{\theta}_{\text{IV}}, \hat{\mathbf{a}}) = \frac{0.1405 + 0.4156z^{-1} + 0.4180z^{-2} + 0.1361z^{-3}}{1 + 0.4252z^{-1} + 0.2343z^{-2} - 0.5672z^{-3}} \tag{3.59}$$

$$\bar{G}(z, \hat{\theta}, \hat{\mathbf{a}}) = \frac{0.1404 + 0.3945z^{-1} + 0.3814z^{-2} + 0.1065z^{-3}}{1 + 0.3665z^{-1} + 0.1902z^{-2} - 0.6136z^{-3}} \tag{3.60}$$

The results obtained in this case study are supposed to vary for different experiments since $e(k)$ is a randomly generated sequence. We therefore repeat the experiment described so far 1000 times by considering different generations for $e(k)$. The estimated coefficients obtained for both FD-VF and IV-FD-VF methods are represented by their corresponding

Table 11 – Gradient of the nonlinear objective function $V(\theta)$ at $t = 15$.

	FD-VF	IV-FD-VF
$\partial V/\partial r_0$	-0.0029 $\times 10^{-5}$	0.0009 $\times 10^{-11}$
$\partial V/\partial r_1$	0.9062 $\times 10^{-5}$	-0.2317 $\times 10^{-11}$
$\partial V/\partial r_2$	-0.1210 $\times 10^{-5}$	0.3419 $\times 10^{-11}$
$\partial V/\partial r_3$	-0.5029 $\times 10^{-5}$	-0.0701 $\times 10^{-11}$
$\partial V/\partial d_1$	-1.4704	-0.2357 $\times 10^{-11}$
$\partial V/\partial d_2$	5.9295	0.4833 $\times 10^{-11}$
$\partial V/\partial d_3$	-16.4975	0.0404 $\times 10^{-11}$

estimated probability density functions in Fig. 25. In this figure, note that dotted vertical lines represent the true values of the coefficients of $G_0(z)$ in (3.56). From Fig. 25, it is observed that only the IV formulation is able to provide concise estimates around the true system coefficients. Meanwhile, FD-VF presents a clear bias for most of its estimates.

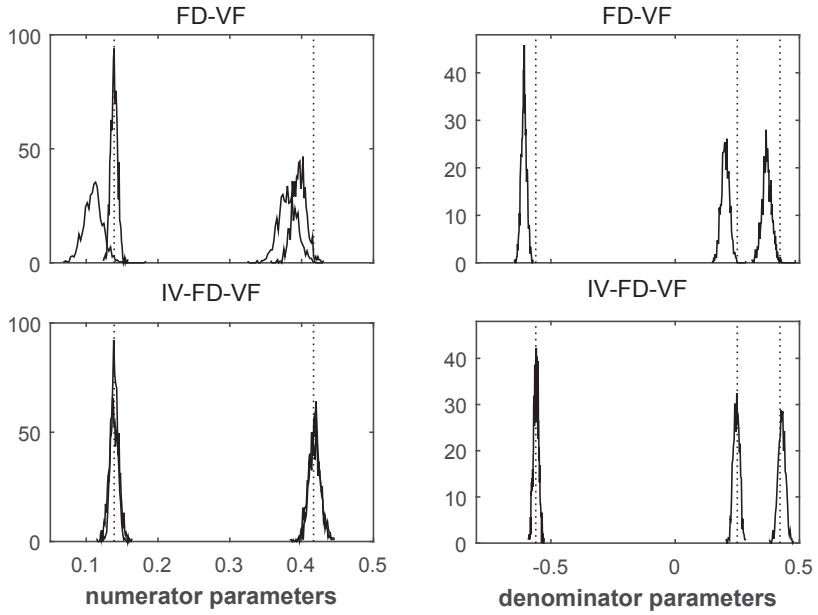

Figure 25 – Estimated probability density functions (solid lines) and coefficients of $G_0(z)$ (represented by vertical dotted lines).

3.3.3 Example III: Inductive potential transformer modeling

Three 525kV SF6 insulated inductive potential transformers (IPT) of a Brazilian gas insulated substation presented dielectric failures due to unknown circumstances. Engineers designated to investigate such failures believe such an issue has happened due to high-frequency overvoltages occurred during substation switchings.

The idea here is to estimate models which are capable of representing frequency

responses (over a wide frequency range) extracted from a "healthy" IPT sample. Then, associated with a proper modeling of the substation, such models could be used to simulate (within electromagnetic transient simulators such as EMPT-RV, for instance) if substation switchings indeed produce overvoltages which exceed the insulation breakdown voltages specified by the IPT designer. In this thesis, we concentrate our attention only to the process of identifying IPT frequency responses.

Fig. 26 depicts the type of IPT under investigation. As shown in Fig. 27, it is composed of a high voltage winding and two low voltage windings. Terminals are labeled as shown in this figure.

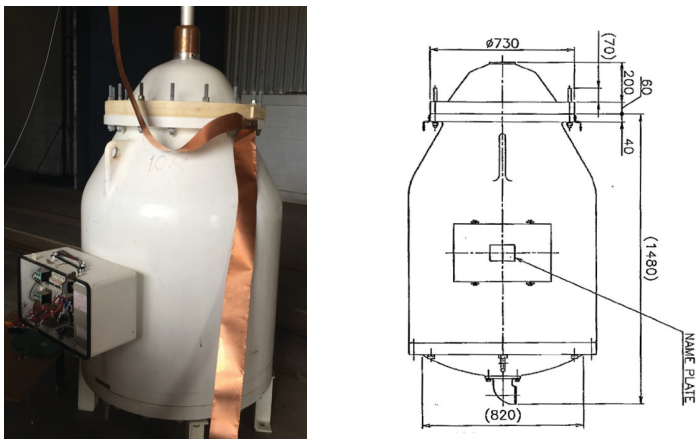

Figure 26 – IPT under investigation (left) and its corresponding sketch (right).

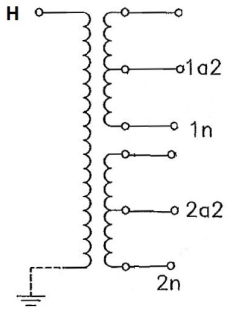

Figure 27 – IPT windings and terminals.

Initially, in this case study, we consider only admittance data extracted from the high voltage winding. Specifically, it is considered $Y(\omega) = I_{\mathrm{H}}(\omega)/V_{\mathrm{H}}(\omega)$ data collected based on two different scenarios:

- Scenario #1: Terminals 1a2, 1n, 2a2 and 2n are all grounded.

- Scenario #2: Terminals 1a2, 1n, 2a2 and 2n are all left opened.

Magnitude curves extracted from the IPT are shown in Figs. 28 and 29 for Scenarios #1 and #2, respectively. These figures also show the resulting fitted frequency responses obtained when applying both regular FD-VF and IV-FD-VF with a model composed of $N = 4$ continuous-time partial fractions. As it can be observed, although regular FD-VF and IV-FD-VF are both capable of estimating the IPT frequency responses, IV-FD-VF presents a better fit to the data.

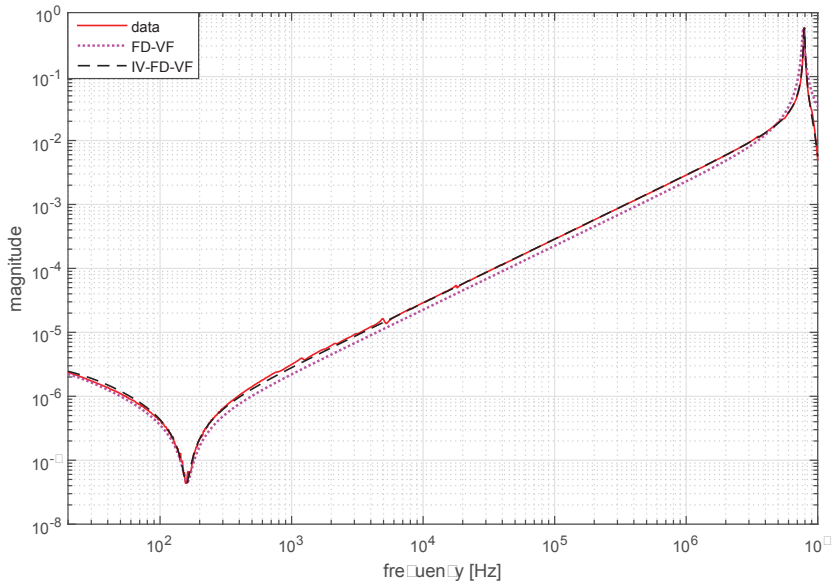

Figure 28 – IPT data extracted for Scenario #1 and resulting model frequency responses.

Now, it is considered a scenario where the IPT is modeled as a (3×3) MIMO system (i.e., a system with three inputs and three outputs). Specifically, it is considered admittance data (depicted in Fig. 30) extracted from the IPT terminals H, 1a2, and 2a2 (terminals 1n and 2n have been maintained grounded). The resulting admittance matrix has the following form:

$$\begin{bmatrix} I_{\mathrm{H}}(\omega) \\ I_{1\mathrm{a}2}(\omega) \\ I_{2\mathrm{a}2}(\omega) \end{bmatrix} = \begin{bmatrix} Y_{11}(\omega) & Y_{12}(\omega) & Y_{13}(\omega) \\ Y_{21}(\omega) & Y_{22}(\omega) & Y_{23}(\omega) \\ Y_{31}(\omega) & Y_{32}(\omega) & Y_{33}(\omega) \end{bmatrix} \begin{bmatrix} V_{\mathrm{H}}(\omega) \\ V_{1\mathrm{a}2}(\omega) \\ V_{2\mathrm{a}2}(\omega) \end{bmatrix}, \tag{3.61}$$

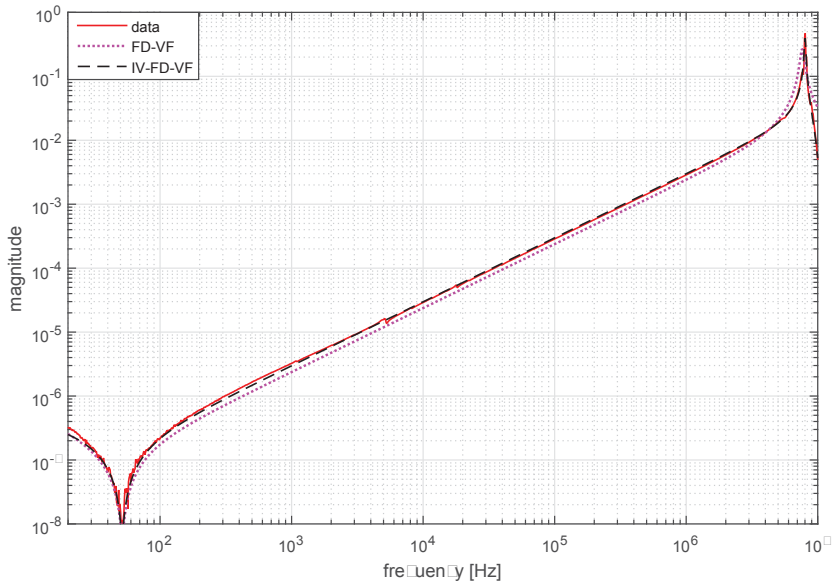

Figure 29 – IPT data extracted for Scenario #2 and resulting model frequency responses.

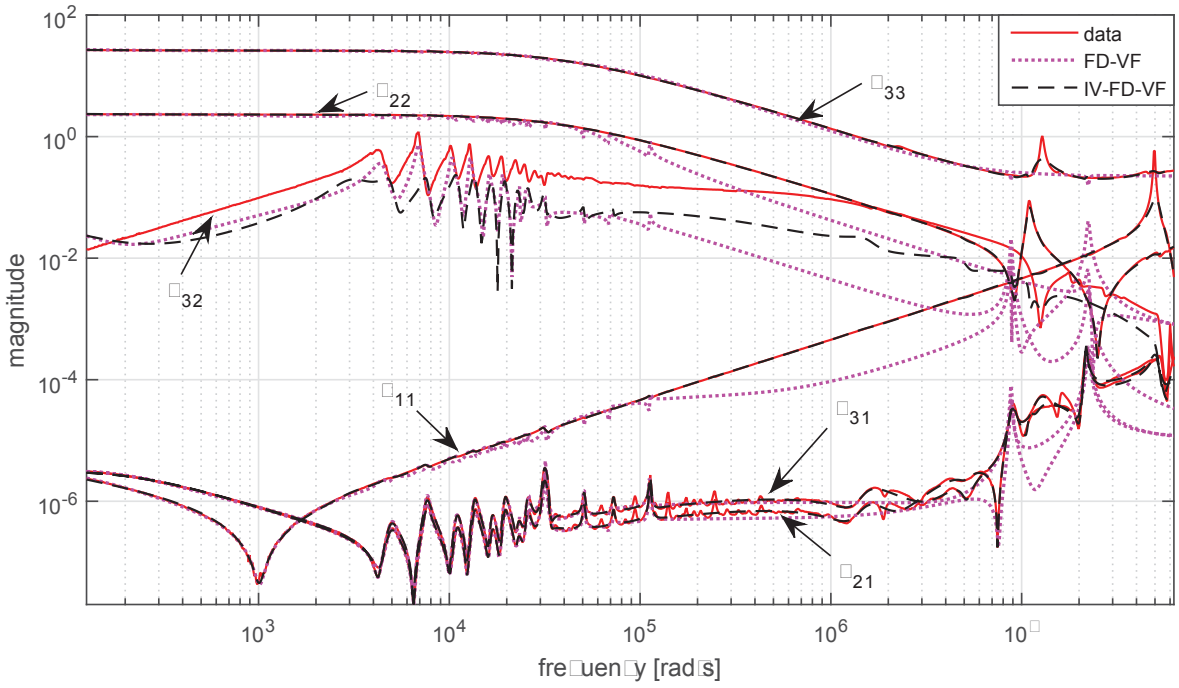

Figure 30 – Admittance data extracted from the IPT when it is modeled as a (3×3) MIMO system. The figure also depicts the resulting model frequency responses.

or, more compactly,

$$\mathbf{I}(\omega) \;=\; \mathbf{Y}(\omega)\,\mathbf{V}(\omega). \tag{3.62}$$

The objective is to model the IPT admittance elements of $\mathbf{Y}(\omega)$ via both regular FD-VF and IV-FD-VF. Here, it is assumed the system is reciprocal, meaning $\mathbf{Y}(\omega)$ satisfies $\mathbf{Y}^{\mathrm{T}}(\omega) = \mathbf{Y}(\omega)$. Therefore, one can identify the entire matrix $\mathbf{Y}(\omega)$ by modeling only, for instance, the admittance elements $Y_{11}(\omega)$, $Y_{22}(\omega)$, $Y_{33}(\omega)$, $Y_{21}(\omega)$, $Y_{31}(\omega)$, $Y_{32}(\omega)$. As it can be observed through Fig. 30, by adopting a model order $N = 50$, the IV-FD-VF iterations present a superior fit for most admittance measurements. This result is also suggested by Fig. 31, which depicts the objective function value $J(\theta)$ through iterations. In this case, note that the IV-FD-VF has been initialized only after 150 FD-VF iterations.

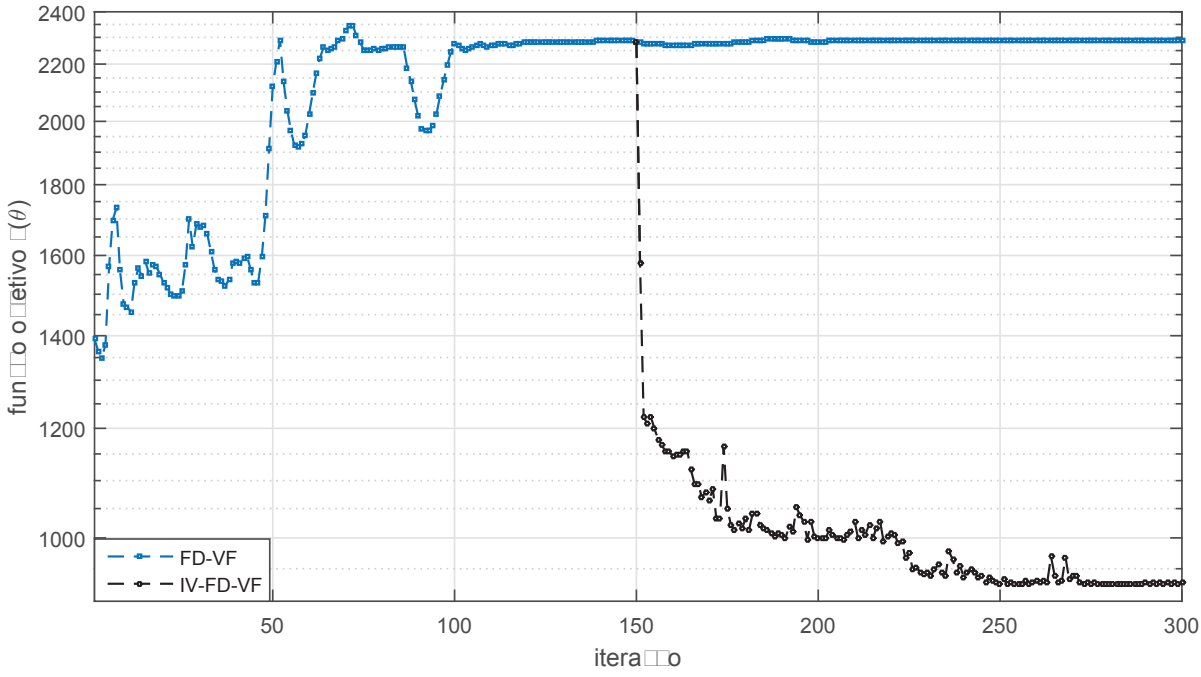

Figure 31 – Objective function value $J(\theta)$ through iterations.

We now investigate a second case study which considers a 550/0.1166kV SF6 insulated IPT.

Fig. 32 depicts the IPT used in the experiment. Admittance data from this IPT (depicted in Fig. 33) has been extracted within Institutos Lactec, Curitiba, Paraná, Brazil (OLIVEIRA *et al.*, 2019).

As it can be observed through Fig. 33, by adopting a model order $N = 50$, the IV-FD-VF iterations once again present a superior fit for most admittance measurements.

Figure 32 – Second IPT under investigation.

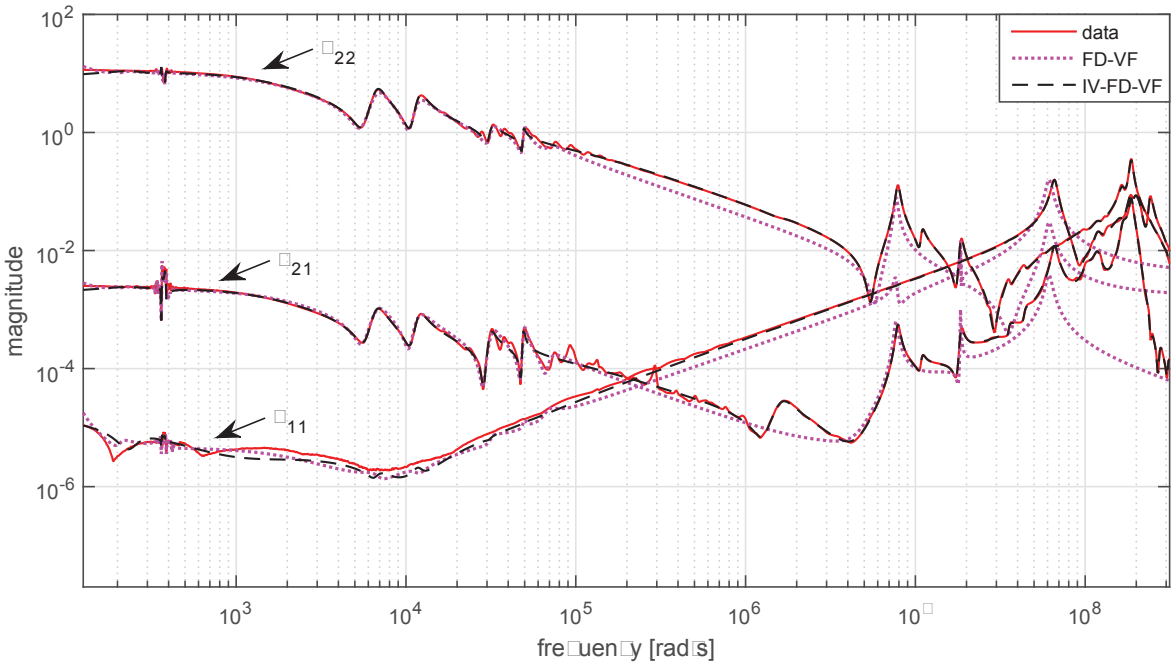

Figure 33 – Admittance data extracted from a second IPT when it is modeled as a (2×2) MIMO system. The figure also depicts the resulting model frequency responses.

This result is also suggested by Fig. 34, which depicts the objective function value $J(\theta)$ through iterations. In this case, note that it has been chosen to initialize IV-FD-VF after 30 regular FD-VF iterations.

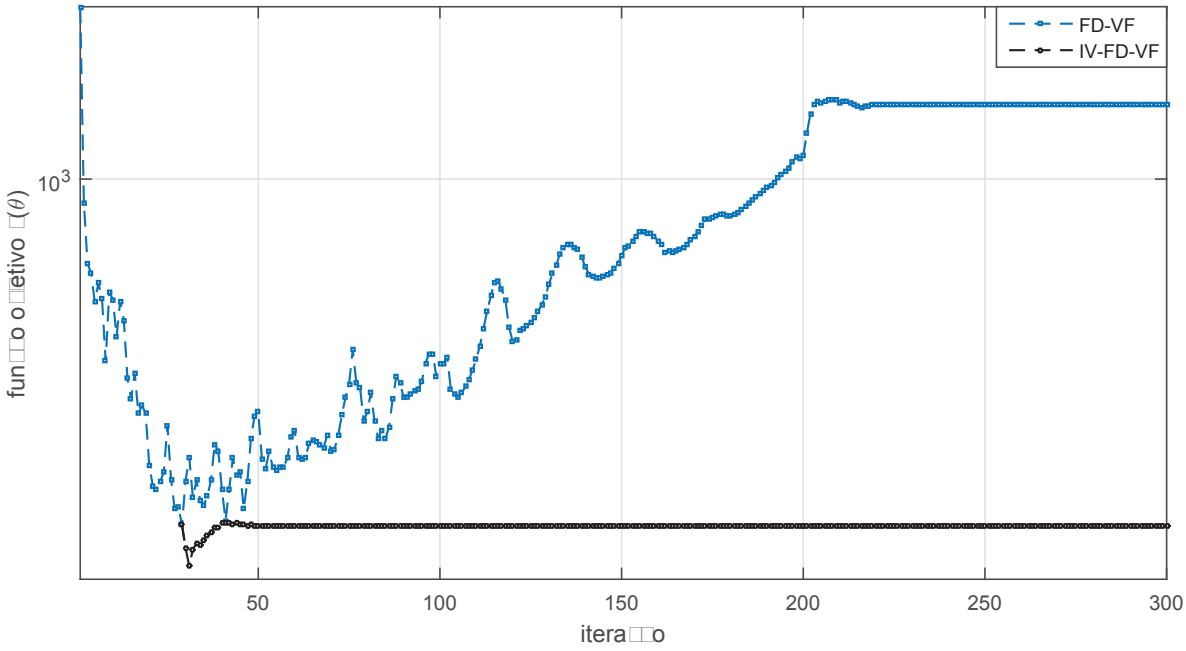

Figure 34 – Objective function value $J(\theta)$ through iterations when modeling a second IPT.

3.4 Final considerations of the chapter

In this chapter, it has been addressed the problem of formulating VF algorithms for system identification based on frequency-domain (FD) data. In particular, based on a unifying FD-VF approach, it has been presented a MIMO generalization of the SISO IV-based FD-VF method originally proposed in (SCHUMACHER; OLIVEIRA, 2019). Such an IV method, denoted by IV-FD-VF, can be similarly applied for estimating models formed either by continuous- or discrete-time RBF sets. The key advantage of IV-FD-VF lies in the fact that it is proved to guarantee optimal solutions after algorithm convergence (see Section 3.5.3). One can observe this important optimality property does not depend on the nature of the noise that corrupts estimation data. Numerical results presented in Section 3.3 have shown IV-FD-VF may provide superior fitting performance when compared to standard FD-VF algorithms such as, for instance, *vectfit3* (PACKAGE, 2008). The results presented in this chapter have also shown IV-FD-VF may provide asymptotically unbiased estimates when modeling linear time-invariant systems corrupted by colored noise.

3.5 Chapter appendices

3.5.1 Appendix A: Derivation of equation (3.42)

Assuming x and y denote two complex quantities, the following properties are here used for derivation of equation (3.42):

$$|x|^2 = x^* x \tag{3.63}$$

$$(xy)^* = x^* y^* \tag{3.64}$$

$$(x-y)^* = x^* - y^* \tag{3.65}$$

$$\frac{\partial}{\partial\theta}\left(x(\theta)y(\theta)\right) = \frac{\partial}{\partial\theta}\left(x(\theta)\right)y(\theta) + \frac{\partial}{\partial\theta}\left(y(\theta)\right)x(\theta) \tag{3.66}$$

$$x + x^* = 2\Re\mathrm{e}\left\{x\right\} \tag{3.67}$$

$$\Re\mathrm{e}\left\{-x\right\} = -\Re\mathrm{e}\left\{x\right\} \tag{3.68}$$

By applying properties (3.63)–(3.65) to (3.18)–(3.19), it follows that

$$J(\theta) = \sum_{v=1}^{V}\sum_{k=1}^{K} W_{(v)}^*(\alpha_k)\left(G_{(v)}'^*(\alpha_k) - \hat{G}_{(v)}^*(\alpha_k)\right) W_{(v)}(\alpha_k)\left(G_{(v)}'(\alpha_k) - \hat{G}_{(v)}(\alpha_k)\right). \tag{3.69}$$

Since only term $\hat{G}_{(v)}(\alpha_k)$ is function of θ (see equations (3.14)–(3.17)), based also on (3.66), we can write

$$\frac{\partial}{\partial\theta}J(\theta) = \sum_{v=1}^{V}\sum_{k=1}^{K}(x_1 + x_2) \tag{3.70}$$

with

$$x_1 = \frac{\partial}{\partial\theta}\left(W_{(v)}^*(\alpha_k)\left(G_{(v)}'^*(\alpha_k) - \hat{G}_{(v)}^*(\alpha_k)\right)\right) W_{(v)}(\alpha_k)\left(G_{(v)}'(\alpha_k) - \hat{G}_{(v)}(\alpha_k)\right), \tag{3.71}$$

$$= -W_{(v)}^*(\alpha_k)\left(\frac{\partial}{\partial\theta}\hat{G}_{(v)}^*(\alpha_k)\right) W_{(v)}(\alpha_k)\left(G_{(v)}'(\alpha_k) - \hat{G}_{(v)}(\alpha_k)\right), \tag{3.72}$$

and

$$
\begin{aligned}
x_2 &= \frac{\partial}{\partial\theta}\left(W_{(v)}(\alpha_k)\left(G'_{(v)}(\alpha_k)-\hat{G}_{(v)}(\alpha_k)\right)\right)W^*_{(v)}(\alpha_k)\left(G'^*_{(v)}(\alpha_k)-\hat{G}^*_{(v)}(\alpha_k)\right), && (3.73)\\
&= -W_{(v)}(\alpha_k)\left(\frac{\partial}{\partial\theta}\hat{G}_{(v)}(\alpha_k)\right)W^*_{(v)}(\alpha_k)\left(G'^*_{(v)}(\alpha_k)-\hat{G}^*_{(v)}(\alpha_k)\right), && (3.74)\\
&= x_1^*. && (3.75)
\end{aligned}
$$

Finally, from (3.19) and (3.67)–(3.68), one can rewrite

$$
\frac{\partial}{\partial\theta}J(\theta)=\sum_{v=1}^{V}\sum_{k=1}^{K}-2\Re\mathrm{e}\left\{W^*_{(v)}(\alpha_k)\left(\frac{\partial}{\partial\theta}\hat{G}_{(v)}(\alpha_k)\right)^* e_{(v)}(\alpha_k)\right\}. \tag{3.76}
$$

As it can be observed in equation (3.14), the v-th set of residues $\{c_i^{(v)}\}$ appear only at their corresponding v-th modeling transfer function $\hat{G}_{(v)}(\alpha_k)$. When it comes to (3.76), this means

$$
\begin{bmatrix}\frac{\partial}{\partial c_0^{(v)}}J(\theta)\\ \cdots \\ \frac{\partial}{\partial c_N^{(v)}}J(\theta)\end{bmatrix}=\sum_{k=1}^{K}-2\Re\mathrm{e}\left\{W^*_{(v)}(\alpha_k)\left(\begin{bmatrix}\frac{\partial}{\partial c_0^{(v)}}\\ \cdots \\ \frac{\partial}{\partial c_N^{(v)}}\end{bmatrix}\hat{G}_{(v)}(\alpha_k)\right)^* e_{(v)}(\alpha_k)\right\},\quad v=1,\cdots,V \tag{3.77}
$$

Meanwhile, all modeling transfer functions $\hat{G}_{(v)}(\alpha_k)$, $v=1,\cdots,V$ are simultaneously parametrized by the same set of residues $\{d_i\}$, so that

$$
\begin{bmatrix}\frac{\partial}{\partial d_1}J(\theta)\\ \cdots \\ \frac{\partial}{\partial d_N}J(\theta)\end{bmatrix}=\sum_{v=1}^{V}\sum_{k=1}^{K}-2\Re\mathrm{e}\left\{W^*_{(v)}(\alpha_k)\left(\begin{bmatrix}\frac{\partial}{\partial d_1}\\ \cdots \\ \frac{\partial}{\partial d_N}\end{bmatrix}\hat{G}_{(v)}(\alpha_k)\right)^* e_{(v)}(\alpha_k)\right\}. \tag{3.78}
$$

Since parameters within θ are arranged as shown in (3.17), one can use definitions (3.43) and (3.44) in equations (3.77) and (3.78) to write $\frac{\partial}{\partial\theta}J(\theta)$ as in (3.79), being this

expression equivalent to (3.42).

$$\frac{\partial}{\partial\theta}J(\theta)=\begin{bmatrix}\sum_{k=1}^{K}-2\Re\mathrm{e}\left\{\mathbf{i}_{(1)}^{*}(\alpha_k)\ e_{(1)}(\alpha_k)\right\}\\ \cdots\\ \sum_{k=1}^{K}-2\Re\mathrm{e}\left\{\mathbf{i}_{(V)}^{*}(\alpha_k)\ e_{(V)}(\alpha_k)\right\}\\ \sum_{v=1}^{V}\sum_{k=1}^{K}-2\Re\mathrm{e}\left\{\mathbf{i}_{(v)}^{\prime *}(\alpha_k)\ e_{(v)}(\alpha_k)\right\}\end{bmatrix}. \tag{3.79}$$

3.5.2 Appendix B: Derivation of equation (3.46)

Generally, if $\mathbf{x}\in\mathbb{C}^{N\times 1}$ and $y\in\mathbb{C}^{1\times 1}$, then $\Re\mathrm{e}\{\mathbf{x}^{*}y\}=\begin{bmatrix}\Re\mathrm{e}\{\mathbf{x}\} & \Im\mathrm{m}\{\mathbf{x}\}\end{bmatrix}\begin{bmatrix}\Re\mathrm{e}\{y\}\\ \Im\mathrm{m}\{y\}\end{bmatrix}$.

By means of this property, one can rewrite Equation (3.45) as follows

$$\sum_{k=1}^{K}\begin{bmatrix}\begin{bmatrix}\Re\mathrm{e}\{\mathbf{i}_{(1)}(\alpha_k)\} & \Im\mathrm{m}\{\mathbf{i}_{(1)}(\alpha_k)\}\end{bmatrix}\begin{bmatrix}\Re\mathrm{e}\{\tilde{e}_{(1)}(\alpha_k)\}\\ \Im\mathrm{m}\{\tilde{e}_{(1)}(\alpha_k)\}\end{bmatrix}\\ \cdots\\ \begin{bmatrix}\Re\mathrm{e}\{\mathbf{i}_{(V)}(\alpha_k)\} & \Im\mathrm{m}\{\mathbf{i}_{(V)}(\alpha_k)\}\end{bmatrix}\begin{bmatrix}\Re\mathrm{e}\{\tilde{e}_{(V)}(\alpha_k)\}\\ \Im\mathrm{m}\{\tilde{e}_{(V)}(\alpha_k)\}\end{bmatrix}\\ \sum_{v=1}^{V}\begin{bmatrix}\Re\mathrm{e}\{\mathbf{i}'_{(v)}(\alpha_k)\} & \Im\mathrm{m}\{\mathbf{i}'_{(v)}(\alpha_k)\}\end{bmatrix}\begin{bmatrix}\Re\mathrm{e}\{\tilde{e}_{(v)}(\alpha_k)\}\\ \Im\mathrm{m}\{\tilde{e}_{(v)}(\alpha_k)\}\end{bmatrix}\end{bmatrix}=\mathbf{0}, \tag{3.80}$$

or, equivalently,

$$\sum_{k=1}^{K}\begin{bmatrix}\Re\mathrm{e}\{\mathbf{N}(\alpha_k)\} & \Im\mathrm{m}\{\mathbf{N}(\alpha_k)\}\end{bmatrix}\begin{bmatrix}\Re\mathrm{e}\{\tilde{e}_{(1)}(\alpha_k)\}\\ \cdots\\ \Re\mathrm{e}\{\tilde{e}_{(V)}(\alpha_k)\}\\ \Im\mathrm{m}\{\tilde{e}_{(1)}(\alpha_k)\}\\ \cdots\\ \Im\mathrm{m}\{\tilde{e}_{(V)}(\alpha_k)\}\end{bmatrix}=\mathbf{0}, \tag{3.81}$$

where

$$\mathbf{N}(\alpha_k) = \begin{bmatrix} \mathbf{i}_{(1)}(\alpha_k) & \mathbf{0} & \cdots & \mathbf{0} \\ \mathbf{0} & \mathbf{i}_{(2)}(\alpha_k) & \cdots & \mathbf{0} \\ \cdots & \cdots & \cdots & \cdots \\ \mathbf{0} & \mathbf{0} & \cdots & \mathbf{i}_{(V)}(\alpha_k) \\ \mathbf{i}'_{(1)}(\alpha_k) & \mathbf{i}'_{(2)}(\alpha_k) & \cdots & \mathbf{i}'_{(V)}(\alpha_k) \end{bmatrix}. \tag{3.82}$$

Now, since $\tilde{e}_{(v)}(\alpha_k)$ is defined as shown in (3.23), and by considering $\hat{\theta}_{\mathrm{IV}}$ represents our IV estimate for vector θ, one can also write

$$\Re\mathrm{e}\{\tilde{e}_{(v)}(\alpha_k)\} = \Re\mathrm{e}\{W_{(v)}(\alpha_k)G'_{(v)}(\alpha_k)\} - \Re\mathrm{e}\{\mathbf{m}^{\mathrm{T}}_{(v)}(\alpha_k)\}\hat{\theta}_{\mathrm{IV}}, \tag{3.83}$$

$$\Im\mathrm{m}\{\tilde{e}_{(v)}(\alpha_k)\} = \Im\mathrm{m}\{W_{(v)}(\alpha_k)G'_{(v)}(\alpha_k)\} - \Im\mathrm{m}\{\mathbf{m}^{\mathrm{T}}_{(v)}(\alpha_k)\}\hat{\theta}_{\mathrm{IV}}, \tag{3.84}$$

where $\hat{\theta}_{\mathrm{IV}}$ has been assumed to be real-valued.

Finally, by using these definitions alongside with Equations (3.24), (3.28)–(3.31), (3.33), (3.47), (3.48) one can rewrite (3.81) as shown in (3.46).

3.5.3 Appendix C: Proof of theorem 3.2.1

In order to prove theorem 3.2.1, we make explicit dependences on θ and $\overline{\mathbf{p}}$ that involved variables might have. One can identify if a specific variable depends on θ or $\overline{\mathbf{p}}$ by inspection of equations presented in Sections 3.1 and 3.2.

If $\hat{\theta}_{\mathrm{LO}}$ denotes a local optimum of $J(\theta)$, then it necessarily satisfies the local/global

optimality condition $\left.\dfrac{\partial J}{\partial \theta}\right|_{\theta=\hat{\theta}_{\mathrm{LO}}} = \mathbf{0}$. Based on equation (3.42), this means

$$\begin{bmatrix} \displaystyle\sum_{k=1}^{K} \Re\mathrm{e}\left\{\mathbf{i}^{*}_{(1)}(\alpha_k, \hat{\theta}_{\mathrm{LO}}, \overline{\mathbf{p}})\ e_{(1)}(\alpha_k, \hat{\theta}_{\mathrm{LO}}, \overline{\mathbf{p}})\right\} \\ \cdots \\ \displaystyle\sum_{k=1}^{K} \Re\mathrm{e}\left\{\mathbf{i}^{*}_{(V)}(\alpha_k, \hat{\theta}_{\mathrm{LO}}, \overline{\mathbf{p}})\ e_{(V)}(\alpha_k, \hat{\theta}_{\mathrm{LO}}, \overline{\mathbf{p}})\right\} \\ \displaystyle\sum_{v=1}^{V}\sum_{k=1}^{K} \Re\mathrm{e}\left\{\mathbf{i}'^{*}_{(v)}(\alpha_k, \hat{\theta}_{\mathrm{LO}}, \overline{\mathbf{p}})\ e_{(v)}(\alpha_k, \hat{\theta}_{\mathrm{LO}}, \overline{\mathbf{p}})\right\} \end{bmatrix} = \mathbf{0}. \tag{3.85}$$

Meanwhile, when it comes to the IV-FD-VF approach, approximations $e_{(v)}(\alpha_k, \theta, \overline{\mathbf{p}}) \approx \tilde{e}_{(v)}(\alpha_k, \hat{\theta}^{t}_{\mathrm{IV}}, \overline{\mathbf{p}}^{t})$, $\mathbf{i}_{(v)}(\alpha_k, \theta, \overline{\mathbf{p}}) \approx \tilde{\mathbf{i}}_{(v)}(\alpha_k, \overline{\mathbf{p}}^{t})$ and $\mathbf{i}'_{(v)}(\alpha_k, \theta, \overline{\mathbf{p}}) \approx \tilde{\mathbf{i}}'_{(v)}(\alpha_k, \hat{\theta}^{t-1}_{\mathrm{IV}}, \overline{\mathbf{p}}^{t})$ make it possible to formulate the approximated problem:

$$\begin{bmatrix} \displaystyle\sum_{k=1}^{K} \Re\mathrm{e}\left\{\tilde{\mathbf{i}}^{*}_{(1)}(\alpha_k, \overline{\mathbf{p}}^{t})\ \tilde{e}_{(1)}(\alpha_k, \hat{\theta}^{t}_{\mathrm{IV}}, \overline{\mathbf{p}}^{t})\right\} \\ \cdots \\ \displaystyle\sum_{k=1}^{K} \Re\mathrm{e}\left\{\tilde{\mathbf{i}}^{*}_{(V)}(\alpha_k, \overline{\mathbf{p}}^{t})\ \tilde{e}_{(V)}(\alpha_k, \hat{\theta}^{t}_{\mathrm{IV}}, \overline{\mathbf{p}}^{t})\right\} \\ \displaystyle\sum_{v=1}^{V}\sum_{k=1}^{K} \Re\mathrm{e}\left\{\tilde{\mathbf{i}}'^{*}_{(v)}(\alpha_k, \hat{\theta}^{t-1}_{\mathrm{IV}}, \overline{\mathbf{p}}^{t})\ \tilde{e}_{(v)}(\alpha_k, \hat{\theta}^{t}_{\mathrm{IV}}, \overline{\mathbf{p}}^{t})\right\}, \end{bmatrix} = \mathbf{0}, \tag{3.86}$$

where $\overline{\mathbf{p}}^{t}$ is specified so that polynomial $\hat{F}(\alpha, \overline{\mathbf{p}})$ equals the estimate obtained for polynomial $F(\alpha, \theta, \overline{\mathbf{p}})$ during the previous algorithm iteration, i.e, so that equation (3.87) is satisfied.

$$\hat{F}(\alpha, \overline{\mathbf{p}}^{t}) = F(\alpha, \hat{\theta}^{t-1}_{\mathrm{IV}}, \overline{\mathbf{p}}^{t-1}). \tag{3.87}$$

Now, if there is a sufficiently small positive value ε and a sufficiently large iteration number t_c such that $\left|\hat{\theta}^{t_c}_{\mathrm{IV}} - \hat{\theta}^{t_c+j}_{\mathrm{IV}}\right| < \varepsilon$ and $|\overline{\mathbf{p}}^{t_c} - \overline{\mathbf{p}}^{t_c+j}| < \varepsilon$ for all $j \in \mathbb{N}$, then one can consider $\hat{\theta}^{t}_{\mathrm{IV}}$ and $\overline{\mathbf{p}}^{t}$ assume fixed values $\hat{\theta}'_{\mathrm{IV}}$ and $\overline{\mathbf{p}}'$ for any $t \geq t_c$.

For iteration $t = t_c + 1$, it follows from equation (3.87) that

$$\hat{F}(\alpha, \overline{\mathbf{p}}^{t_c+1}) = F(\alpha, \hat{\theta}^{t_c}_{\mathrm{IV}}, \overline{\mathbf{p}}^{t_c}). \tag{3.88}$$

Once

$$\hat{\theta}_{\mathrm{IV}}^{t_c+1} = \hat{\theta}_{\mathrm{IV}}^{t_c} = \hat{\theta}'_{\mathrm{IV}} \quad \text{and} \quad \overline{\mathbf{p}}^{t_c+1} = \overline{\mathbf{p}}^{t_c} = \overline{\mathbf{p}}', \tag{3.89}$$

one can also rewrite (3.88) as

$$\hat{F}(\alpha, \overline{\mathbf{p}}') = F(\alpha, \hat{\theta}'_{\mathrm{IV}}, \overline{\mathbf{p}}'), \quad \text{so that} \quad \hat{F}(\alpha, \overline{\mathbf{p}}')/F(\alpha, \hat{\theta}'_{\mathrm{IV}}, \overline{\mathbf{p}}') = 1. \tag{3.90}$$

Based on these results, it becomes possible to rewrite equation (3.86) for iteration $t = t_c + 1$ as

$$\left[\begin{array}{c} \sum_{k=1}^{K} \Re\mathrm{e}\left\{\mathbf{i}^*_{(1)}(\alpha_k, \hat{\theta}'_{\mathrm{IV}}, \overline{\mathbf{p}}')\ e_{(1)}(\alpha_k, \hat{\theta}'_{\mathrm{IV}}, \overline{\mathbf{p}}')\right\} \\ \cdots \\ \sum_{k=1}^{K} \Re\mathrm{e}\left\{\mathbf{i}^*_{(V)}(\alpha_k, \hat{\theta}'_{\mathrm{IV}}, \overline{\mathbf{p}}')\ e_{(V)}(\alpha_k, \hat{\theta}'_{\mathrm{IV}}, \overline{\mathbf{p}}')\right\} \\ \sum_{v=1}^{V}\sum_{k=1}^{K} \Re\mathrm{e}\left\{\mathbf{i}'^*_{(v)}(\alpha_k, \hat{\theta}'_{\mathrm{IV}}, \overline{\mathbf{p}}')\ e_{(v)}(\alpha_k, \hat{\theta}'_{\mathrm{IV}}, \overline{\mathbf{p}}')\right\} \end{array}\right] = \mathbf{0} \tag{3.91}$$

since, by means of definitions in (3.89)–(3.90), (3.20)–(3.21) and (3.50)–(3.52),

$$\begin{aligned} \tilde{e}_{(v)}(\alpha_k, \hat{\theta}_{\mathrm{IV}}^{t_c+1}, \overline{\mathbf{p}}^{t_c+1}) &= \tilde{e}_{(v)}(\alpha_k, \hat{\theta}'_{\mathrm{IV}}, \overline{\mathbf{p}}') \\ &= \frac{F(\alpha_k, \hat{\theta}'_{\mathrm{IV}}, \overline{\mathbf{p}}')}{\hat{F}(\alpha_k, \overline{\mathbf{p}}')} W_{(v)}(\alpha_k) G'_{(v)}(\alpha_k) - W_{(v)}(\alpha_k) \frac{B^{(v)}(\alpha_k, \hat{\theta}'_{\mathrm{IV}}, \overline{\mathbf{p}}')}{\hat{F}(\alpha_k, \overline{\mathbf{p}}')} \\ &= \frac{F(\alpha_k, \hat{\theta}'_{\mathrm{IV}}, \overline{\mathbf{p}}')}{F(\alpha_k, \hat{\theta}'_{\mathrm{IV}}, \overline{\mathbf{p}}')} W_{(v)}(\alpha_k) G'_{(v)}(\alpha_k) - W_{(v)}(\alpha_k) \frac{B^{(v)}(\alpha_k, \hat{\theta}'_{\mathrm{IV}}, \overline{\mathbf{p}}')}{F(\alpha_k, \hat{\theta}'_{\mathrm{IV}}, \overline{\mathbf{p}}')} \\ &= e_{(v)}(\alpha_k, \hat{\theta}'_{\mathrm{IV}}, \overline{\mathbf{p}}') \end{aligned} \tag{3.92}$$

$$\begin{aligned}
\tilde{\mathbf{i}}_{(v)}(\alpha_k, \overline{\mathbf{p}}^{t_c+1}) &= \tilde{\mathbf{i}}_{(v)}(\alpha_k, \overline{\mathbf{p}}') \\
&= \begin{bmatrix} W_{(v)}(\alpha_k) \\ W_{(v)}(\alpha_k)\boldsymbol{\Phi}(\alpha_k, \overline{\mathbf{p}}') \end{bmatrix} \\
&= \begin{bmatrix} W_{(v)}(\alpha_k) \\ \dfrac{\hat{F}(\alpha_k, \overline{\mathbf{p}}')}{F(\alpha_k, \hat{\theta}'_{\mathrm{IV}}, \overline{\mathbf{p}}')} W_{(v)}(\alpha_k)\boldsymbol{\Phi}(\alpha_k, \overline{\mathbf{p}}') \end{bmatrix} \\
&= \mathbf{i}_{(v)}(\alpha_k, \hat{\theta}'_{\mathrm{IV}}, \overline{\mathbf{p}}')
\end{aligned} \tag{3.93}$$

$$\begin{aligned}
\tilde{\mathbf{i}}'_{(v)}(\alpha_k, \hat{\theta}^{t_c}_{\mathrm{IV}}, \overline{\mathbf{p}}^{t_c+1}) &= -W_{(v)}(\alpha_k)\widetilde{G}'_{(v)}(\alpha_k, \hat{\theta}^{t_c}_{\mathrm{IV}}, \overline{\mathbf{p}}^{t_c+1})\boldsymbol{\Phi}(\alpha_k, \overline{\mathbf{p}}^{t_c+1}) \\
&= -W_{(v)}(\alpha_k)\widetilde{G}'_{(v)}(\alpha_k, \hat{\theta}'_{\mathrm{IV}}, \overline{\mathbf{p}}')\boldsymbol{\Phi}(\alpha_k, \overline{\mathbf{p}}') \\
&= -W_{(v)}(\alpha_k)\left(\frac{\hat{F}(\alpha_k, \overline{\mathbf{p}}')}{F(\alpha_k, \hat{\theta}'_{\mathrm{IV}}, \overline{\mathbf{p}}')}\right)^2 \widetilde{G}'_{(v)}(\alpha_k, \hat{\theta}'_{\mathrm{IV}}, \overline{\mathbf{p}}')\boldsymbol{\Phi}(\alpha_k, \overline{\mathbf{p}}') \\
&= \mathbf{i}'_{(v)}(\alpha_k, \hat{\theta}'_{\mathrm{IV}}, \overline{\mathbf{p}}')
\end{aligned} \tag{3.94}$$

Expression (3.91) matches exactly with the local optimality condition in (3.85), meaning that $\hat{\theta}'_{\mathrm{IV}}$ is guaranteed a local (if not the global) optimum of $J(\theta)$.

4 CONCLUSIONS

This thesis has addressed and promoted the problem of formulating VF algorithms for both time- and frequency-domain system identification. When it comes to time-domain, in Chapter 2, VF algorithms have been developed within a ringdown context, so that oscillatory (as well as purely exponential) dynamics (modes) of power systems could be effectively estimated through transient data sets. When it comes to frequency-domain, in Chapter 3, this thesis has presented a unifying FD-VF method which can be similarly applied for estimating models formed either by continuous- or discrete-time RBFs. Numerical examples presented in Chapter 2 have focused on actual ringdown data sets extracted from NAEI and BIP systems. Meanwhile, numerical examples presented in Chapter 3 have focused mainly on frequency response data extracted from actual transformers.

Specifically, in Chapter 2, it has been shown that the single-signal RTD-VF method (SCHUMACHER; OLIVEIRA; KUIAVA, 2018) is capable of providing superior fitting performance over recognized techniques, such as Prony (HAUER; DEMEURE; SCHARF, 1990) and Matrix Pencil (CROW; SINGH, 2005), as well as over its counterpart RFD-VF method previously proposed in (PAPADOPOULOS *et al.*, 2016), which is described in frequency-domain and therefore relies on performing DFTs of ringdown data sequences.

By simultaneously processing multiple ringdown signals possibly distributed over different locations of a power system, it has also been shown in Chapter 2 that the multi-signal RTD-VF approach proposed in (SCHUMACHER; OLIVEIRA; KUIAVA, 2019) may provide superior results when compared to single-signal RTD-VF, in which ringdown signals are estimated independently, i.e., on at a time. In addition, if regular multi-signal RTD-VF is transformed into the so-called multi-signal IV-RTD-VF iterations (see also (SCHUMACHER; OLIVEIRA; KUIAVA, 2019)), then it is possible to further refine solutions provided by regular multi-signal RTD-VF.

On the other hand, in Chapter 3, it has been shown that the IV-FD-VF method

(SCHUMACHER; OLIVEIRA, 2019) may provide superior fitting performance when compared to standard FD-VF algorithms such as, for instance, *vectfit3* (PACKAGE, 2008), which is still one of the most popular implementations of standard FD-VF.

Finally, by means of theorems 2.6.1 and 3.2.1, presented in Chapters 2 and 3, respectively, it has been highlighted that in both time-domain and frequency-domain contexts addressed in this thesis the key advantage of the presented IV-based VF approaches is to guarantee that local optimums are necessarily obtained after algorithm convergence. This important optimality property is independent on the nature of noise that corrupts estimation data, since no assumption about it is adopted while proving these theorems (see Sections 2.9.4 and 3.5.3). Such propositions have also been confirmed by means of the numerical examples of Sections 2.7.2 and 3.3.2, which provide statistical analysis based on data samples corrupted by colored noise.

REFERENCES

AGUIRRE, L. A. *Introdução à Identificação de Sistemas: técnicas lineares e não-lineares aplicadas a sistemas reais*. 3. ed. Belo Horizonte: Editora da UFMG, 2007. Cited in page 17.

ÅSTRÖM, K. J. *Computer-Controlled Systems*. 3. ed. [S.l.]: Prentice Hall, 1996. Cited in page 16.

BAROCIO, E.; PAL, B. C.; THORNHILL, N. F.; MESSINA, A. R. A dynamic mode decomposition framework for global power system oscillation analysis. *IEEE Transactions on Power Systems*, v. 30, n. 6, p. 2902–2912, 2015. Cited in page 25.

CANIZARES, C.; FERNANDES, T.; GERALDI Jr., E.; GERIN-LAJOIE, L.; GIBBARD, M.; HISKENS, I.; KERSULIS, J.; KUIAVA, R.; LIMA, L.; DEMARCO, F.; MARTINS, N.; PAL, B. C.; PIARDI, A.; RAMOS, R.; DOS SANTOS, J.; SILVA, D.; SINGH, A. K.; TAMIMI, B.; VOWLES, D. Benchmark models for the analysis and control of small-signal oscillatory dynamics in power systems - IEEE task force on benchmark systems for stability controls. *IEEE Transactions on Power Systems*, v. 32, n. 1, p. 715–722, 2017. Cited 2 times in pages 22 and 31.

CHEN, C. T. *Linear System Theory and Design*. 3. ed. New York: Oxford University Press, 1999. Cited 4 times in pages 39, 56, 75, and 77.

CHOI, B.-K.; CHIANG, H.-D.; LI, Y.; LI, H.; CHEN, Y.-T.; HUANG, D.-H.; LAUBY, M. Measurement-based dynamic load models: derivation, comparison, and validation. *IEEE Transactions on Power Systems*, v. 21, n. 3, p. 1276–1283, 2006. Cited in page 25.

CHOMPOOBUTRGOOL, Y.; VANFRETTI, L. Identification of power system dominant inter-area oscillation paths. *IEEE Transactions on Power Systems*, v. 28, n. 3, p. 2798–2807, 2013. Cited in page 25.

Cigre WG A2/C4.39. *Electrical Transient Interaction Between Transformer and the Power System, Part 1 Expertise and Part 2 Case Studies*. 2014. Cited in page 18.

CROW, M. L.; SINGH, A. The matrix pencil for power system modal extraction. *IEEE Transactions on Power Systems*, v. 20, n. 1, p. 501–502, 2005. Cited 11 times in pages 22, 24, 25, 26, 29, 41, 45, 58, 65, 74, and 121.

DESCHRIJVER, D.; HAEGEMAN, B.; DHAENE, T. Orthonormal Vector Fitting: A robust macromodeling tool for rational approximation of frequency domain responses. *IEEE Transactions on Advanced Packaging*, v. 30, n. 2, p. 216–225, 2007. Cited 5 times in pages 17, 19, 34, 88, and 89.

DESCHRIJVER, D.; MROZOWSKI, M.; DHAENE, T.; DE ZUTTER, D. Macromodeling of multiport systems using a fast implementation of the vector fitting method. *IEEE Microwave and Wireless Components Letters*, v. 18, n. 6, p. 383–385, 2008. Cited 2 times in pages 19 and 100.

DOSIEK, L.; PIERRE, J. W. Multichannel techniques for the estimation of power system electromechanical modes. In: *16th IFAC Symposium on System Identification*. [S.l.: s.n.], 2012. p. 1013–1018. Cited 2 times in pages 25 and 47.

DOSIEK, L.; PIERRE, J. W. Estimating electromechanical modes and mode shapes using the multichannel ARMAX model. *IEEE Transactions on Power Systems*, v. 28, n. 2, p. 1950–1959, 2013. Cited 2 times in pages 25 and 47.

EREMIA, M.; SHAHIDEHPOUR, M. *Handbook of Electrical Power System Dynamics: Modeling, Stability, and Control*. [S.l.]: Wiley-IEEE Press, 2013. Cited in page 16.

FRAX-101. *Sweep Frequency Response Analyzer*. 2013. [Online]. Available: www.megger.com. Cited in page 100.

GILSON, M.; WELSH, J. S.; GARNIER, H. Frequency-domain instrumental variable based method for wide band system identification. In: *American Control Conference*. [S.l.: s.n.], 2013. p. 1663–1668. Cited in page 21.

GLICKMAN, M.; O'SHEA, P.; LEDWICH, G. Estimation of modal damping in power networks. *IEEE Transactions on Power Systems*, v. 22, n. 3, p. 1340–1350, Aug 2007. ISSN 0885-8950. Cited in page 23.

GRIVET-TALOCIA, S. Package macromodeling via time-domain Vector Fitting. *IEEE Microwave and Wireless Components Letters*, v. 13, n. 11, p. 472–474, 2003. Cited 6 times in pages 17, 19, 24, 26, 29, and 74.

GRIVET-TALOCIA, S.; GUSTAVSEN, B. *Passive Macromodeling: Theory and Applications*. New Jersey: John Wiley and Sons Inc., 2016. Cited 21 times in pages 17, 18, 19, 20, 25, 34, 35, 37, 38, 39, 40, 54, 55, 56, 58, 86, 88, 89, 93, 94, and 95.

GUSTAVSEN, B. Computer code for rational approximation of frequency dependent admittance matrices. *IEEE Transactions on Power Delivery*, v. 17, n. 4, p. 1093–1098, 2002. Cited 3 times in pages 17, 19, and 88.

Gustavsen, B. Wide band modeling of power transformers. *IEEE Transactions on Power Delivery*, v. 19, n. 1, p. 414–422, 2004. Cited 2 times in pages 18 and 100.

GUSTAVSEN, B. Improving the pole relocating properties of Vector Fitting. *IEEE Transactions on Power Delivery*, v. 21, n. 3, p. 1587–1591, 2006. Cited 4 times in pages 17, 18, 19, and 100.

GUSTAVSEN, B. Study of transformer resonant overvoltages caused by cable-transformer high-frequency interaction. *IEEE Transactions on Power Delivery*, v. 25, n. 2, p. 770–779, 2010. Cited in page 18.

GUSTAVSEN, B.; SEMLYEN, A. Rational approximation of frequency domain responses by Vector Fitting. *IEEE Transactions on Power Delivery*, v. 14, n. 3, p. 1052–1061, 1999. Cited 11 times in pages 17, 18, 19, 24, 39, 56, 86, 88, 89, 93, and 100.

HAUER, J. F.; DEMEURE, C. J.; SCHARF, L. L. Initial results in Prony analysis of power system response signals. *IEEE Transactions on Power Systems*, v. 5, n. 1, p. 80–89, 1990. Cited 9 times in pages 22, 23, 24, 26, 29, 41, 58, 74, and 121.

HENDRICKX, W.; DHAENE, T. A discussion of "rational approximation of frequency domain responses by Vector Fitting. *IEEE Transactions on Power Systems*, v. 21, n. 1, p. 441–443, 2006. Cited in page 18.

HEUBERGER, P. S. C.; VAN DEN HOF, P. M. J.; WAHLBERG, B. *Modelling and Identification with Rational Orthogonal Basis Functions*. London: Springer-Verlag, 2005. Cited 3 times in pages 17, 20, and 86.

HIGHAM, N. J. The scaling and squaring method for the matrix exponential revisited. *SIAM J. Matrix Anal. Appl.*, v. 26, n. 4, p. 1179–1193, 2005. Cited in page 79.

HWANG, J. K.; LIU, Y. Noise analysis of power system frequency estimated from angle difference of discrete fourier transform coefficient. *IEEE Transactions on Power Delivery*, v. 29, n. 4, p. 1533–1541, Aug 2014. ISSN 0885-8977. Cited 3 times in pages 22, 41, and 63.

HWANG, J. K.; LIU, Y. Identification of interarea modes from ringdown data by curve-fitting in the frequency domain. *IEEE Transactions on Power Systems*, v. 32, n. 2, p. 842–851, 2017. Cited 9 times in pages 5, 22, 23, 24, 41, 44, 45, 58, and 63.

IEEE Std C57.149. *Guide for the Application and Interpretation of Frequency Response Analysis for Oil Immersed Transformers. IEEE Power and Energy Society*. 2012. Cited 2 times in pages 100 and 101.

IHLENFELD, L. P. R. K.; OLIVEIRA, G. H. C.; SANS, M. R. A data passivity-enforcement preprocessing approach to multiport system modeling. *IEEE Transactions on Power Delivery*, v. 31, n. 3, p. 1351–1359, 2016. Cited in page 18.

JEREMIAS, T.; ZIMMER, V.; DECKER, I. C.; E Silva, A. S.; AGOSTINI, M. N. Estudo de oscilações eletromêcanicas no sistema elétrico brasileiro utilizando medidas fasoriais sincronizadas ("study of electromechanical oscillations in the brazilian electric system using phasor measurement units"). In: *XIX Congresso Brasileiro de Automatica*. [S.l.: s.n.], 2012. p. 2364–2371. Cited 3 times in pages 5, 46, and 69.

JUANG, J.; PAPPA, R. S. An eigensystem realization algorithm for modal parameter identification and model reduction. *Journal of Guidance, Control, and Dynamics*, v. 8, n. 5, p. 620–627, 1985. Cited in page 25.

KHAZAEI, J.; FAN, L.; JIANG, W.; MANJURE, D. Distributed prony analysis for real-world PMU data. *Electric Power Systems Research*, v. 133, p. 113–120, 2016. Cited 2 times in pages 25 and 47.

KNOCKAERT, L. Comments on "macromodeling of multiport systems using a fast implementation of the vector fitting method". *IEEE Microwave and Wireless Components Letters*, v. 19, n. 9, p. 602–602, 2009. Cited in page 19.

KONTIS, E. O.; PAPADOPOULOS, T. A.; Barzegkar-Ntovom, G. A.; CHRYSOCHOS, A. I.; PAPAGIANNIS, G. K. Modal analysis of active distribution networks using system identification techniques. *International Journal of Electrical Power and Energy Systems*, v. 100, p. 365–378, 2018. Cited 3 times in pages 25, 65, and 67.

KONTIS, E. O.; PAPADOPOULOS, T. A.; CHRYSOCHOS, A. I.; PAPAGIANNIS, G. Measurement-based dynamic load modeling using the vector fitting technique. *IEEE Transactions on Power Systems*, v. 33, n. 1, p. 338–351, 2018. Cited in page 25.

KUNDUR, P. *Power System Stability and Control*. New York: McGraw-Hill, 1994. Cited 2 times in pages 22 and 31.

LI, X.; CUI, H.; JIANG, T.; XU, Y.; JIA, H.; LI, F. Multichannel continuous wavelet transform approach to estimate electromechanical oscillation modes, mode shapes and coherent groups from synchrophasors in bulk power grids. *International Journal of Electrical Power and Energy Systems*, v. 96, p. 222–237, 2018. Cited in page 25.

LJUNG, L. *System Identification: Theory for the User*. 2. ed. New Jersey: Prentice Hall, 1999. Cited 2 times in pages 16 and 17.

LJUNG, L.; GLAD, T. *Modeling of Dynamic Systems*. New Jersey: Prentice Hall, 1994. Cited in page 16.

MAHMOOD, F.; HOOSHYAR, H.; LAVENIUS, J.; BIDADFAR, A.; LUND, P.; VANFRETTI, L. Real-time reduced steady-state model synthesis of active distribution networks using pmu measurements. *IEEE Transactions on Power Delivery*, v. 32, n. 1, p. 546–555, 2017. Cited in page 25.

MEDFASEE. 2017. [Online]. Available: http://www.medfasee.ufsc.br/temporeal/. Cited 6 times in pages 8, 22, 30, 41, 63, and 67.

MEKONNEN, Y. S.; SCHUTT-AINÉ, J. E. Broadband macromodeling of sampled frequency data using z-domain Vector-Fitting method. In: *IEEE Workshop on Signal Propagation on Interconnects*. [S.l.: s.n.], 2007. p. 45–48. Cited in page 19.

MESSINA, A. R.; VITTAL, V. Extraction of dynamic patterns from wide-area measurements using empirical orthogonal functions. *IEEE Transactions on Power Systems*, v. 22, n. 2, p. 682–692, 2007. Cited in page 25.

MUNOZ-HERNANDEZ, G. A.; MANSOOR, S. P.; JONES, D. I. *Modelling and Controlling Hydropower Plants*. [S.l.]: Springer, 2013. Cited in page 16.

NING, J.; PAN, X.; VENKATASUBRAMANIAN, V. Oscillation modal analysis from ambient synchrophasor data using distributed frequency domain optimization. *IEEE Transactions on Power Systems*, v. 28, n. 2, p. 1960–1968, 2013. Cited in page 25.

NING, J.; SARMADI, S. A. N.; VENKATASUBRAMANIAN, V. Two-level ambient oscillation modal estimation from synchrophasor measurements. *IEEE Transactions on Power Systems*, v. 30, n. 6, p. 2913–2922, 2015. Cited in page 25.

NOURI, B.; ACHAR, R.; NAKHLA, M. S. z-domain orthonormal basis functions for physical system identifications. *IEEE Transactions on Advanced Packaging*, v. 33, n. 1, p. 293–307, 2010. Cited 2 times in pages 19 and 86.

OLIVEIRA, G. H. C.; IHLENFELD, L. P. R. K.; RODRIGUES, L. F. M.; ROCHA, A. C. O.; SANTO, D. J. D. E. Sobre o uso de parâmetros s para aprimorar modelos de tp indutivos presentes em gis. In: *XXV Seminário Nacional de Produção e Transmissão de Energia Elétrica*. [S.l.: s.n.], 2019. p. 1–9. Cited in page 111.

OLIVEIRA, G. H. C.; RODIER, C.; IHLENFELD, L. P. R. K. LMI-based method for estimating passive blackbox models in power systems transient analysis. *IEEE Transactions on Power Delivery*, v. 31, n. 1, p. 3–10, 2016. Cited in page 18.

ONS. *Daily Preliminary Information of Operation 02/02/2011*. 2011. [Online]. Available in Portuguese: www.ons.org.br. Cited 2 times in pages 30 and 46.

PACKAGE vectfit3. *Frequency-Domain Vector Fitting Implementation*. 2008. [Online]. Available: http://www.sintef.no/projectweb/vectfit/. Cited 6 times in pages 19, 27, 84, 100, 113, and 122.

PAPADOPOULOS, T. A.; CHRYSOCHOS, A. I.; KONTIS, E. O.; PAPAGIANNIS, G. K. Ringdown analysis of power systems using Vector Fitting. *Electric Power Systems Research*, v. 141, p. 100–103, 2016. Cited 10 times in pages 18, 24, 26, 29, 41, 42, 58, 65, 74, and 121.

PATERNINA, M. R. A.; TRIPATHY, R. K.; Zamora-Mendez, A.; DOTTA, D. Identification of electromechanical oscillatory modes based on variational mode decomposition. *Electric Power Systems Research*, v. 167, p. 71–85, 2019. Cited in page 25.

PINTELON, R.; SCHOUKENS, J. *System Identification: A Frequency Domain Approach*. 2. ed. [S.l.]: Wiley-IEEE Press, 2012. Cited in page 16.

PORDANJANI, I. R.; CHUNG, C. Y.; MAZIN, H. E.; XU, W. A method to construct equivalent circuit model from frequency responses with guaranteed passivity. *IEEE Transactions on Power Delivery*, v. 26, n. 1, p. 400–409, 2011. Cited in page 88.

RAMIREZ, A. Vector fitting-based calculation of frequency-dependent network equivalents by frequency partitioning and model-order reduction. *IEEE Transactions on Power Delivery*, v. 24, n. 1, p. 410–415, 2009. Cited in page 17.

RENMU, H.; JIN, M.; HILL, D. Composite load modeling via measurement approach. *IEEE Transactions on Power Systems*, v. 21, n. 2, p. 663–672, 2006. Cited in page 25.

SANATHANAN, C. K.; KOERNER, J. Transfer function synthesis as a ratio of two complex polynomials. *IEEE Transactions on Automatic Control*, v. 8, n. 1, p. 56–58, 1963. Cited in page 18.

SCHUMACHER, R. Identificação de sistemas via bases de funções racionais e métodos iterativos baseados em variáveis instrumentais. *Dissertação de mestrado, Universidade Federal do Paraná*, 2017. Cited 2 times in pages 20 and 105.

SCHUMACHER, R.; LIMA, E. G.; OLIVEIRA, G. H. C. RF power amplifier behavioral modeling based on Takenaka-Malmquist-Volterra series. *Circuits, Systems and Signal Processing*, v. 35, n. 7, p. 2298–2316, 2016. Cited in page 20.

SCHUMACHER, R.; OLIVEIRA, G. H. C. An optimal vector fitting method for estimating frequency-dependent network equivalents in power systems. *Electric Power Systems Research*, v. 150, p. 96–104, 2017. Cited 9 times in pages 17, 19, 21, 25, 26, 27, 34, 84, and 104.

SCHUMACHER, R.; OLIVEIRA, G. H. C. A unifying method to construct rational basis functions for linear and nonlinear systems. *Circuits, Systems, and Signal Processing*, v. 37, n. 6, p. 2394–2412, 2018. Cited 6 times in pages 19, 20, 27, 78, 84, and 87.

SCHUMACHER, R.; OLIVEIRA, G. H. C. An optimal and unifying vector fitting method for frequency-domain system identification. *International Journal of Electrical Power and Energy Systems*, v. 104, p. 326–334, 2019. Cited 7 times in pages 21, 27, 84, 88, 100, 113, and 122.

SCHUMACHER, R.; OLIVEIRA, G. H. C.; KUIAVA, R. A novel time-domain linear ringdown method based on vector fitting for estimating electromechanical modes. *Electric Power Systems Research*, v. 160, p. 300–307, 2018. Cited 15 times in pages 18, 24, 26, 29, 30, 33, 37, 38, 41, 54, 55, 58, 69, 74, and 121.

SCHUMACHER, R.; OLIVEIRA, G. H. C.; KUIAVA, R. A multi-signal instrumental variable vector fitting method for estimating inter-area electromechanical modes of power systems. *International Journal of Electrical Power and Energy Systems*, v. 111, p. 1–13, 2019. Cited 9 times in pages 18, 26, 27, 29, 48, 58, 63, 74, and 121.

SCHUMACHER, R.; OLIVEIRA, G. H. C.; MITCHELL, S. D. An iterative approach for selecting poles on complex frequency localizing basis function-based models. *Journal of Control, Automation and Electrical Systems*, v. 26, n. 4, p. 380–389, 2015. Cited in page 19.

SHI, G. On the nonconvergence of the Vector Fitting algorithm. *IEEE Transactions on Circuits and Systems II: Express Briefs*, v. 63, n. 8, p. 718–722, 2016. Cited 2 times in pages 21 and 25.

STEIGLITZ, K.; MCBRIDE, L. E. A technique for the identification of linear systems. *IEEE Transactions on Automatic Control*, v. 10, n. 4, p. 461–464, 1965. Cited in page 18.

STOJANOVIĆ, D. P.; KORUNOVIĆ, L. M.; MILANOVIĆ, J. V. Dynamic load modelling based on measurements in medium voltage distribution network. *Electric Power Systems Research*, v. 78, n. 2, p. 228–238, 2008. Cited in page 25.

SUSUKI, Y.; MEZIC, I. Nonlinear koopman modes and coherency identification of coupled swing dynamics. *IEEE Transactions on Power Systems*, v. 26, n. 4, p. 1894–1904, 2011. Cited in page 25.

THAMBIRAJAH, J.; BAROCIO, E.; THORNHILL, N. Comparative review of methods for stability monitoring in electrical power systems and vibrating structures. *IET Generation, Transmission and Distribution*, v. 4, n. 10, p. 1086–1103, 2010. Cited in page 22.

THOMAS, B.; SAVADAMUTHU, U. Impulse breakdown characteristics of aged oil impregnated paper. *IEEE Transactions on Dielectrics and Electrical Insulation*, v. 24, n. 4, p. 2354–2361, 2017. Cited in page 18.

TRUDNOWSKI, D. J.; JOHNSON, J. M.; HAUER, J. F. Making prony analysis more accurate using multiple signals. *IEEE Transactions on Power Systems*, v. 14, n. 1, p. 226–231, 1999. Cited 2 times in pages 25 and 47.

TRUDNOWSKI, D. J.; PIERRE, J. W.; ZHOU, N.; HAUER, J. F.; PARASHAR, M. Performance of three mode-meter block-processing algorithms for automated dynamic stability assessment. *IEEE Transactions on Power Systems*, v. 23, n. 2, p. 680–690, 2008. Cited 3 times in pages 22, 23, and 63.

UBOLLI, A.; GUSTAVSEN, B. Comparison of methods for rational approximation of simulated time-domain responses: ARMA, ZD-VF, and TD-VF. *IEEE Transactions on Power Delivery*, v. 26, n. 1, p. 279–288, 2011. Cited 2 times in pages 17 and 19.

VAN DEN BOSCH, P. P. J.; VAN DER KLAUW, A. C. *Modeling, Identification and Simulation of Dynamical Systems*. 1. ed. Florida: CRC Press, 1994. Cited in page 17.

VAN DEN HOF, P. M. J.; HEUBERGER, P. S. C.; BOKOR, J. System identification with generalized orthonormal basis functions. *Automatica*, v. 31, n. 12, p. 1821–1834, 1995. Cited in page 20.

VOORHOEVE, R.; OOMEN, T.; VAN HERPEN, R.; STEINBUCH, M. On numerically reliable frequency-domain system identification: new connections and a comparison of methods. In: *19th IFAC World Congress*. [S.l.: s.n.], 2014. v. 47, n. 3, p. 10018–10023. Cited 2 times in pages 17 and 21.

WADDUWAGE, D. P.; ANNAKKAGE, U. D.; NARENDRA, K. Identification of dominant low-frequency modes in ring-down oscillations using multiple Prony models. *IET Generation, Transmission and Distribution*, v. 9, n. 15, p. 2206–2214, 2015. Cited in page 32.

WONG, N.; LEI, C. IIR approximation of FIR filters via discrete-time Vector Fitting. *IEEE Transactions on Signal Processing*, v. 56, n. 3, p. 1296–1302, 2008. Cited in page 19.

YE, Y.; LIU, Y. Monitoring power system disturbances based on distribution-level phasor measurements. In: *2012 IEEE PES Innovative Smart Grid Technol.* [S.l.: s.n.], 2012. p. 1–8. Cited 3 times in pages 22, 41, and 63.